GEOLOGICAL AND GEOTECHNICAL STUDIES OF SOME LANDSLIDES IN AND AROUND KOHIMA TOWN, NAGALAND

BY

MEHILO APON

Submitted in partial fulfillment of the requirement of the
Degree of Doctor of Philosophy in Geology
of Nagaland University
2024

PLAGIARISM-FREE UNDERTAKING

Name of Research Scholar	Mr. Mehilo Apon
Ph.D. Registration Number	Ph.D/GEL/00092 of 28th August, 2017
Title of Ph.D. thesis	Geological and geotechnical studies of some landslides in and around Kohima town, Nagaland
Name & Institutional Address of the Supervisor	Prof. G.T. Thong, Department of Geology, Nagaland University, Kohima Campus, Meriema - 797004
Name of the Department & School	Department of Geology / School of Sciences
Date of submission	
Date of plagiarism check	31.07.2024
Percentage of similarity detected by the DrillBit software	9 %

I hereby declare / certify that the Ph.D. thesis submitted by me is complete in all respects, as per the guidelines of the Nagaland University for this purpose. I also certify that the thesis (soft copy) has been checked for plagiarism using DrillBit plagiarism detection software. It is also certified that the contents of the electronic version of the thesis are the same as the final hard copy of the thesis. A copy of the report generated by the DrillBit plagiarism detection software is also enclosed.

(Name & Signature of the Scholar)

Date:

Place:

Name & Signature of the Supervisor with seal:

NAGALAND UNIVERSITY

August 2024

DECLARATION

I, Mr. Mehilo Apon, hereby declare that the subject matter of this thesis is the record of work done by me, that the contents of this thesis did not form basis of the award of any previous degree to me or to the best of my knowledge to anybody else, and that the thesis has not been submitted by me for any research degree in any other University/Institute.

This is being submitted to the Nagaland University for the degree of Doctor of Philosophy in Geology.

Candidate

Head   Supervisor

NAGALAND

Glenn T. Thong
Senior Professor
Department of Geology

UNIVERSITY

☎ *0370 - 2240515*
Mobile 09436000479
E-mail *glen2t03@yahoo.com*
glennthong@nagalanduniversity.ac.in

Kohima Campus, Meriema - 797004

CERTIFICATE

The thesis presented by Mr. Mehilo Apon, M.Sc., bearing Registration No. Ph.D/GEL/00092 (28th August 2017) embodies the results of investigations carried out by him under my supervision and guidance.

I certify that this work has not been presented for any degree elsewhere and that the candidate has fulfilled all conditions laid down by the University.

Place:

G.T. THONG

Date:

Supervisor

ACKNOWLEDGEMENT

PREFACE

Mountainous regions are prone to landslides, especially during the monsoon. The slopes of hilly terrain, particularly those of tectonically active regions, are usually made up of weak rocks and covered by low-strength soils. The study area is a part of the rising Arakan-Yoma Ranges and is marked by faults, thrusts, and other lineaments. Various tectonic events have taken a toll in this region, thereby extensively destabilising the slopes. With fast-paced urbanisation and development, human activities have aggravated the condition of the weak terrain. The region is also prone to heavy and continuous rainfall during the monsoon, which often triggers landslides. This study was carried out in the northern part of Kohima town, which was affected by six landslides following heavy and continuous rains in 2017 and 2018.

An attempt is made to determine the characteristics of the soils and rocks of the study area. Various geotechnical and geomechanical methods were employed to determine the properties of the soils and rocks respectively. Considering the dynamic nature of the region, an attempt was also made to determine the stresses that have been instrumental in shaping Kohima town.

This study is made up of six chapters. Chapter 1 gives a general overview of the study area along with information on the general location of the study area. It also deliberates on the works done by different researchers in similar fields of geotechnical and geological parameters. The objectives of this study are stated in this chapter. The geological setting of the study area is elaborated in Chapter 2. Chapter 3 covers the various materials and methodologies that have been taken up in the landslide zones, leading to multiple analyses being expounded in thorough detail. Chapter 4 of the thesis portrays the results of geotechnical analyses, which had been conducted on the slope materials of the affected areas. It has been illustrated with charts and figures. Each of the study areas begins with a detailed description of the impact and extent of the landslides. The different back analyses and precipitation analyses follow it. The results of slope mass rating and kinematic, structural, and paleostress analyses are illustrated in Chapter 5. In the final chapter, some appropriate and applicable remedial and mitigation measures follow the discussions of the results. A summary of the works and the results forms the conclusion in this chapter.

CONTENTS

LIST OF FIGURES

LIST OF TABLES

PARTICULARS OF CANDIDATE

NAME OF THE CANDIDATE   : Mr. Mehilo Apon

DEGREE   : Ph.D.

DEPARTMENT   : Geology

TITLE OF DISSERTATION   : Geological and geotechnical studies of some landslides in and around Kohima town, Nagaland

DATE OF ADMISSION   : 28th August 2017

APPROVAL OF RESEARCH PROPOSAL   : 16th August 2018

REGISTRATION No. & DATE   : Ph.D/GEL/00092 (28th August 2017)

Head of Department

BIODATA OF THE CANDIDATE

1. **Research papers published**

   - **Mehilo Apon,** Notoka K, C. Nokendangba Chang, Meripeni Ezung, Glenn T. Thong, Temsulemba Walling (2024) Analysis of an anthropogenically-induced landslide with emphasis on geological precursors. *Results in Earth Sciences* (Elsevier). (ISSN: 2211-7148), Vol. 2, pp. 100020. https://doi.org/10.1016/j.rines.2024.100020

   - C. Nokendangba Chang, Meripeni Ezung, **Mehilo Apon**, Supongtemjen, Temsulemba Walling & Glenn T. Thong (2021) Assessment of landslides along NH 29 in the Kevüza area, Kohima, Nagaland. *Indian Geotechnical Journal* (Springer), vol. 51, pp. 841–860. https://doi.org/10.1007/s40098-021-00566-z

   - Meripeni Ezung, Temsulemba Walling, C. Nokendangba Chang, **Mehilo Apon**, C. Chelladurai, C. (2019) Application of electrical resistivity method for land instability study at the Nagaland Medical College (NMC) site, Kohima, Nagaland. *Advances in Environmental Research of Northeast India*, pp. 231-240. K. Khelchandra Singh (Ed).

2. **Presentation of paper**

   - "Application of UAV data for landslide studies in Pezielietsie colony, Kohima, Nagaland". Online International Conference on Earth & Environmental Sciences, Natural Resource Management & Climate Change with Special Focus on Eastern Himalayas. Department of Geology, Sikkim University (8th to 9th October 2020).

   - "Geological studies of the 2017-landslide in part of Peraciezie Colony, Kohima, Nagaland". National Conference on Emerging Trends in Environmental Research. Department of Environmental Science, Pachhunga University College, Aizawl, Mizoram (31st October to 2nd November 2019).

   - "Study of Nhachüko landslide, Kohima, Nagaland". 3rd National Geo-Research Scholars Meet. Wadia Institute of Himalayan Geology, Dehradun, Uttarakhand (6th to 8th June 2019).

3. **Workshops and Seminars/Webinars attended**

- "Global Seismology & Tectonics" - International Virtual Workshop organized by the Geoscience & Technology Division, CSIR-NEIST, Jorhat, Assam, India (20th to 30th September, 2022)

- 36th International Geological Congress (Virtual), Delhi, India (20th to 22nd March, 2022)

- "Local Groundwater Related Issues and Participatory Groundwater Management" online training course held at Department of Geology, Nagaland University, Kohima, Nagaland organized by Central Ground Water Board, North Eastern Region, Guwahati (28th February, 2022)

- "Basic Hydrological Applications (QGIS)" - Webinar training at The Geographical Information System Lab (TGIS) Online Platform, Ahmedabad, Gujarat (9th January, 2021)

- "Advanced R Programming" - Webinar training at The Geographical Information System Lab (TGIS) Online Platform, Ahmedabad, Gujarat (27th November, 2021)

- "Basic R Programming" - Webinar training at The Geographical Information System Lab (TGIS) Online Platform, Ahmedabad, Gujarat (20th November, 2021)

- "RS & GIS Applications in Natural Resource Management" online course conducted by Indian Institute of Remote Sensing, Dehradun (8th to 26th November, 2021)

- "Global Seismology & Tectonics" - International Virtual Workshop organized by the Geoscience & Technology Division, CSIR-NEIST, Jorhat, Assam, India (20th to 30th September, 2021)

- "Global Navigation Satellite System (GNSS)" online course conducted by Indian Institute of Remote Sensing, Dehradun (13th to 24th September, 2021)

- e-Training on "Transect Mapping in the Nagaland-Manipur Ophiolite Belt" conducted by RTD, NER, Shillong (5th October, 2020 to 09th October, 2020)

- "Indo-Canadian Workshop on Interactive Design in Geotechnical Engineering: Theory to Practice" organised by National Institute of Technology, Karnataka, Surathkal (India), Indian Geotechnical Society, Surathkal Chapter, Institute of Technology, Kanpur (India), TC 206 of ISSMGE (Interactive Geotechnical Design) and University of Ottawa (Canada) (24th September, 2020 – 2nd October, 2020).

- e-Training on "Engineering Geology and Landslide Studies" conducted by RTD, SR, GSITI, Hyderabad (21st September, 2020 to 26th September, 2020).

- "3 days Virtual National Seminar on Sedimentation, Tectonics and Metallogeny of North-East India" jointly organised by North-Eastern Hill University, Shillong and Geological Society of India, Bengaluru (21st September, 2020 to 23rd September, 2020).

- e-Training on "Basics of GIS and its Application" conducted by CGMT Division of GSI Training Institute, Hyderabad (17th September, 2020 to 19th September, 2020).

- "5 Days National Level Webinar on "Landslide & its Effects-A case study on Kodagu" from (8th September, 2020 to 12th September, 2020).

- e-Training on "Basic Training Course on Earthquake Geology, Active Fault Mapping and Seismo-tectonic Studies" conducted by RTD, CR, GSITI, Nagpur (17th to 21st August, 2020)

- Webinar on "Recent Earthquakes in Indo-Burmese Ranges" organized by Department of Geology, Pachhunga University College, Aizawl, Mizoram (6th to 7th August, 2020)

- National Workshop on "Recent Advances in Geosciences" conducted by Department of Geosciences Dr. B.R. Ambedkar University, Etcherla, Srikakulam (31st July, 2020)

- ESRI User Conference India 2020 (14th to 16th July, 2020)

- International Webinar on "Recent Advances In Geotechnical Engineering Research & Practice (RAGeo-RP)" organized by Department of Civil and Environmental Engineering, IIT Patna in association with Indian Geotechnical

Society (IGS) Bihar & Jharkhand Chapter; Nepal Geotechnical Society (NGS) and Centre for Earthquake Engineering Research (CEER), IIT Patna (01st to 10th July, 2020)

- 4th National Geo-Research Scholars Meet 2020 webinar organized by Wadia Institute of Himalayan Geology, Dehradun (23rd to 24th June, 2020)

- Certificate course on "Fundamentals of Photogrammetry and Cartography" online course conducted by Indian Institute of Remote Sensing, ISRO Dehradun (12th June to 12th July, 2020)

- 1st Indo-Japan webinar series on "Geotechnics for Disaster Mitigation" organized by Indian Geotechnical Society, Surathkal Chapter, India, National Institute of Technology Karnataka, Surathkal, India, Indian Institute of Technology Tirupati, India and Kyushu University, Japan (8th to 13th June, 2020)

- Short Term Course (online) on "Disaster Management and its Mitigation" organized by Department of Civil Engineering, Aligarh Muslim University, Aligarh, under TEQIP – III (20th to 21st May, 2020)

- International Training Course on "Landslide Risk Assessment and Mitigation (LARAM-India 2020)". Civil Engineering Department, IIT Roorkee. Organised by IIT Roorkee India, Indian Geotechnical Society (Roorkee Chapter), University of Salerno Italy and Norwegian University of Science and Technology, Norway (17th – 22nd February, 2020)

- National Workshop on Sequence Stratigraphy and Basin Analysis. Department of Geology, Nagaland University, Kohima Campus, Meriema (26th to 30th November, 2018)

4. **Consultancy**

- Site Investigation of Nagaland Medical College, Kohima (2019)

- Expert Committee - Recommendations for subsidence and landslide at old Kohima Municipal Council dumping site on NH-29 (2018)

CHAPTER 1

INTRODUCTION

The Indian subcontinent northeastern region includes Nagaland. The region represents a severely dissected mobile belt of the Burmese Orogen, which is the westernmost morphotectonic unit. Nagaland's geodynamically vulnerable area is undergoing severe and ongoing tectonic disturbances, which is causing large-scale folding and faulting of the rocks. It has resulted in considerable crumpling, jointing, shearing, and the crumbling of the rock masses. Various geomorphic processes have weathered and eroded the weaker rocks, causing large-scale slope instability.

Downward movement of earth material along slopes under the influence of gravity, triggered by incessant rainfall and seismic and anthropogenic activities is called landslide (Varnes, 1978; Crozier, 1986; Brunsden and Prior, 1987; Cruden, 1991; Dai and Lee, 2002; Luirei et al., 2023). Landslides are common geological disasters in mountainous terrain, which may or may not be caused by water (Singh et al., 2021; Zhang et al., 2023a, b). Slope morphology is important, as it controls slope stability conditions (Singh et al., 2021). Landslides have a significant relation with moderate (5º-15º) and relatively steep slopes (15º-30º) (Skilodimou et al., 2018). Landslide speeds range widely from very slow (a few mm/year) to extremely fast (over 5 m/s) of which very fast and extremely fast landslides have a probability of killing a large number of people (Turner, 2018). Damage to property, infrastructure, and even loss of lives are observed along its path (Bogoslovsky and Ogilvy, 2012; Froude and Petley, 2018; Velayudham et al., 2021). According to the database of the International Association of Engineering Geology (IAEG), landslides are responsible for around 14% of natural hazard injuries and deaths globally (Aleotti and Chowdhury, 1999). Landslides may be regional events, but even the largest and most spectacular landslides rarely lead to national disaster declarations (Turner, 2018).

Recent developments, such as mountain slope cutting for road widening, blasting, dam construction, and infrastructural development on moderate to steep slopes have caused major concerns (Sati et al., 2023). The sedimentary rocks of the region are extensively jointed, fractured, crushed, and worn, making them prone to landslides (Pandey et al., 2021; Singh et al., 2021). As highways are built along steep

slopes and highly sheared rocks, human activity has worsened slope stability (Luirei et al., 2023). Slope re-profiling, groundwater flow perturbations and rapid pore pressure changes, modification of surface water and overland flows, degradation of surface due to land use changes, and inappropriate constructions are some factors affecting slope stability due to anthropogenic stress (Jaboyedoff et al., 2016).

The orientation of joint sets is critical in determining the safety of a slope. When discontinuities, faults, and other weak zones form a continuous failure path and are oriented towards a slope, they may induce failure (Gokceoglu et al., 2000). Seismic disturbances are accountable for weakening slopes, lowering the factor of safety, and ultimately resulting in failure (Mebrahtu et al., 2022).

Rainfall-induced landslides are caused when water infiltrates the ground, creating a positive pore-fluid pressure, changing soil suction, and raising soil unit weight (Cignetti et al., 2019; Mebrahtu et al., 2022). Pore water is a key factor in understanding the processes from landslide initiation to sediment discharge influenced by rainfall-induced landslides (Yamaguchi et al., 2023). Landslides have a major impact on the hydrological response of local areas (Ran et al., 2015). The frequency and density of landslides increase as the amount of rainfall increases (Skilodimou et al., 2018). Evaluation of the volume of a potential landslide on a slope is vital for hazard mitigation (Sun et al., 2020). Rainfall of >700 mm is strongly related to landslide events (Skilodimou et al., 2018). During severe rainfall, the physical properties of slope materials are altered, and the pore pressure and weight of slope material greatly increase, while cohesion significantly decreases, making slopes unstable (Lehmann et al., 2013; Mebrahtu et al., 2022).

1.1   Area of study

The area of investigation is included in the Survey of India (SoI) topographic sheet no. 83K/2/NW and encompasses the northern and western regions of Kohima town. This area lies within 25°40'00" - 25°45'00" north latitudes and 94°02'30" - 94°07'30" east longitudes. Six areas of slope instability (Fig. 1.1) that occurred during the monsoon, have been taken up for this study.
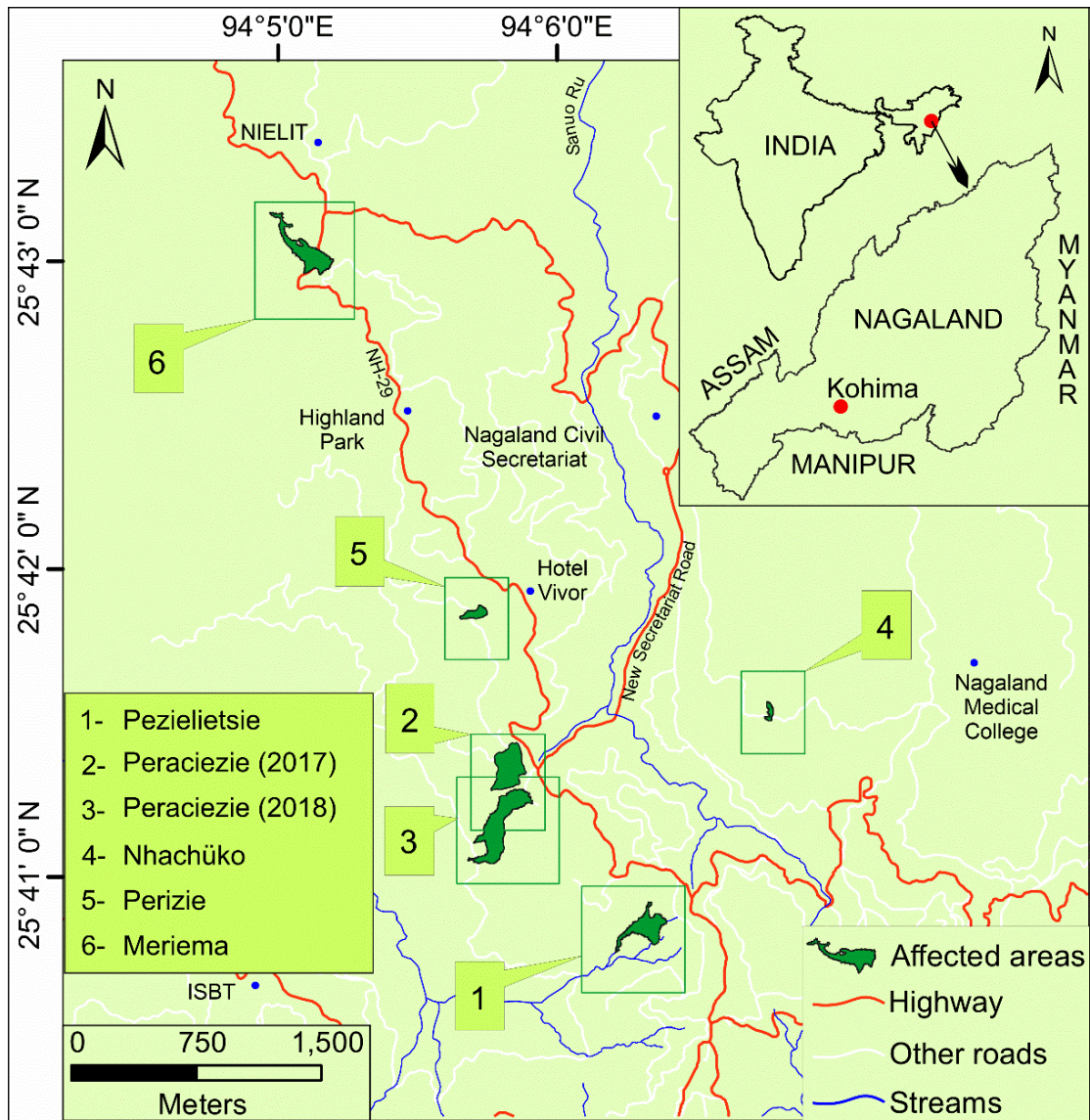
Fig. 1.1: Location map

1.1.1 Geomorphology

The geography of Kohima is characterised by severely dissected denudational hills, cliffs, narrow valleys, and deep gorges. Mount Japfü is situated in the southern region of Kohima and rises with an altitude of 3014 meters. The hill ranges trend roughly NE-SW and are roughly parallel to one another. The western section of Kohima district is made up of low to moderate hills comprising sandstone, siltstone, shale, and mudstone. The north-central portion of the district comprises steep, linear structural hills and narrow valleys made up of sedimentary rocks that are, to some extent, weathered and crushed. The south-central section of the district is made up of curvilinear and irregularly shaped, denuded structural hills with minor valleys formed

of hard, compact sandstone, siltstone, and shale. The average elevation of Kohima Town is 1444 meters above mean sea level.

1.1.2 Climate and rainfall

The annual rainfall of Kohima ranges between 1634 and 1817 mm, placing it in a fairly high rainfall zone (Kusre and Singh, 2012). The average annual rainy days reported is 116.2, with the highest duration during the monsoon (June to October) of 82.3 days (Dabral et al., 2019). The least annual rainfall in Kohima was 1075.6 mm in 1985, while the highest was 2616.1 mm in 1993 (Supongtemjen, 2012). The southwest monsoon contributes most rainfall to Kohima during August and September. The region experiences a temperate climate, with summer temperature around 28°C and winter lows of roughly 6°C.

1.1.3 Drainage

Discontinuities like joints and fractures, through which groundwater in the area discharges, control the drainage patterns of Kohima. They are asymmetrical, narrow, and deep. The study area is distinguished by parallel drainage patterns dominated by first- and second-order streams. These erosive streams discharge large volumes of water during the monsoon. Dzuyie Rü, Sanuo Rü, Chadoucha Rü, Hapuma Rü, Zed Rü, Pfuratsie Rü, and Dzüza Rü are some major streams flowing through Kohima.

1.2 Objectives

Several landslide episodes affects Kohima with the arrival of the monsoon, affecting the population and damaging infrastructure. This township is undergoing rapid urbanisation, so understanding the landslide scenario has become crucial. Therefore, the subsequent objectives have been engaged for this study:

a) To determine the geotechnical parameters of the rocks and soils
b) To identify the possible modes of slope failure
c) To suggest appropriate preventive and/or mitigation measures

1.3 Literature Review

Landslides are a familiar sight in hilly terrain. A slow or sudden movement of earth material transpires when a trigger of landslide initiates the movement under

gravitational effect (Cruden, 1991; Cruden and Varnes, 1996). The trigger can be anything from a vibration to incessant rainfall. Its effects extend from infrastructure damage to loss of lives globally (Assis et al., 2019; Garcia-Delgado et al., 2022; Montoya-Araque and Montoya-Noguera, 2023). Landslides are often impacted by slope, slope materials, rainfall, earthquakes, and land usage (Bradley et al., 2019; Trisnawati et al., 2022). Topographic elements, such as elevation, hypsometry, aspect, slope, geological setting (structural and stratigraphic features), and human-induced causes are all factors to be considered (Jaboyedoff et al., 2016; Froude and Petley, 2018; Zieher et al., 2023). Climate change is expected to have a detrimental effect on the severity and frequency of natural disasters such as landslides (Zieher et al., 2023). Long-term variations in air temperature and precipitation may impact the hydro-meteorology and trigger landslides in mountain environments (Stoffel and Huggel, 2012). Each year, thousands of people are killed and injured by landslides, which often cause large financial damages, both directly and indirectly, by destroying infrastructure, property, agricultural lands, highways, and other routes (Froude and Petley, 2018; Shabbir et al., 2023).

1.3.1 Classification of landslides

Several workers have proposed landslide classification schemes (Campbell, 1951; Zaruba and Mencl, 1969; Crozier, 1973; Coch, 1995; Smith, 2013). Recognising the type of landslide is essential in any scientific investigation because it provides an assortment of information about the type of movement, rate of material movement, etc. This simplifies the study of surface instability by condensing the numerous specifics of related events into a few easily recognised elements based on shared characteristics (Crozier, 1984; Msilimba, 2002).

The classification of Varnes (1978) of 29 landslide types has further been reclassified by Hungr et al. (2014) to 32. Table 1.1 illustrates the classification by Hungr et al. (2014), which is predicated on the modification of landslide-forming material and its congruity with conventional geotechnical and geological nomenclature for rocks and soils.

Table 1.1: Hungr et al. (2014) landslide classification system (After Varnes, 1978)

Type of movement	Rock	Soil
Fall	Rock fall	Boulder/debris/silt fall
Topple	Rock block topple	Gravel/sand/silt topple

	Rock flexural topple	
	Rock rotational slide	Clay/silt rotational slide
	Rock planar slide	Clay/silt planar slide
Slide	Rock wedge slide	Gravel/sand/debris slide
	Rock compound slide	Clay/silt compound slide
	Rock irregular slide	
Spread	Rock slope spread	Sand/silt liquefaction spread
		Sensitive clay spread
Flow	Rock avalanche	Sand/silt/debris dry flow
		Sand/silt/debris flow-slide
		Sensitive clay flow-slide
		Debris flow
		Mudflow
		Debris flood
		Debris avalanche
		Earthflow
		Peat flow
Slope deformation	Mountain slope deformation	Soil slope deformation
	Rock slope deformation	Soil creep
		Solifluction

1.3.1.1 Falls

A fall is a vertical movement that is rapid or very fast and can occur in rocks or debris. This variant of landslide has low moisture content (Summerfield, 2014). Falls are more common on steep slopes (Keller and Blodgett, 2007). Discontinuities are the main controlling factors. Seismic events, rain storms, rapid snow melt, freeze-thaw cycles of water in joints, root penetration and wedging, or stress relief after deglaciation can activate falls (Zellmer, 1987; Wieczorek et al., 1995, 2000; Vidrih et al., 2001; Dorren, 2003). Falls are generally observed on slopes with 70°-90° angles (Ritchie, 1963).

1.3.1.2 Topples

The rotation of a rock block along a fixed base is referred to as toppling. Toppling may involve one or more blocks. Toppling failure mechanisms were initially divided into three types: block, flexural, and block-flexural by Goodman and Bray (1976). Continuous columns of rock descending steeply towards the slope and breaking in flexure and bending forward are referred to as flexural toppling. Block-flexural toppling is a complicated process characterised by pseudo-continuous flexure along large blocks, separated by a number of cross joints (Alejano, 2021). The weight of rock masses and other discontinuity sets parallel to the slope direction are believed

to be the most essential elements impacting slope stability (Goodman and Kieffer, 2000).

1.3.1.3 Slides

A slide is a downslope movement of soil or rock mass caused by a surface break. Slides are either rotational or translational, and moisture levels may be low or moderate (Summerfield, 2014). Translational landslides are shallower and traverse significantly longer than rotational failures because the mass moves along a plane (Burns, 2013; Melo et al., 2022). Typically, during the slide event, their slide planes are activated. Rotational slides, on the other hand, have a curved surface of rupture and cause slumps due to backward slippage (Smith, 2013).

1.3.1.4 Flows

Flows are commonly observed on gentle slopes (Keller and Blodgett, 2007). Flow is a movement of unconsolidated materials that can be quick or sluggish, depending on the material and moisture (Summerfield, 2014). Debris flows are the most common type of flow. They are potentially damaging phenomena that occur in numerous mountain regions worldwide (Hungr et al., 2001; Ciccarese et al., 2020). In some instances, debris flows may be turbulent owing to high flow velocity, whereas in others, they are laminar as a result of high viscosity. Debris flows are extremely erratic, beginning on steep slopes and flowing down valleys to deposit at the mouths of debris-flow gullies (Wang et al., 2015).

1.3.2 Slope deformation

Slope deformation refers to the large-scale gravitational deformation of high, steep mountainous slopes. They are characterised by complex, sluggish, or incomprehensible rates of movements, and include ridges, benches, fractures, ditches, and bulges (Hungr et al., 2014). This complicated process precludes any credible forecast of future evolution. It is quite challenging to stabilise these massive soil/rock formations, and living in such unstable places is possible, albeit at a high cost in terms of building and infrastructure maintenance (Picarelli et al., 2022).

1.3.3 Previous studies in the region

Sondhi (1941), the first researcher on land instability, carried out landslide studies along the Dimapur-Manipur road section in Nagaland. Sharda and Bhambay (1980) created slope classification maps and gave a geotechnical report of Kohima

town. Lotha (1994) investigated several landslides of Kohima. Bhattacharjee et al. (1998) investigated some weak sections of NH 39. The Central Road Research Institute (CRRI, 2000a) expressed concern over some weak zones between Chumukedima and Maram. Aier (2005), Walling (2005), Sothu (2009), Supongtemjen (2012), and Khalo (2016) also conducted slope stability studies in and around Kohima town and the AH 1, as well as generated landslide hazard zonation maps and proposed corrective/mitigation measures. Jamir (2013) assessed slope stability and produced a map of landslide susceptibility for Mokokchung town. Slope instability of the Noklak Township was studied by Jamir et al. (2022). Kemas et al. (2004), Aier et al. (2005), Walling et al. (2005), Singh et al. (2008), Aier et al. (2009a), Aier et al. (2009b), Sothu et al. (2009), Aier et al. (2011), Jamir et al. (2011), Sothu et al. (2011), Aier et al. (2012), Supongtemjen and Thong (2014), Supongtemjen et al. (2015), Khalo et al. (2016), Walling et al. (2016), Kedovikho and Krishnaiah (2020) and Chang et al. (2021) contributed to landslide literature of the region by studying slope instability in and around Kohima. A map of landslide susceptibility of Kohima district was prepared by Yadav et al. (2023).

1.3.4 Geological parameters

1.3.4.1 Slope morphometry

Slope morphometric indices demonstrated by Mehrotra et al. (1994), can be utilised to decipher several classes of slope movement processes. Slope morphometry is an examination of angles of slope and the relative relief of an area. Landslides have occurred on slopes greater than 30° in 81% of cases. Debris flows can develop on slopes steeper than 30°. This is a lower limit that is slightly shallower than slopes that create debris slides (Terzaghi, 1950). Terrain roughness is measured by its relative relief.

Materials move downward and outward on unstable slopes. This is typically caused by high pore pressure and steep slope changes in the terrain (CRRI, 2000b), which is defined by the safety factor. The factor of safety of a slope is the ratio of the total resisting forces that work to prevent failure to the sum of driving forces that tend to cause failure (Piteau and Peckover, 1989). Natural slope failure destroys vegetation, exposing the soil surface to further erosion (Choubey and Lallenmawia, 1987). When natural slopes are transformed to cut slopes for the construction of highways, bridges, dams, and other engineered constructions, they get steeper (Das et

al., 2010; Vishal et al., 2010). When suitable scientific methodologies are not employed, such slopes become prone to failure.

1.3.4.2 Hydrogeology

The mobilised mass in a landslide typically impacts the uppermost, in-situ soil horizons of the weathering profile or hillside sedimentary deposits accumulated on pre-existing rock material (Sidle and Ochiai, 2006; Borrelli et al., 2018). During a rainstorm event, some of the water runs off the terrain surface, while the rest infiltrates into the soil, affecting pore pressures and thus, the effective stresses and shear strength. As a result, landslides can be triggered by either a drop in suction when unsaturated, or an increase in positive pore pressure due to rise in the water table (Sidle and Bogaard, 2016; Conte et al., 2022).

Slope, lithology, structure, weathering, soil composition, vegetation, and rainfall influence drainage. Because the groundwater table drops during the dry season, most places are dry. Certain regions however, are perpetually wet, indicating high water tables. High water tables imply a high absorption rate and very little drainage, resulting in water logging. During the monsoon, much of Kohima town receives high rainfall, which seep into the soils and raises the water table. Some landslides in Kohima are due to toe erosion by streams. However, the bulk of instabilities occur on free slopes, where stream influence is not the primary cause (Walling, 2005).

Groundwater movement through clay-bearing strata, such as shales, accelerates the weathering process by causing physical and chemical changes. Weathered shales with high total porosity, but low effective porosity and permeability, causes water to accumulate in the pores, resulting in the rise of hydrostatic pressure (Singh et al., 2016). Water in expansive clays, which have low permeability and are prone to weathering, reduces the shear strength (Ykhlef et al., 2023).

1.3.4.3 Structure and lineaments

Geological and structural contexts along slopes play a significant role in the mass wasting processes (Fookes et al., 1966; Varnes, 1978; Massonnet and Feigl, 1998). Favourable structures in slope deformation are distinguished by a certain arrangement of rock complexes, especially when they transpire along slopes or ridges

of local topography (Kandpal and Pant, 1995). Bedding planes, joints, and faults are the major geological discontinuities that affect slopes. Some authors consider these structural traits as key landslide-exacerbating variables (Agliardi et al., 2013; Galeandro et al., 2013; Doglioni and Simeone, 2014). High-hazard slopes have the same dip direction as geological features (Cerri et al., 2017). Groundwater presence is often noted along faulted and weathered, or crushed zones (Hasan et al., 2021).

Water intrusion along bedding planes and joints is usually responsible for rock failure; shale tends to swell when exposed to water, thereby putting pressure on clay-filled joints. Deep tectonic fractures beneath ground surface can cause substantial damage, including brittle and plastic deformation (Zischinsky, 1969; Ambrosi and Crosta, 2006; Willenberg et al., 2008; Jaboyedoff et al., 2011, 2013).

Numerous studies on the impact of faults on landslides have found a substantial association (Chen et al., 2014; Bucci et al., 2016; Penna et al., 2016; Tsai et al., 2018). Sen et al. (2015) discovered numerous types of movement along faults, including debris flows, earth falls, and rock slides. In a morphological reconstruction study, Chang et al. (2018) correlated landslide activity with active normal faulting in the Tatun Volcanic Complex in northern Taiwan. Based on morphotectonic characteristics, LiDAR-derived DEM, aerial images, and field measurements, Chen et al. (2019) successfully deciphered the influence of thrusting on deep-seated, slope gravitational deformation.

1.3.4.4 Lithology

The lithology may affect slope stability (Peruccacci et al., 2012; Henriques et al., 2015). Hill slopes are usually made up of several types of rocks and soils. These rocks may have diverse mineral assemblages with varying component strengths and mineral or rock grain linkages. The number of steep slopes and landslides, as well as the distribution of landslide magnitude, are influenced by lithology and rock strength (Roda-Boluda et al., 2018). Landslides are most likely to occur in fractured and worn rocks. Weathering also affects the shear strength of rocks significantly (Piteau and Peckover, 1989; Guo and Wang, 2017). When water is present, carbonaceous shale's strength significantly decreases, which promotes the formation of landslides (Su et al., 2021). The presence of discontinuities also influences the shear strength of a rock mass, as failure surfaces in rock masses tend to follow such pre-existing

discontinuities. When load is removed, clay minerals tend to absorb and adsorb water. Water travels between clay particles, increasing their volume and reducing the bonding forces between them. As a result, clay investigations are very important. Rocks with mineral components that can be transformed into clay minerals, will weather to generate masses with a clay mineral composition. The presence of clay minerals in rocks diminishes their strength (Trisnawati et al., 2022).

1.3.4.5 Rainfall

The complex interaction of soil, rock set-up, and rainwater is what propels a rainfall-induced landslide. Rainfall is the most common landslide-causing trigger throughout the world in numerous locations (Yu et al., 2021; Montoya-Araque and Montoya-Noguera, 2023; Oorthuis et al., 2023). Landslides are more likely to happen when the ground is wet and the water table is high. Landslides are commonly found in regions with high annual mean rainfall. High-intensity rainfall episodes normally generate translational landslides, whereas low-intensity and long-duration rainfall events frequently cause rotational, deep-seated landslides (Rahimi et al., 2011). Severe rainstorms, especially those that take place during the rainy season and those that follow extended wet spells, have been identified as the triggers for some of the most destructive landslides in this region (Thong et al., 2004; Aier, 2005). The preceding rainfall amount has a substantial impact on soil moisture content, which affects the overall stability of the landslide.

1.3.5   Geotechnical parameters

1.3.5.1 Moisture content

The moisture content (W_C) of a soil is defined as the weight of water (w_l) divided by the weight of solid soil (w_d) in a given amount of soil. It is expressed as:

$$W_C = \frac{w_l}{w_d}$$

The moisture content is usually stated as a percentage. When formulas are used to describe relationships between quantities, they can be expressed as fractions. Natural moisture content refers to the water content of a soil in its natural state. A knowledge of water content is necessary for soil compaction control, estimating soil consistency limitations, and calculating the stability of earthworks and foundations (Hazreek et al., 2018; Guo et al., 2023).

1.3.5.2 Atterberg limits

The Atterberg or Consistency limits are a fundamental gauge of the character of fine-grained soils. These limits may exist in the solid, semi-solid, plastic, or liquid stages, dependent upon the water content of soil. The consistency and behaviour of a soil varies by state, as does its engineering properties. As a result, the boundary between each condition can be determined based on a change in the conduct of the soil (Atterberg, 1911).

When remoulded, the cohesiveness shown by the particles in clayey soils tends to be disrupted due to variations in water content. As the amount of water of the soil is lowered from virtually a suspension, the soil goes through numerous phases of consistency. These consistency limits, which include the liquid, plastic, and shrinkage limits, have been arbitrarily identified as the water contents at which the soil moves from one of these stages to the next. The water content of fine-grained soil greatly influences its consistency. It aids in an understanding of soil-water behaviour and by extension, the engineering properties (Oluyemi-Ayibiowu and Akinleye, 2019; Wu et al., 2020).

Liquid limit

The liquid limit (W_L) of a soil is the water content that corresponds to the arbitrary limit between its liquid and plastic states of consistency. It is the moisture content at which clay transitions from liquid to plastic. It is defined as the least water content at which the soil remains liquid, yet has a low shear strength against flowing that may be tested using standard methods (Casagrande, 1932).

Plastic limit

The plastic limit (W_P) of a soil denotes the water content that corresponds to an arbitrary limit between the plastic and the semi-solid states of consistency of the environment. Plasticity is the property of soil that allows it to be rapidly flexed without rupture, elastic rebound, or volume change. It specifies the lowest water content at which soil may disintegrate when rolled into a thread. The plasticity is affected by mineral composition and particle size (Chen et al., 2023).

Shrinkage limit

The shrinkage limit (W_S) is the arbitrary water content at which soil tends to move from the plastic to the semi-solid state of consistency, that is, the lowest water

content between the semi-solid and solid states. It is defined as the maximum water content at which a drop in the amount of water does not lead to a decrease in soil mass volume. When the moisture content of a soil reaches its shrinkage limit, the soil begins to alter in volume, and the soil becomes semi-solid. It will eventually become semi-liquid after more soaking and lead to subsidence in the area. The shrinkage limit is useful for determining soil swelling and shrinking capacity. During alternating wet and dry seasons, most soils experience cyclical swelling and shrinkage. Subsidence occurs when soils shrink. When wet, expansive soils swell, fissures form, raising soil levels due to swelling, distortion, and fracture development. Such features are common during cyclic drying-wetting situations (Chang et al., 2021).

1.3.5.3 Shear strength parameters

The resistance of soil particles to deformation caused by continuous shear displacement under the action of shear stresses is defined as the soil shear strength (Punmia, 1994). To analyse soil stability problems such as bearing capacity, slope stability, and lateral pressure on earth-retaining structures, a thorough grasp of shearing resistance is required. Soil shear strengths can be determined in the laboratory using a variety of procedures, including the triaxial compression test and the direct shear test (Punmia, 1994).

Shear test types reliant on drainage conditions

Before deciding on a method, the probable conditions before and during the tests are to be examined, as these can have far-reaching impact on the outcomes. The shearing strength of cohesionless or coarse-grained soil can be measured in both dry and saturated conditions. Cohesive or fine-grained soil is typically evaluated while saturated. Shear tests on such saturated soils are classed as unconsolidated undrained, consolidated undrained, or drained, depending on whether drainage is permitted before and during the test (Huang et al., 2023).

Unconsolidated undrained test

Drainage is not permitted at any point of the test, either before or after the application of normal stress or during the application of shear stress. As a result, no time is available for pore-water pressure dissipation and subsequent soil consolidation; no major volume changes are envisaged. Undrained tests are frequently performed on low-permeability soils. This is the most adverse condition that could

arise in geotechnical engineering practice, and is thus replicated in shear testing. Testing is allowed for a very short period till failure (Huang et al., 2023).

Consolidated undrained test

During the application of the normal stress, full drainage is permitted, but no drainage is permitted during the application of shear stress. As a result, no volume changes occur during shearing, and excess pore pressure occurs (Pirzada et al., 2023).

Drained test

Drainage is fully permitted at every stage of this test. The soil is consolidated under the applied stress and is tested for shearing by applying shear stresses very slowly. Practically, no excess pore pressure develops at any stage while volume changes take place (Nguyên et al., 2019).

Direct shear test

A soil sample with a square or circular cross-section used in the direct shear test, is compressed in a shear box that is divided in two and allowed to fail along a predefined plane. A graph is created to represent the applied normal stress and the equivalent shear stress for at least three to four tests at various normal values of stress. This graph is used to calculate the cohesion (c) and internal friction angle (ϕ), and used to determine the shear strength of the soil (Yang et al., 2021; Subashchandrabose and Jeyapriya, 2023).

1.3.6 Rock mass rating and slope mass rating

Bieniawski (1973) established the rock mass rating (RMR) system as a geomechanical classification system for rocks. The RMR incorporates the most important geologic criteria of influence into a single overall comprehensive index of rock mass quality. The RMR system classifies a rock mass based on five factors:

a) Uniaxial compressive strength (UCS) of the rock

b) Rock quality designation (RQD)

c) Discontinuity spacing

d) Discontinuity condition

e) Groundwater condition

Rock strength can be evaluated in the field or in the laboratory using a Schmidt hammer or a Point Load Index Tester (PLIT) respectively. In the laboratory,

the rock sample is compressed between conical steel plates until failure occurs. The point load index can be measured using diametric axial blocks, or irregular lumps based on the size and shape of the test specimens. A multitude of factors influences the bearing strength of rocks, including rock type, weathering extent, mineralogical structure, rock composition, faults/fractures, rock deformation, water infiltration, etc. (Cai et al., 2020; Hasan et al., 2021).

The RQD was developed by Deere et al. (1966) for a quantitative evaluation of rock mass quality from drill core logs. RQD is a core recovery method that is based on the frequency of cracks and softening of rock mass encountered during drilling. If core drilling is not possible, RQD can be approximated using the empirical relationship of Palmström (1982), RQD = 115-3.3Jv, where Jv is the total volumetric joint count for all joint sets.

The structural discontinuities in rocks in which a slope is excavated have a considerable influence on the stability of the slope. A discontinuity is a planar surface that represents a shift in the physical or chemical properties of a soil or rock mass. Direction, persistence, roughness, and infilling are essential properties in jointed rock, slope stability investigations. The size of blocks that can slide from the face is defined by the persistence of discontinuities and their spacing (Mavrouli et al., 2015; Umili et al., 2020).

Groundwater condition is a key criterion for determining the stability of a slope. The presence of groundwater in the rock mass affects the stability of the slope by lowering the shear strength of the possible failure surface. Water pressure increases the forces tending to induce sliding in tension fractures or nearly vertical fissures, reducing stability. Changes in the water content of some rocks, notably shales, can induce faster weathering and a loss of strength. Groundwater is responsible for the influence of water pressure in underground excavations (Yang et al., 2019).

The roughness of a joint surface is a measure of the intrinsic unevenness and waviness of the surface of a discontinuity, relative to its mean plane. Surface roughness has a significant influence on shear behaviour of rock joints (Wang et al., 2023), that is, the joint roughness coefficient enhances shear strength (Gentier et al., 2000; Tang and Wong, 2016). The friction angle of a rough surface is composed of

two components, the friction of the rock material (ϕ) and the interlocking induced by surface irregularities.

The slope mass rating (SMR) is a quantitative measure used on rock masses to assess the stability of rock slopes. Romana (1985) significantly contributed by applying rock mass classification to the assessment of rock slope stability. SMR is derived empirically from RMR by adding adjustment parameters for discontinuous orientations.

1.3.7 Kinematic analyses

The study of a body's geometrically possible motion without accounting for the forces at play is known as kinematics. Kinematic analysis is concerned with movement direction. It is commonly used in slope stability studies to determine if blocks or masses of rock can move along geologic structures and slide out of the face of a slope (Nasution et al., 2021; Rahman et al., 2023).

Plane failure

Translational failure refers to failure along a plane. It happens when a mass of rock slides down a slope along a weak plane. The failure plane will be sub-parallel to the slope. A cell must have both strike and dip components for planar failure. For the strike component, the strike of the slope is compared to the strike of the bedding. If the strikes are within 20° of one another, the cell is considered strike-critical. The slope dip is compared to the apparent dip of the bedding to analyse the dip component. The cell is designated as dip-critical if the apparent dip is less than the slope dip. Where a cell is both strike-critical and dip-critical, it is an area of potential plane failure. A cell that is both strike- and dip-critical is an area of possible plane collapse (Kwan, 2004).

Wedge failure

A type of translational failure is wedge failure. When rock masses slide over two intersecting discontinuities, a wedge-shaped slope may collapse, generating a wedge-shaped block, that dip out of the cut slope at an oblique angle. Within the shaded area, there is a plunge of two crossing discontinuities that is more than the friction angle of the slope material but less than the dip angle of the slope face (Oktarianty 2019).

Toppling failure

Toppling is a type of failure in which a unit or units rotate forward about a horizontal axis under the influence of gravity and other factors. It occurs when rocks along a slope are affected by discontinuities that are closely spaced and steeply inclined, and dip into the slope (Zheng et al., 2021; Luo et al., 2023).

Identification of mode of failure

The type of slope materials involved in a slide is used to identify the likely mode of failure. There are two categories into which the geologic materials can be separated: in-situ rocks and overburden comprising soil and debris. In soil and debris, rotational failure is typical, whereas translational and toppling failure occur frequently in in-situ rocks (Zhang et al., 2020; Zheng et al., 2021).

1.3.8 Paleostress analyses

Paleostress analysis was taken up to determine the geological aspect of the landslide study. This includes slickensides of faulted surfaces. Slickensides carry distinct slip surfaces, which bear the record of geological deformations. They are formed from shallow to great depths (Doblas, 1998). Slickensides are attributed to shear fractures, many of which are known to generate earthquakes (Borradaile, 2015). Fault gouge on the surfaces form distinct linear structures due to the growth of mineral fibers called slickenlines. The identification of this structure aids in determining the slip direction of a fault (Hancock, 1985; Angelier, 1994). Fault surfaces may also contain different sets of slickensides embossed on the other. Continuous and slow creeping of the rocks on fractures can typically result in polishing of the mineralized surface.

A straight slickenline/slickenfibre may denote translational type of fault movement. A curved slickenline points to preservation of direction of propagation of earthquake rupture, which various authors have recently studied (Mandal and Chakraborty, 1989; Kearse et al., 2019; Kearse and Kaneko, 2020; Macklin et al., 2021; Aoki et al., 2023). Slickensides frequently form stair-steps, causing fractures on which they form to step down in a single direction, allowing the sense of shear to be determined. The significance of this fabric is that the minerals grow according to the slip vector, resulting in slickensides that are parallel to the highest shear stress and thus the paleoslip vector of the fault surface. Slickensides are thus extremely valuable,

particularly in paleostress studies (Brandes and Tanner, 2019). Paleostress inversion is the process of determining paleostress history using evidence discovered in rocks, based on the assumption that former tectonic stresses should have left traces in the rocks (Wallace, 1951; Doblas, 1998; Simón, 2019). Slickenside lineation helps calculate paleostress tensors (Diabat, 2009). An interpretation in terms of stress orientation is given by the tensors to kinematic study of brittle characteristics (Tranos et al., 2022). Paleostress tensor analysis allows for the determination of the stress history of a study area.

1.3.9 *Back analyses*

Back analysis estimates the shear strength of a slope, which can be used to verify the results derived from laboratory work. The back calculated values of shear strength usually tends to be better, though there are uncertainties in this analysis (Hussain et al., 2010). Deterministic and probabilistic methods are used to perform back analysis (Duncan et al., 2014). Identifying a specific set of parameters that may cause slope failure is carried out with the deterministic method. Probabilistic method is necessitated when back-analysing several sets of slope stability parameters with uncertainty (Zhang et al., 2010; Mandal et al., 2017). A wealth of information is provided by the probabilistic back analysis compared to that offered by deterministic back analysis, matching with that of real life data. This proves to be beneficial for engineering modelling of construction as well as slope stability analysis (Nassirzadeh et al., 2024). The Liquid Equilibrium Method (LEM) and Finite Element Method (FEM) are used for back analysing a slope condition. The LEM's primary goal is to reduce shear strength of the material with a safety factor to achieve equilibrium against shear stresses. Since FEM is a helpful technique for assessing slopes with complex layouts, it does not require assumptions about the shape or location of the failure surface. All types of failure conditions can be modelled using FEM (Mandal et al., 2017).

Factor of safety

The Factor of safety (FoS) describes the stability of a specific slope and is based on the notion of limited equilibrium, which is the condition in which forces seeking to induce sliding are exactly balanced by forces resisting sliding. As a result, the ratio of total force available to resist sliding to total force tending to induce sliding can be defined as FoS.

When a slope is on the point of failure, a condition of restricted equilibrium exists in which the resisting and pushing forces are equal, and it is assumed that FoS=1 in this condition. When the slope is stable, the resistive forces exceed the destabilising forces, resulting in FoS>1; slopes with FoS<1 are unstable. After obtaining the mode of failure and shear strength values, stability equations are worked out analytically by taking into account the resisting and mobilising forces along the discontinuities to determine the FoS of that specific slope. The FoS of a landslide is a more basic criterion to analyse the stability of a landslide than the shear strength (Bai et al., 2022).

1.3.10 Precipitation analyses

Climate change is most likely to have an impact on landslides by increasing precipitation intensity (Chiang and Chang, 2011; Handwerger et al., 2019). The spatial arrangement and amount of rainfall play a crucial role in connecting precipitation to landslides. Landslide risk is particularly affected by changes in precipitation in urban areas (Johnston et al., 2021). Changes in drainage conditions, through flow, infiltration rates, and/or the hydraulic conductivities of slope materials are some of the mechanisms through which the stability of a slope is affected by precipitation (Iverson, 2000; Crozier, 2010). Landslides may occur when a slope is subjected to light rain over an extended period (Lee et al., 2022).

Hilly regions have the disadvantage of poor spatial representation of precipitation patterns, which is generally due to the constrained positioning of rain gauges. Moreover, data obtained from rain gauges for precipitation time series is often incomplete and inconsistent (Yu et al., 2020; Wang et al., 2020). The problem of missing or partial records of rainfall or precipitation are addressed by remotely sensed rainfall data, which offer a reliable option. The high spatial resolution and the consistency of its time series, offers benefits of using this data (Hounguè et al., 2021). The Global Precipitation Measurement (GPM) is a collaborative mission between NASA and JAXA (Japan Aerospace Exploration Agency), aimed at offering precise precipitation data worldwide using satellite remote-sensing technology, with a focus on high spatiotemporal resolution (Kirschbaum et al., 2017; Pan et al., 2023). The basic aim of the GPM mission is to improve precipitation measurements through understanding the physics and space-time variability of precipitation across the Earth (Kidd et al., 2020). In contrast to the previous Tropical Rainfall Measuring Mission

(TRMM), the GPM focused on studying tropical and subtropical precipitation, has the capability to detect light rain (< 0.5 mm/hr) with a spatial resolution of 0.1°×0.1° (Huffman et al., 2019).

CHAPTER 2

GEOLOGICAL SETTING

The NW-SE crustal collision between the Indian Plate and the Burma microplate resulted in the litho-tectonic units and intricate geodynamics of Nagaland. These units, whose rocks are folded and commonly affected by reverse faults, are exposed as NE-SW-trending linear ranges with steep hills and narrow valleys. Tensile fractures and normal faults have formed parallel to the crustal compression direction. Nagaland is subdivided into three morphotectonic divisions. From east to west, they are the Naga Hills Ophiolite, Inner Fold Belt (IFB) comprising the Patkai Synclinorium in the north and Kohima Synclinorium in the south, and the Belt of Schuppen (Mathur and Evans, 1964). Kohima lies within the Kohima Synclinorium of the IFB of Nagaland. It comprises the folded and thrusted Disang and Barail groups of rocks (Table 2.1; Fig. 2.1) of Upper Cretaceous-Eocene and Oligocene ages respectively. The Disang are represented by thick layers of splintery shale with thin intercalations of siltstone/sandstone, whereas the Barail comprise thick layers of sandstone with thin intercalations of papery shale (Geological Survey of India, 2011).

Table 2.1: Lithostratigraphic succession of Kohima (After Mathur and Evans, 1964; DGM, 1978; Ghose et al., 2010)

Age	Group	Formation	Palaeogene Inner Fold Belt
Oligocene to Upper Eocene	Barail	Renji	Grey, fine to medium-grained, hard, medium-bedded iron-bearing sandstone with thin horizons of lenticular siltstone interbedded with grey shale
		Jenam	Alternating sandstone, siltstone, and grey to dark grey shale with some coal seams
		Laisong	Light grey, fine to medium grained, hard, and medium bedded sandstone, with occasional plant imprints and burrows, with intercalations of shale
Upper Cretaceous to Eocene	Disang	Upper	Grey, khaki grey, and black splintery shales with silty interbands, lensoidal sandstones, and rhythmites
		Lower	
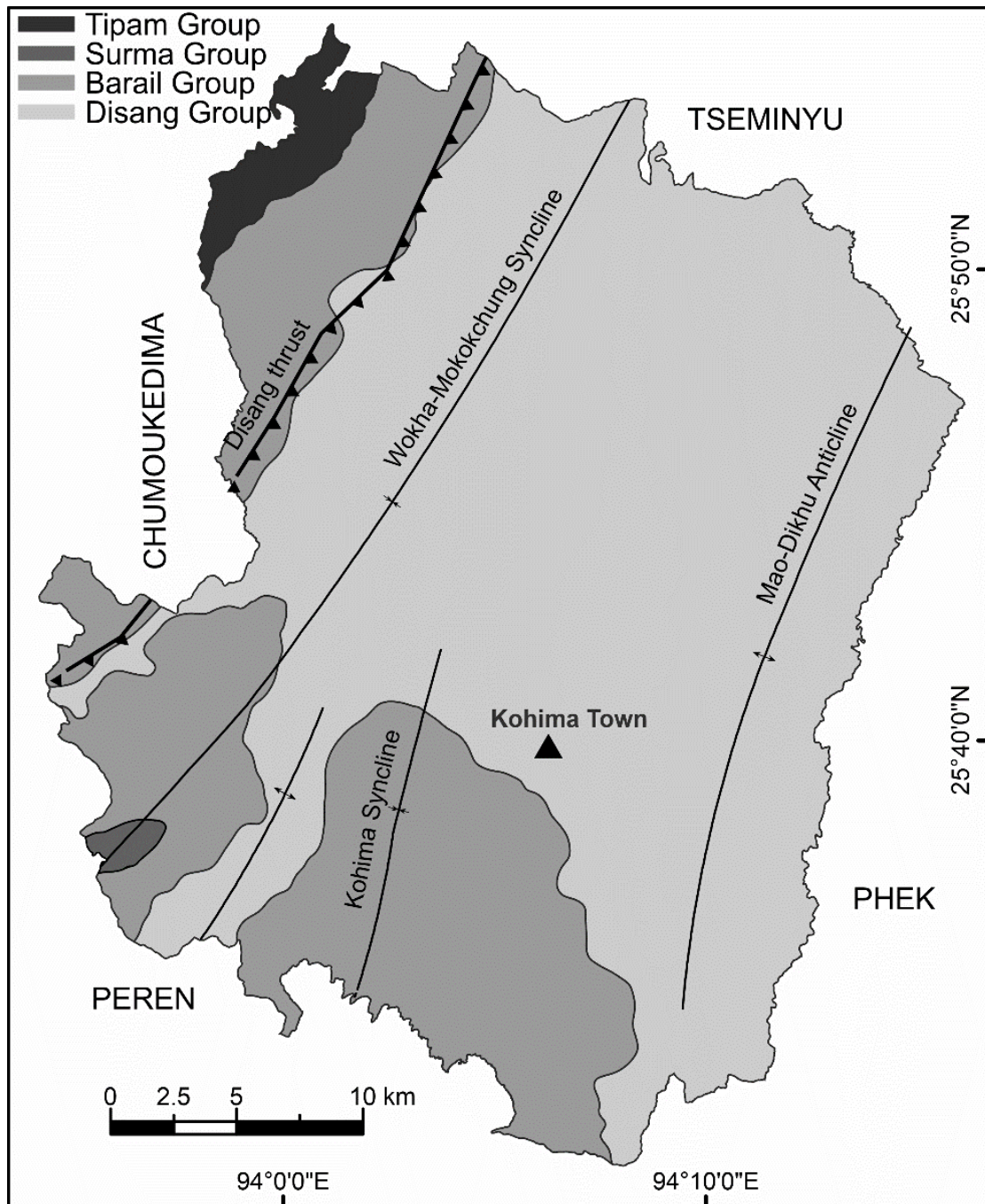
Fig. 2.1: Geological map of Kohima (After GSI, 2011)

The region has witnessed three deformational episodes (F1, F2, F3), of which evidence of F1 deformation, representing early Alpine-Himalayan events (Roy and Kacker, 1986) is lacking in Nagaland. Post-collisional features, F2 and F3, are clearly imprinted in the rocks of Nagaland. Thrusting in the region is due to F2 movements. The Pliocene-Quaternary movements, which have resulted in the formation of small folds and strike-slip faults, are thought to be due to F3 movements (Roy and Kacker,

1986). Numerous neotectonic traces found in the study area, such as extreme deformation of the rocks, are attributed to F3 movements.

2.1   Disang Group

Mallet (1876) named the monotonous splintery shale succession the Disang Group, after the Disang River, thereby providing the earliest geological information of the region. The splintery nature of the shale is attributed to the intersection of bedding and prominent fracture cleavage (Soibam, 1998). The Disang, the oldest of the Tertiary sequence of Nagaland, consists of flysch sediments (Directorate of Geology & Mining, 1978). It is made up of khaki grey to black shales with sandy and silty interbands, as well as thin, hard, intercalated siltstones. Argillaceous sediments are dominant in the Lower Disang Formation, while the Upper Disang Formation is more arenaceous (Sinha et al., 1982). The thickness of the arenaceous sediments increases, and grades upward into the Barail Group. The Disang shales tend to be spheroidally weathered and form concretions, while shale pellets are formed parallel to the bedding (Devdas and Gandhi, 1985; Sarma, 1985).

2.2   Barail Group

The Disang is conformably overlain by the Barail Group of rocks, which are of Upper Eocene - Oligocene age. The Barail derives its name from the Barail Range in the North Cachar Hills of Assam. Thick sequences of sandstone with thin intercalations of shales are observed in this group of rocks. The Laisong, Jenam, and Renji formations, in decreasing order of age, are part of the Barail Group.

2.2.1   *Laisong Formation*

The Laisong Formation exposed in the western part of Kohima, is characterised by very hard, grey, thin-bedded sandstones alternating with hard, sandy shale.

2.2.2   *Jenam Formation*

The Jenam is mostly composed of thick sandstone beds with intercalations of sandy shale and calcareous and iron-stained shale.

2.2.3   *Renji Formation*

The Renji sandstones, extending beyond the south and southwest borders of Nagaland into Manipur and Assam, are thickly layered, hard, ferruginous, and intercalated with some shale. The main structural setup of this belt reveals NNE-SSW

trending folds that are normally open towards the west, but become closely compacted near the eastern edge of the ophiolites.

CHAPTER 3

METHODOLOGY

Topographic maps of the Survey of India (SoI) and remotely sensed data are used to extract thematic and metric information for use in Geographical Information Systems (GIS). The Pezielietsie, Peraciezie, Perizie, Nhachüko, and Meriema areas were georeferenced using the SoI topographic map No. 83 K/2/NW at a scale of 1:5,000 (1970-71 survey). Input data was manually digitised and maps created using ArcGIS 10.7 software. Besides satellite imagery, UAV (Unmanned Aerial Vehicle) mapping was carried out in all the slide-affected areas using a drone (DJI Phantom 4 Pro+). Employing the structure-from-motion (SfM) technique, the Agisoft Metashape program was used to create a point cloud having a 3D coordinate system that was generated photogrammetrically. Google Earth (GE) imagery was used to translate the structures in the study area onto the contour map. Satellite-based rainfall data from the international Global Precipitation Measurement (GPM) mission was used to assess landslides in the area of interest after Kirschbaum and Stanley (2018).

3.1 Geotechnical parameters of soil

Soil samples were randomly collected from various sites of the study area. A trowel was used to remove about 10 kg of sample from pits excavated to depths devoid of organic materials. Small amounts of samples were collected in containers and weighed in the field using a portable weighing apparatus. These were then analysed in the laboratory to assess the moisture content of the soils.

3.1.1 Sample preparation

The samples were prepared in compliance with American standards (ASTM D421-85, 2007). Depending on the quantity of moisture in the soils, the samples were spread out and left to dry for a number of days. The dried soil samples were triturated, and fractions passing through ASTM sieve no. 40 (425 µm) were used to calculate the Atterberg limits, while those that passed through ASTM sieve no. 10 (2 mm) were utilised for direct shear tests. Distilled water was employed as the mixing ingredient to eliminate the risk of reactivity with minerals in the soil and reduce the risk of accuracy. The soil in the mixed state was left for at least 24 hours to achieve uniform moisture distribution for consistency limit testing.

The moisture content of the soils was evaluated using the oven-dried method. The containers with soil samples were initially weighed. The samples were then kept heated at 104°C in a thermostatically controlled oven for 24 hours. The moisture content was calculated by weighing the sample again after drying and calculating the difference.

3.1.2   Atterberg limits

3.1.2.1 Liquid limit

Cone penetrometer method

A cylindrical cup was filled with around 150 grams of thoroughly combined moist soil paste and levelled to the trough. It was then placed on the base of the cone penetrometer. The cone point was adjusted such that it just touched the surface of the soil paste in the cup. The vertical rod was let go, allowing the cone to sink into the soil paste on its own weight for 5 seconds. Approximately 20 grams of the cone penetration area were extracted to determine the moisture content relative to the weight after being dried in an oven. The test was repeated until a penetration range of 14 to 28 mm was obtained. This test was performed for up to four readings. A graph depicting the water content and cone penetration was prepared. The straight line that fit the best was then sketched. The moisture level that corresponded to a 20 mm cone penetration was selected as the liquid limit of the soil.

3.1.2.2 Plastic limit

The rolling thread method (BIS, 1985) was used to assess the plastic limit. On a glass plate, eight (8) grams of earth were compressed into a ball and hand-rolled into a thread with a consistent diameter of 3 millimeter. The procedure was repeated until the thread crumbled at a diameter of 3 mm. The disintegrated soil thread was collected in a container, and moisture content evaluated. This test was repeated to obtain at least three sets of data, and the average was used to determine the plastic limit of the soil, which is given as a percentage.

3.1.2.3 Index properties

Plasticity index

The plastic range is the extent of consistency at which soil shows plastic qualities. The values of plasticity index (I_P) vary from non-plastic to excessively plastic (Table 3.1). The larger the disparity between liquid and plastic limits, the more plastic

the soil is. A cohesionless soil has a plasticity index of zero. The soil's plasticity index is determined by calculating the numerical gap between the liquid limit (W_L) and plastic limit (W_P):

$$I_P = W_L - W_P \qquad (3.1)$$

In sandy soils, it is important to establish the plastic limit initially. If the plastic limit cannot be identified, the soil is considered non-plastic. When the plastic limit equals or surpasses the liquid limit, the plasticity index becomes zero.

Table 3.1: Soil classification according to Plasticity Index (Anon, 1979)

Plasticity Index (%)	Description
< 1	Non-plastic
1 - 7	Slightly plastic
7 - 17	Moderately plastic
17 - 35	Highly plastic
> 35	Extremely plastic

Liquidity index

The ratio of natural water content of soil to its plastic limit (W_P) divided by its plasticity index is known as the liquidity index; it is also called the water plasticity ratio. W_C denotes the water content.

$$I_L = \frac{W_C - W_P}{I_P} \qquad (3.2)$$

Consistency index

The consistency index (I_C) is computed by dividing the liquid limit of the soil minus the natural moisture content by the plasticity index:

$$I_C = \frac{W_L - W_C}{I_P} \qquad (3.3)$$

The consistency index is used to investigate the field behaviour of saturated fine-grained soils. Thus, if the consistency index of a soil equals unity, it is at the plastic limit. Additionally, a soil at its liquid limit has an I_C of 0 (Table 3.2). If I_C is greater than one, the soil is semisolid and stiff. When the soil has a negative consistency index, it contains more water than its liquid limit and acts more like a liquid. There is a conflict between the consistency and liquidity indexes. They represent the condition of the soil in the field. As the consistency index increases, the shear strength also increases.

Table 3.2: I_L and I_C values based on soil consistency (Atterberg, 1911)

Consistency	Liquidity Index	Consistency Index
Semisolid or solid-state	Negative	>1
Very stiff (moisture content = plastic limit)	0	1
Very soft (moisture content = liquid limit)	1	0
Liquid state (when disturbed)	>1	Negative

3.1.2.4 Plasticity chart

The plasticity chart can categorise fine-grained organic soils based on liquid limit and plasticity index qualities. Using the plasticity chart, several parameters of clays and silts are correlated, such as their dry strength, compressibility, and consistency at the plastic limit, with the Atterberg limits (Casagrande, 1932).

The Indian Bureau of Standards (BIS, 1970) has adopted the Unified Soil Classification System (USCS) as their code of practice for soil classification and identification, with some modifications to the plasticity chart. By drawing vertical lines at liquid limits $W_L=35\%$ and $W_L=50\%$, the graph is separated into six areas (Fig. 3.1). The A-line separates clays with low ($W_L=35\%$), medium ($35\% <W_L<50\%$), and high plasticity ($W_L>50\%$) from inorganic silts or organic clays. The ordinate represents the plasticity index, while the abscissa represents the liquid limit. CL-ML soils have a plasticity index ranging from 4 to 7. The following group symbols are used in the general classification (Murthy, 2003):

CL, CI, CH - Inorganic clays of low, medium, and high plasticity respectively

ML - Low plasticity of Inorganic silt

OL - Low plasticity of Organic silts or organic silt-clays

OI - Organic clays of medium plasticity

MI - Inorganic silts or silty sands of medium plasticity

MH - Inorganic silts of high compressibility

OH - Organic clays of high compressibility or plasticity

The soils of a given group may contain blends of one or more components of other soils, including fine sand.
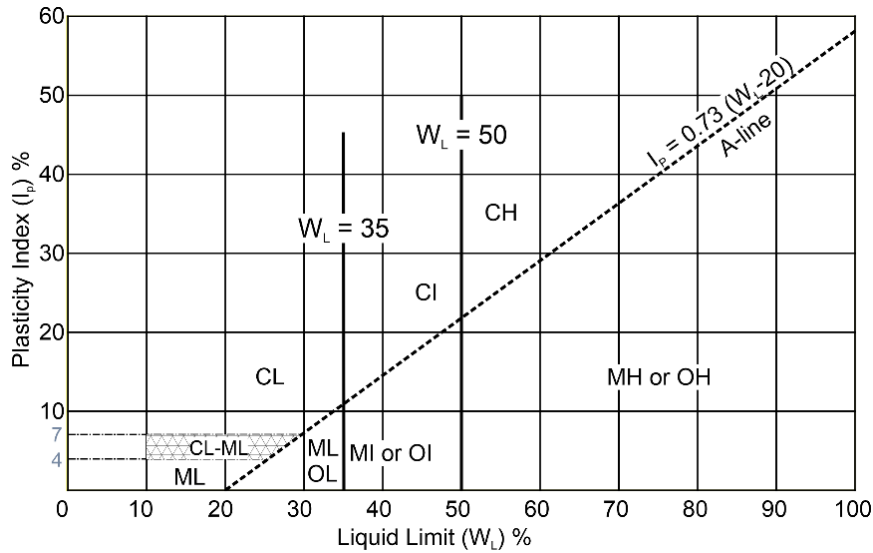
Fig. 3.1: Plasticity chart according to BIS, 1970

3.1.2.5 Shrinkage limit

A sufficient amount of distilled water was added to 30 g of soil in an evaporating dish to fill in any soil gaps and make the soil pasty enough to be readily put into the shrinkage dish without trapping air bubbles. The volume of the shrinkage dish (V), which is also the volume of the wet soil pat, was calculated, by filling the shrinkage dish with mercury and weighing the mercury in the shrinkage dish using a measuring cylinder. The entire soil paste was put into the dish and weighed (W). The dish was then dried at 105°C and cooled, after which the weight of the dry soil mass (Wo) was determined. The dried soil pat was placed in a glass cup containing mercury. The soil pat was pressed into the glass cup with the help of a glass plate. The displaced mercury was collected, and its volume (Vo) calculated and shrinkage limit (IS: 2720-6, 1972) determined. It is computed using the following equation:

$$W_S = \left\{ \left(\frac{W - W_o}{W_o} \right) - \left(\frac{V - V_o}{W_o} \right) \right\} X 100 \qquad (3.4)$$

Here, W_S - shrinkage limit (%)

W - weight of the wet soil (g)

W_o - weight of dried soil (g)

V - wet soil volume (ml)

V_o - dry soil volume (ml)

3.1.2.6 Shear strength of soils

The cohesion (c) and internal friction angle (ϕ) of the remoulded soil samples of the study area were evaluated by direct shear testing, using the consolidated drained test method. It was carried out following standard procedures (BIS, 1986). About 200 g of soil sample was thoroughly mixed in 20 cc distilled water, compacted, and placed in a shear box. The box was placed in a water jacket and positioned on the shearing machine to cause failure along a predetermined horizontal plane between the two sides of the shear box. The loading frame was used to apply the desired normal load in the range of 0.1 to 0.5 kg/cm^2. Readings of shear displacement were obtained at one-minute intervals till failure. The sample was then extracted and moisture content calculated. Shearing was permitted at a low continuous strain rate (0.05 mm/minute) to allow for complete drainage throughout shearing. The test was performed with three similar specimens under increased normal loads. Using the normal and peak shear stresses, the cohesion, internal friction angle, and unconfined compressive strength (σ_{ci}) were derived from RocData software (Rocscience Inc., 2005).

3.2   Rock mass rating and slope mass rating

Determining the lithology, structure, and groundwater conditions required extensive fieldwork. For point load tests, about 20-25 rock samples were acquired from each rock exposure. Their averages were used to calculate the strength. A Brunton compass was used to measure the orientations of the exposed litho-units and structural features. To help comprehend how the slope failed in this area, a number of joint trends were obtained to assess the rock and slope mass rating. Spacings between discontinuities were measured. Visual observations were made to estimate groundwater conditions, and ratings assigned accordingly. Bieniawski (1989) classified groundwater conditions as fully dry, damp, wet, pouring, or gushing. Joint roughness, classified as very rough, rough, somewhat rough, smooth, polished, and slickensided surfaces, was determined by touching joint surfaces with the finger. In total, eight rock slopes were chosen for study, based on availability of abundant structural data in in-situ rocks.

After loading the specimens into the testing apparatus, the platens were closed to make contact with the smallest dimensions of the block or lump—avoid the edges and corners. The distance 'D' between platen contact sites was measured within 2% accuracy. Within a range of ±5%, the smallest specimen width (W) perpendicular to the loading direction was recorded. When the sides are not parallel, W is determined from

W_1, W_2, and W_3, as shown in equation 3.5. The specimen was then loaded to allow failure to occur within 10-60 seconds, and the failure at load 'P' was recorded. If the fracture surface passes through only one loading point, the test should be dismissed as invalid.

$$W = \frac{W_1 + W_2 + W_3}{3} \tag{3.5}$$

3.2.1 Calculation

Uncorrected point load strength (IS) is calculated as P/De^2 where De, the "equivalent core diameter", is given by:

$$D_e^2 = \frac{4A}{\pi} \tag{3.6}$$

Here, A - the smallest cross-sectional area of a plane passing through the platen contact points and π - 3.14.

3.2.2 Size correction

Since IS fluctuates with 'D' in the core diametral test and with 'De' in irregular lump testing, size correction is required in order to use the chart to get a unique point load strength value for the rock sample (Fig. 3.2). A rock specimen or sample's size-corrected Point Load Strength Index, or IS (50), is equal to the value of IS that would have been obtained from a diametral test with D = 50 mm. According to the Rock Mass Rating method (Bieniawski, 1989), if the point load index (PLI) is less than 1 MPa, UCS is preferred over index strength. The corresponding equation for UCS and PLI is:

$$\sigma ci = K \ (PLI) \tag{3.7}$$

Here, K denotes the conversion factor and PLI denotes the point load index.
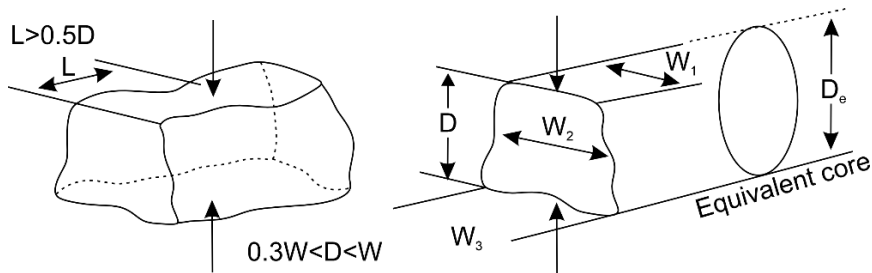
Fig. 3.2: Requirement of specimen shape for irregular lump test

Following Singh et al. (2012), a conversion factor of 14.4 was chosen for shale and 21.9 for sandstone. The discontinuity conditions and their respective ratings (Table 3.3) were used to calculate the RMR values of the rock mass in the study area. Rating

values are assigned to each parameter based on the chart of Bieniawski (1989). RMR values were calculated by adding the ratings. The final RMR value is divided into five categories (Table 3.3). A higher rating for a rock mass indicates better rock mass conditions.

Using the following equation, the SMR was calculated by adding a factorial correction factor based on the joint-slope connection and a factor related to the excavation method to the RMR (Table 3.4):

$$SMR = RMR+(F1{\times}F2{\times}F3)+F4 \qquad\qquad (3.8)$$

a) F1 depends on parallelism between the dip of the slope, α_s and the dip direction of the discontinuity α_j.

b) In the case of planar failure, F2 depends on the dip of the discontinuity β_j, while in toppling failure this parameter is set as 1.

c) F3 indicates the connection between the slope face (β_s) and the joint dip (β_j).

d) F4 denotes the slope excavation method, which ranges from +15 (natural slope) to -8 (slope not suitable for blasting), as shown in Table 3.4.

Table 3.3: Rock mass rating parameters and its ratings (Bieniawski, 1989)

1	**Strength of intact rock material** (MPa)	Point load strength	>10	4-10	2-4	1-2			
		UCS	>250	100-250	50-100	25-50	5-25	1-5	<1
	Rating		15	12	7	4	2	1	0
2	**RQD (%)**		90-100	75-90	50-75	25-50	<25		
	Rating		20	17	13	8	3		
3	**Spacing of discontinuity (m)**		>2	0.6-2	0.2-0.6	0.06-0.2	<0.06		
	Rating		20	15	10	8	5		
4	**Condition of discontinuity**		Very rough, discontinuous, no separation, unweathered	Rough walls, separation <0.1 mm, slightly weathered	Slightly rough, separation <1 mm highly weathered	Slickensides or gouge, <5 mm thick or separation 1-5 mm, continuous	Soft gouge, >5 mm thick or separation >5 mm decomposed rock wall		
	Rating		30	25	20	10	0		
5	**Groundwater conditions**		Completely dry	Damp	Wet	Dripping	Flowing		
	Rating		15	10	7	4	0		
	RMR		>80	61-80	41-60	21-40	<20		
	Class no.		I	II	III	IV	V		
	Classification of rock mass		Very good	Good	Fair	Poor	Very poor		

Table 3.4 shows values of the adjustment factors F1, F2, F3, and F4 for the various joint orientations. The SMR classes (Table 3.5) were calculated using the RMR and adjustment factor values from equation 3.8. SMR values vary from 0 to 100, based on which stability classes are assigned.

Table 3.4: Values of adjustment factors (after Romana, 1985)

Adjustment factors	Case of slope failure		Very favorable	Favorable	Fair	Unfavourable	Very unfavourable
F1	Planar (P)	$\alpha j - \alpha s$					
	Toppling (T)	$\alpha j - \alpha s - 180$	>30°	30°-20°	20°-10°	10°-5°	<5°
	Wedge (W)	$\alpha j - \alpha s$					
	P/W/T	Rating	0.15	0.40	0.70	0.85	1.00
F2	P	βj					
	W	βi	<20°	20°-30°	30°-35°	35°-45°	>45°
	P/W	Rating	0.15	0.40	0.70	0.85	1.00
	T	Rating	1	1	1	1	1
F3	P	$\beta j - \beta s$					
	W	$\beta j - \beta s$	>10°	10°-0°	0°	0°-(-10°)	<-10°
	T	$\beta j + \beta s$	<110°	110°-120°	>120°	-	-
	P/W/T	Rating	0	-6	-25	-50	-60
F4	Natural slope	Pre-splitting	Smooth blasting		Normal blasting		Poor blasting
	15	10	8		0		-8

Table 3.5: Stability classes as per SMR values (after Romana, 1985)

Class No.	V	IV	III	II	I
SMR value	0-20	21-40	41-60	61-80	81-100
Rock mass description	Very poor	Poor	Normal	Good	Very good
Stability	Very unstable	Unstable	Partially stable	Stable	Fully stable
Failure	Large planar or soil-like	Planar or big wedge	Planar along some joints, many wedges	Some block failure	No failure

3.3 Kinematic analyses

Angular correlations between discontinuities and slope surfaces are used to predict possible modes of failure, following Kliche (1999). To establish the main joint sets that influence instability, the joint trends were plotted in Rocscience software (Dips version 8.0) to generate pole density and contour diagrams. These were utilised to create stereographic projections to determine the type of failure mode. Joint projection data

were used for kinematic studies with the Markland Test (Markland, 1972), which was updated by Hocking (1976), Cruden (1978), and Hoek and Bray (1981). Rose diagrams were created to better understand the orientation of lineaments in relation to the regional trend.

RocData software (Rocscience Inc., 2005) was used to calculate friction angles. Uniaxial compressive strength (UCS) based on field estimation (Table 3.6), geological strength index (GSI) (Fig. 3.3), and material constant of the rock (Mi) determined from a qualitative description of the rock material specified in Table 3.7 are among the input parameters. Disturbance factor (Df), rock unit weight, and slope heights were assessed in the field. Df is determined by the degree of disturbance experienced by the rock mass, such as blast damage and/or stress relaxation. It ranges from 0 for undisturbed, in-situ rock masses to 1 for highly disturbed rock masses. As there is no blasting in the area, Df = 0. Based on these parameters, the friction angles were computed automatically.

Table 3.6: Field estimates of UCS of intact rock (Hoek and Brown, 1997)

Field estimate of strength	UCS (MPa)	Examples
Specimen can only be chipped with a geological hammer	>250	Fresh basalt, chert, diabase, gneiss, granite, quartzite
Specimen requires many blows of a geological hammer to fracture	100-250	Amphibolite, sandstone, basalt, gabbro, gneiss, granodiorite, limestone, marble, rhyolite, tuff
Specimen requires more than one blow of a geological hammer to fracture	50-100	Limestone, marble, phyllite, sandstone, schist, shale
Cannot be scraped or peeled with a pocket knife; specimen can be fractured with a single blow from a geological hammer	25-50	Claystone, coal, concrete, schist, shale, siltstone
Can be peeled with a pocket knife with difficulty; shallow indentation made by firm blow with point of geological hammer	5-25	Chalk, rocksalt, potash
Crumbles under firm blows with point of geological hammer; can be peeled by a pocket knife	1-5	Highly weathered or altered rock
Indented by thumbnail	0.25-1	Stiff fault gouge
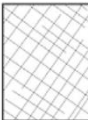
GEOLOGICAL STRENGTH INDEX FOR JOINTED ROCKS (Hoek and Marinos, 2000)

From the lithology, structure and surface conditions of the discontinuities, estimate the average value of GSI. Do not try to be too precise. Quoting a range from 33 to 37 is more realistic than stating that GSI = 35. Note that the table does not apply to structurally controlled failures. Where weak planar structural planes are present in an unfavourable orientation with respect to the excavation face, these will dominate the rock mass behaviour. The shear strength of surfaces in rocks that are prone to deterioration as a result of changes in moisture content will be reduced if water is present. When working with rocks in the fair to very poor categories, a shift to the right may be made for wet conditions. Water pressure is dealt with by effective stress analysis.

SURFACE CONDITIONS

STRUCTURE

DECREASING SURFACE QUALITY ⟹

VERY GOOD
Very rough, fresh unweathered surfaces

GOOD
Rough, slightly weathered, iron stained surfaces

FAIR
Smooth, moderately weathered and altered surfaces

POOR
Slickensided, highly weathered surfaces with compact coatings or fillings or angular fragments

VERY POOR
Slickensided, highly weathered surfaces with soft clay coatings or fillings

DECREASING INTERLOCKING OF ROCK PIECES

INTACT OR MASSIVE - intact rock specimens or massive in situ rock with few widely spaced discontinuities
90 80 — N/A N/A

BLOCKY - well interlocked un-disturbed rock mass consisting of cubical blocks formed by three intersecting discontinuity sets
70

VERY BLOCKY- interlocked, partially disturbed mass with multi-faceted angular blocks formed by 4 or more joint sets
60 50

BLOCKY/DISTURBED/SEAMY - folded with angular blocks formed by many intersecting discontinuity sets. Persistence of bedding planes or schistosity
40 30

DISINTEGRATED - poorly inter-locked, heavily broken rock mass with mixture of angular and rounded rock pieces
20

LAMINATED/SHEARED - Lack of blockiness due to close spacing of weak schistosity or shear planes
N/A N/A 10

Fig. 3.3: Basic GSI chart from geological observations (Hoek and Marinos, 2000)

Table 3.7: Constant Mi values for intact sedimentary rock group (Hoek and Brown, 1997)

Class	Group	Texture			
		Coarse	Medium	Fine	Very fine
Clastic		Conglomerates 21±3	Sandstones 17±4	Siltstones 7±2	Claystones 4±2
		Breccias 19±5		Greywackes 18±3	Shales 6±2
					Marls 7±2
Non-Clastic	Carbonates	Crystalline limestone 12±3	Spariritic limestones 10±2	Micritic limestones 9±2	Dolomites 9±3
	Evaporates		Gypsum 8±2	Anhydrite 12±2	
	Organic				Chalk 7±2

3.4   Structural analyses

Lineaments are rectilinear or curvilinear surficial expressions induced by stresses in the subsurface bedrock. These are identified as continuous or discontinuous features in high-quality satellite imagery or aerial photos. Lineaments of the study area were mapped using Linear Imaging Self Scanner (LISS-4) and Google Earth satellite imagery (Table 3.8). Some of the faults plotted, were confirmed in the field using tectonic features such as slickensides retained in the rocks of the study area. Slickenside is a form of non-penetrative lineation that is used to determine the direction of slide along a fault (Ramsay, 1967; Hancock and Barka, 1987; Petit, 1987; Doblas, 1998; Mukhopadhayay et al., 2019). Faulted features were also checked and quantified in the field with a handheld Global Positioning System (GPS).

Table 3.8: Satellite imageries used in the study

Satellite data / Source	Date acquired	Spatial resolution (m)
LISS-4 (ISRO)	7th January 2019	5.8
Google Earth imagery	March 2022	0.15-15

3.5   Paleostress analyses

Slickenside data (i.e., rake) and fault plane data (dip & dip direction) were recorded for paleostress analyses to deduce the stress tensor of an area. WinTensor program was used to perform the analysis of the paleorecords of stresses (Delvaux,

1993; Delvaux and Sperner, 2003). The Right Dihedron method and the Rotational Optimisation method of the program was used to infer the results.

Based on the vertical stress axes, the stress regime is established, which are extensional (σ1 is vertical), strike slip (σ2 is vertical), and compressional (σ3 is vertical). The stress regimes within these three kinds vary based on the stress ratio (R) - radial extension (σ1 vertical, 0<R<0.25), pure extension (σ1 vertical, 0.25<R<0.75), transtension (σ2 vertical, 0.75<R<1 or 1>R>0.75), and pure strike-slip. Based on the stress regimes, Guiraud et al. (1989) suggest that the stress tensors are represented with the orientation of the horizontal principal stress (S_{Hmax}) as well as the horizontal minimum stress stress axes (S_{hmin}) (Fig. 3.4).

Delvaux et al. (1997) and Delvaux and Sperner (2003) identified compression of three types: pure compression (σ3 vertical, 0.25<R<0.75), pure strike slip (σ2 vertical, 0.75>R>0.25), Pure extension (σ1 vertical, 0.25<R<0.75), and. The stress regime can be stated numerically using the R' index, which ranges from 0.0 to 3.0 and is defined as follows:

R' = R when (σ1 is vertical; extensional stress regime)

R' = 2 - R when (σ2 is vertical; strike-slip stress regime)

R' = 2 + R when (σ3 is vertical; compressional stress regime)

Fig. 3.4: Representations of stress tensors by different stress regimes commended by Guiraurd et al. (1989)

3.6   Back analyses

Back analyses of the affected slopes have been carried out using Rocscience Slide2 software based on the Limit Equilibrium Method (LEM) and probabilistic analysis. The Janbu simplified method used considers normal interslice forces, but

ignores interslice shear force and satisfies overall horizontal driving forces, but not overall resisting forces (Alok et al., 2024; Jaffari, 2014). Due to this reason, the FoS outcome is consistently lower when applying Janbu's method compared to that of Bishop's method (Koutnik et al., 2008). A particular slip surface can exhibit various safety factor values when calculated. Consequently, a range of safety factors is produced, allowing for the determination of the probability of failure for a slope.

A probabilistic analysis using Latin-Hypercube sampling method and global minimum analysis type was executed for the back analysis of the slopes. The Latin Hypercube sampling technique, which is probabilistic in nature, produces results that are similar to those of the Monte Carlo technique, but with a reduced number of samples (Nagy-Göde and Török, 2022). A uniform distribution is set for the parameters to perform the back analysis so as to ensure random samples are generated uniformly over the specified range of each variable.

The following results are computed and displayed along with the charts on conducting a back analysis for a slope:

3.6.1 *Deterministic Safety Factor or FS (deterministic)*

FS (deterministic) is the factor of safety of the Global Minimum slip surface, as determined from a regular (non-probabilistic) slope stability analysis (Djeffal and Belkacemi, 2023).

3.6.2 *Mean Safety Factor or FS (mean)*

The FS (mean) is the average safety factor of the Global Minimum slip surface as determined by the probabilistic analysis.

3.6.3 *Probability of Failure (PF)*

It estimates the failure risks of slopes, which is the ratio of the number of samples with safety factor of less than 1 to the total number of samples (Aminpour et al., 2021). A PF exceeding 50% indicates that over half of the safety outcomes have factors of safety that are below 1.

3.6.4 *Reliability Index (RI)*

The RI shows how far the mean safety factor deviates from the crucial safety factor value of one by the number of standard deviations (Chen et al., 2014). It can be calculated assuming either a normal distribution (Normal RI) or lognormal distribution

(Lognormal RI) of the safety factor results. In Slide2 analyses, both values are displayed. A Reliability Index of atleast 3 is usually recommended as a minimal assurance of safe slope design (Akın, 2017).

3.7   Precipitation analyses

The GPM mission data of NASA initiated in 2014, was used to analyse the number of days and intensity of rainfall that occurred around the landslide areas. Rainfall information gathered from the GPM mission offers detailed and timely rainfall data to scientists around the globe, even every half hour. GPM IMERG is an algorithm that calibrates and integrates TRMM data and surface gauge data to rectify biases in satellite data (Acker and Leptoukh, 2007). The precipitation data (mm/day) were gathered by calculating spatial averages across the study area within the specified date range to generate a time-series output as described by Huffman et al. (2019).

CHAPTER 4

GEOTECHNICAL ANALYSES

Geotechnical analyses was carried out in all the six landslide of the study area, the results of which are given below.

4.1 Pezielietsie Colony

4.1.1 Study area

The research area is located between latitudes 25°40′46.389″ and 25°40′55.427″N and longitudes 94°6′11.056″ and 94°6′22.53″E (Fig. 4.1.1). The crown of the slide is located approximately 1410 m above mean sea level (msl). During the winter, a stream that flows southwest along the northwestern boundary of the study area, dries up. A larger stream flows westward to the south of the landslide zone. The slope profile has an average slope angle of ~23°.

A drain was built to channelise water to the stream channel west-north-west of the landslide zone. Wastes dumped in the drain choked segments of the channel, causing water to flow over the fragile surface. Non-biodegradable plastics and other waste dumped in stream channels have caused landslides in parts of Kohima (Aier et al., 2012).

4.1.2 Consistency limits

The consistency of fine-grained soil is heavily influenced by its moisture content. During heavy rain, slope material become saturated, and the water content may surpass the liquid limit of the soil. The soil then behaves like a fluid, ultimately failing. The average liquid limit ranges from 28.39 to 38.59, and the plasticity index from 9.08 to 19.25 (Table 4.1.1). Snethen et al. (1977) attribute these findings to low degree of expansion. The average shrinkage limit of these samples is 29.25. According to Holtz and Gibbs (1956), such values suggest a relatively low rate of expansion. The average plasticity index of the six soil samples tested is 13.38. The plasticity chart (Fig. 4.1.2) for samples of inorganic silts and clays (BIS, 1970) shows low to moderate plasticity.
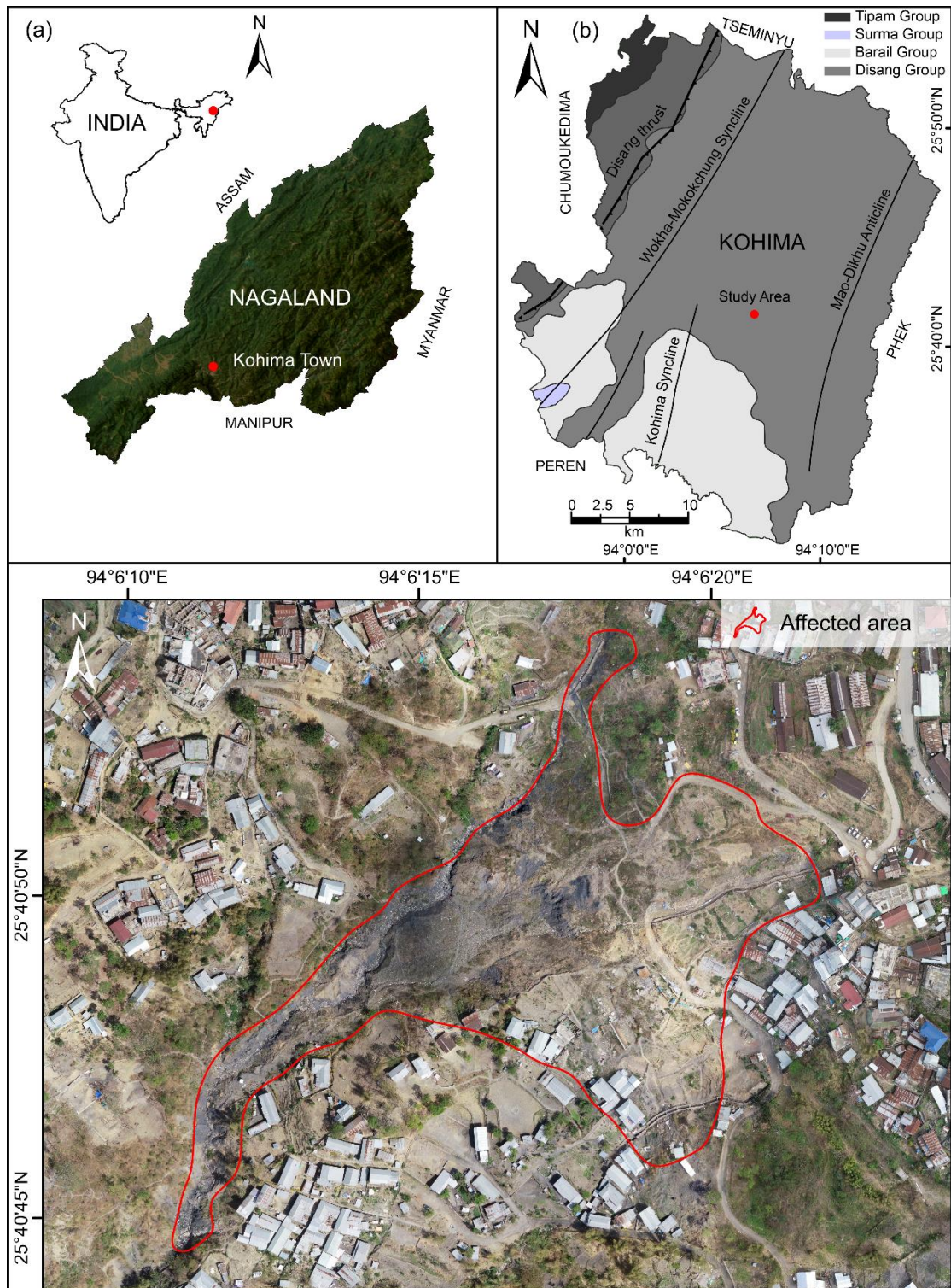
Fig. 4.1.1 Location map of Pezielietsie Colony slide

Table 4.1.1 Consistency limits of six soil samples

Sample No	Liquid limit (W_L)	Plastic limit (W_P)	Plasticity index (I_P)	Shrinkage limit (S_L)
1	36.70	25.89	10.81	31.97
2	33.50	20.65	12.85	30.11

3	28.39	16.48	11.91	26.80
4	32.98	23.90	9.08	30.32
5	33.45	17.10	16.35	24.26
6	38.59	19.34	19.25	32.02
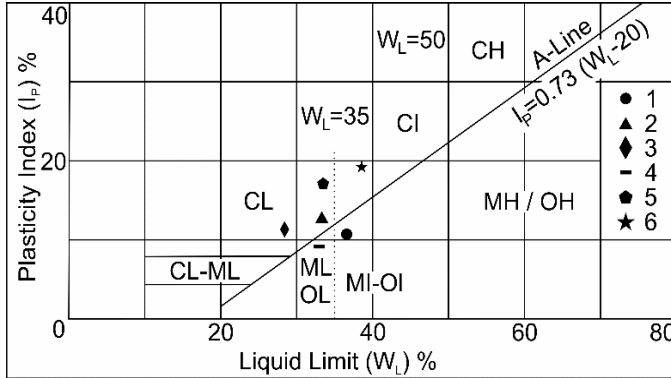
Fig. 4.1.2 Plasticity chart of the soil samples (M - Inorganic silt/very fine sand; C - Inorganic clay; O - Organic silt/clay; L - Low compressible and plastic silt/clay; I - Medium compressible and plastic silt/clay; H - High compressible and plastic silt/clay)

The loss of fine-grained particles by subsurface flows through the fissured surface soils and near-surface rocks of the study area is the reason for the low liquid and shrinkage limits, as well as the low plasticity index. As a result, the intermolecular forces of attraction between soil particles are diminished, and such soils become less cohesive, which changes the consistency and shear strength according to Tabbal et al. (2019).

4.1.3   Direct Shear

Soil samples have been assessed for c, ϕ, and σ_{ci} (Table 4.1.2; Fig. 4.1.3). The 'c' value of silty-clay typically ranges from 10-20 kPa and 'ϕ' from 18°-32° under consolidated conditions (Geotechdata 2020). The samples have extremely low 'c' values. This could be due to heavy rainfall (Matthew et al., 2013; He et al., 2022), which saturates the soils and raises the pore pressure. The somewhat elevated 'ϕ' values indicate loose, coarse soils. Strengths of soils typically vary from extremely soft (<25 kPa) to hard (>400 kPa). Very low values of σ_{ci}, as represented by the soils in this study. According to Das and Sobhan (2018) such soils are very weak and soft.

Table 4.1.2 Shear strength parameters of the soils obtained from direct shear test

Sample	Cohesion (C) (kPa)	Internal Friction Angle (ϕ)	σ_{ci} (kPa)
1	3.12	30.14	10.85

2	0.70	23.73	02.15
3	5.18	29.17	17.66
4	3.53	27.87	11.71
5	5.51	24.84	17.24
6	4.47	24.59	13.94
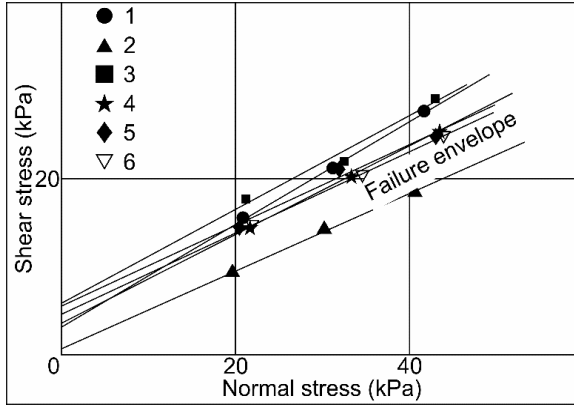
Fig. 4.1.3: Failure curves of samples

4.1.4 Back analysis

Back analysis of the slope was based on the average values of 'c' (3.75 kPa) and 'φ' (26.2°) obtained from direct shear test of soil samples, using a soil unit of 19 kN/m^3 (Geotechnical Info, 2012) and Mohr-Coulomb strength type. The probability analysis (Fig. 4.1.4) portrays a deterministic safety factor of 0.829, with a failure probability of 85.90%. This means that 859 out of 1000 samples produced a FoS <1.

The minimum reliability index (RI) for slope safety is 3 (Kamien, 1997). However, in this area (Fig. 4.1.4), a RI of -1.096 is noted, which is insufficient for slope safety.

Rocscience Slide2 scatter plots (Fig. 4.1.5a) show the link between soil cohesiveness, friction angle, and FoS. For this graphic, a range of 0.99 to 1.01 was chosen so that the relationship between cohesiveness and friction angle is equivalent to a FoS of 1. Approximately 28 spots (red squares) are inside the specified range (Figs. 4.1.5a, b). Any pair of cohesion and friction-angle values within this linear curve (Fig. 4.1.5b) gives a FoS equivalent to 1. The parameters alpha and beta denote the slope and y-intercepts of the line, respectively (Fig. 4.1.5b), resulting in the equation,

Friction angle = -1.18339*cohesion + 35.2541

The sensitivity curves for cohesiveness (Fig. 4.1.6a) and friction angle (Fig. 4.1.6b) with respect to FoS have modest slopes, indicating that changes in soil-parameter values have a moderate impact on slope stability. According to the sensitivity curves, the cohesiveness and friction angle values are 8.85 kPa and 29.97° respectively, corresponding to steady slope conditions at a safety factor of 1. Friction angle variation has a greater impact on the safety factor since the curve (Fig. 4.1.6c) is steeper than the cohesion sensitivity curve.
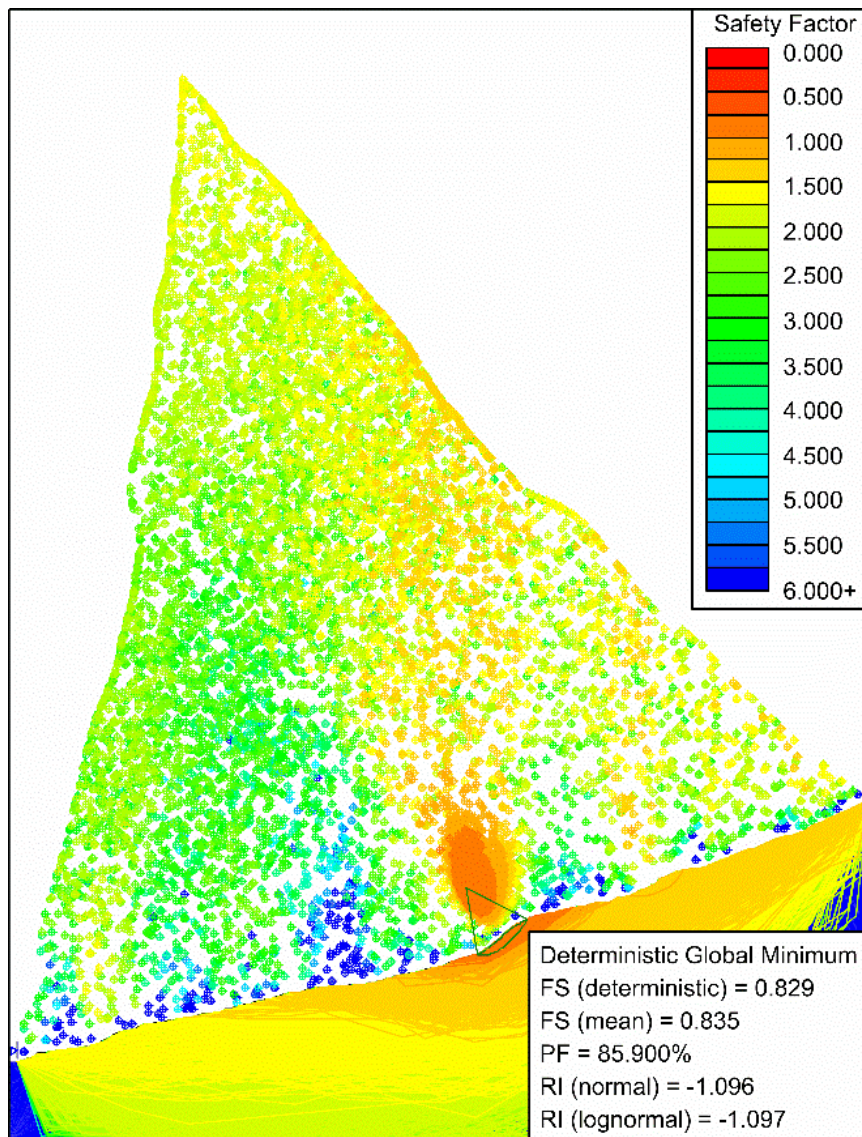
Fig. 4.1.4 Slope stability analysis with global minimum slip surface showing a safety factor of 0.829
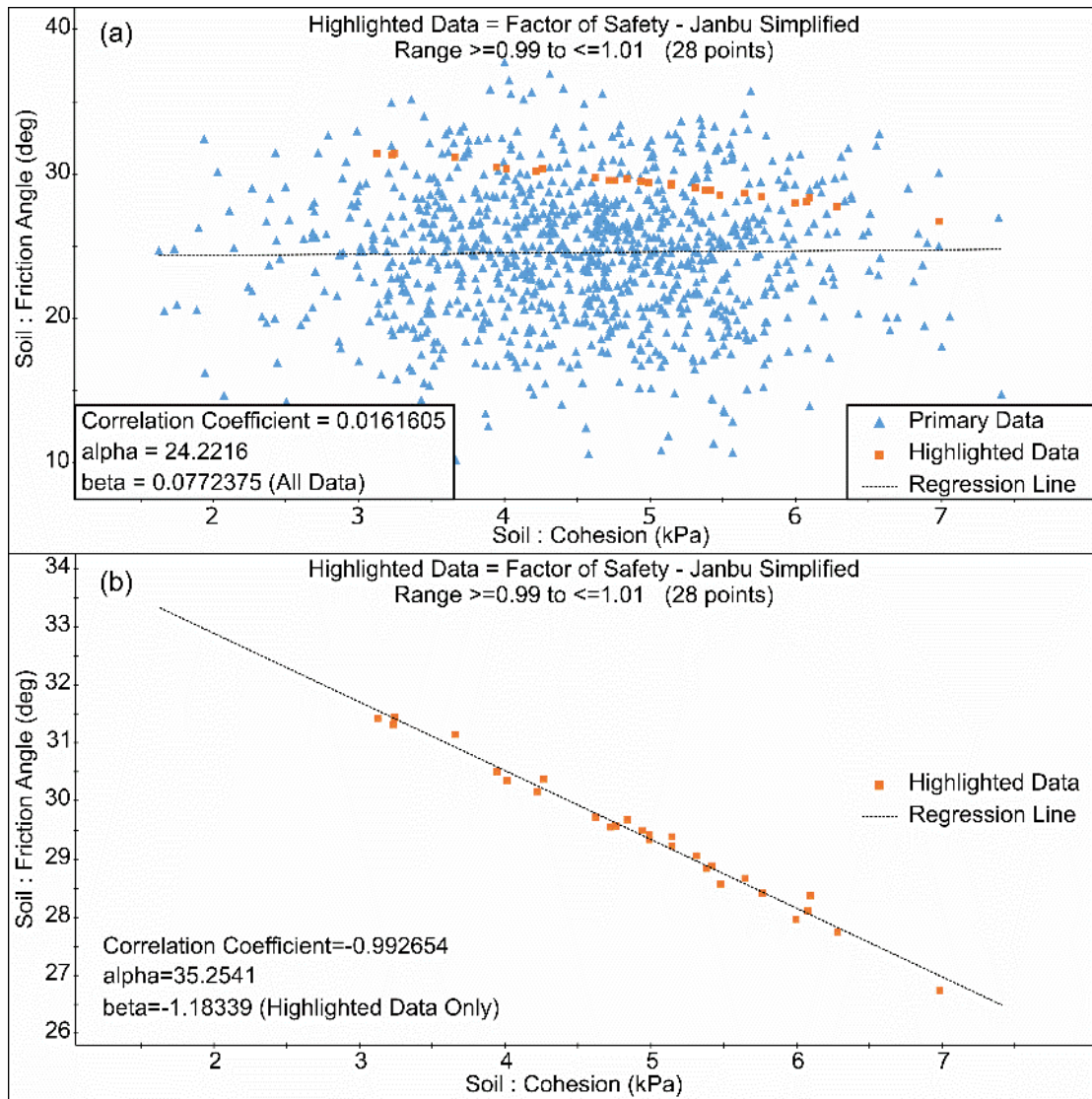
Fig. 4.1.5 (a) Scatter plots of correlation between cohesion and friction angle to the safety factor, (b) Linear best-fit-line relationship between cohesion and friction angle for a FoS=1
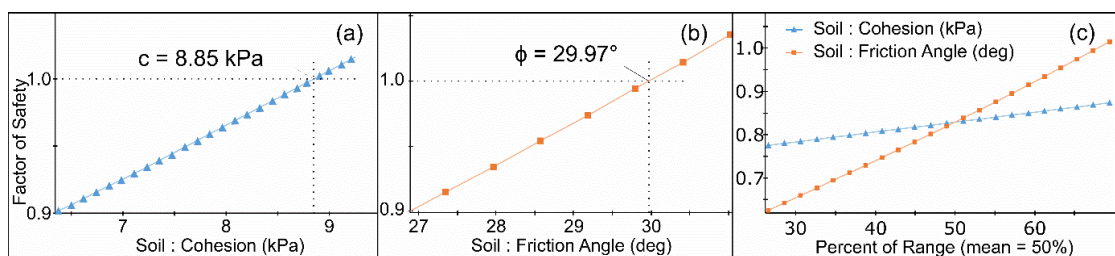
Fig. 4.1.6 Sensitivity curves (a) Cohesion at the FoS equivalent to 1, (b) Friction angle at the FoS equivalent to 1, (c) Plots for soil variables, cohesion, and friction angle

4.1.5 *Precipitation analysis*

Kohima town gets an average annual rainfall of 1634 to 1817 mm, which is considered quite high. In 2017, a minor landslide occurred in the area, indicating

worsening slope conditions. The area received much more rainfall in 2018 (2312.97 mm), including 468.87 mm in July alone (Table 4.1.3). Heavy rains lashed parts of Kohima town from the 28-30 July (Fig. 4.1.7), soaking the fissured soils and rocks of the study area and causing a catastrophic landslide on 31st July.

Table 4.1.3: Precipitation data of Pezielietsie Colony during July 2018

Date	Rainfall (mm)	Date	Rainfall (mm)	Date	Rainfall (mm)	Date	Rainfall (mm)	Date	Rainfall (mm)
1	2.16	8	7.27	15	6.34	22	12.33	29	41.80
2	6.82	9	15.57	16	11.61	23	14.20	30	38.76
3	7.10	10	7.89	17	20.46	24	36.70	31	8.13
4	3.70	11	21.68	18	9.70	25	43.75		
5	1.65	12	17.86	19	7.65	26	19.07		
6	7.38	13	7.29	20	10.76	27	14.08		
7	8.05	14	6.15	21	12.11	28	37.84	**Total**	**468.87**
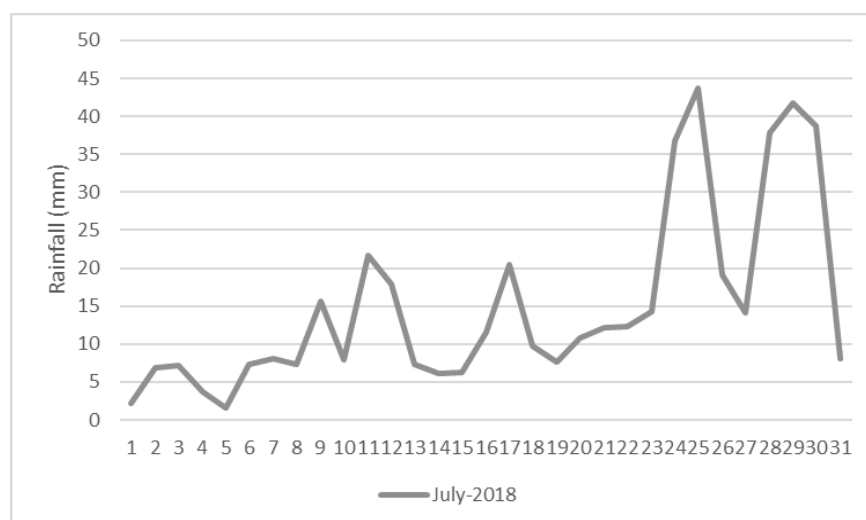
Fig. 4.1.7 Precipitation curve of Pezielietsie Colony

4.2   Peraciezie Colony (2017)

4.2.1   Study area

The Peraciezie Colony (hereafter referred to as PRC-A) is located at the northern end of Kohima town (Fig. 4.2.1). It is a thriving sector that caters to the ever-increasing requirements of the populace, be it natives or people from rural areas in pursuit of work and education. The National Highway (NH) 2 passes through the eastern fringe of the colony. This colony houses schools, offices, business establishments, and an increasing number of residential households. The colony was

affected by two landslides, one in 2017 and another in 2018, at two sites, a few hundred meters apart.
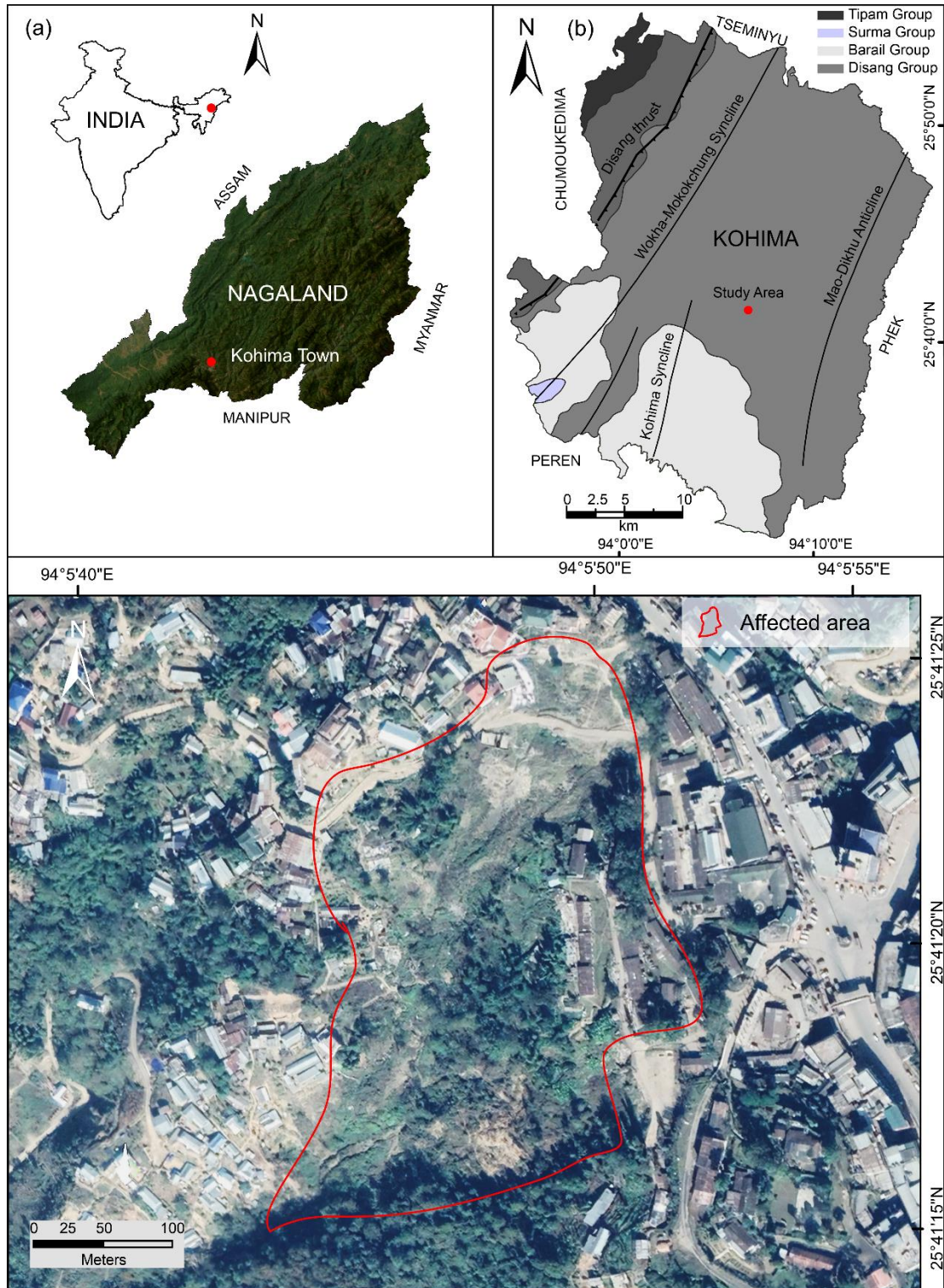
Fig. 4.2.1: Location map of Peraciezie Colony slide, 2017 (Google Earth, November 2017)

On 12th June 2017, a landslide took place in the wee hours at 25°41'22.95"N and 94°5'48.33"E, at an elevation of 1417 above msl. It damaged an area of ~42,500 m^2 and around 20 houses, rendering several families homeless (https://easternmirrornagaland.com/21-houses-destroyed-by-landslide-in-kohima-town/; https://morungexpress.com/landslides-destroy-over-20-houses-kohima; https://employee.gsi.gov.in/cs/groups/public/documents/document/b3zp/mtyx/~edisp/dcport1gsigovi161646.pdf). It also damaged two roads that connected part of the colony with the rest of Kohima town. The colony was also left reeling in complete darkness as electric poles collapsed during the episode. It was reported that the sliding process began about 3 days earlier due to incessant rains. Due to sliding and subsidence, a particular stretch of road has been realigned several times during the monsoon. The unstable slope too is affected every monsoon. A section of the Border Roads Task Force (BRTF) camp on the left flank of the slide was severely affected. A retaining wall has been erected at the toe to arrest further sliding. Numerous perennial springs are noted near the toe of the slide.

4.2.2 *Consistency limits*

Soil samples were collected from November to January. The liquid limit (W_L) ranges between 24.50 and 46.50%. The water content of the six samples is lower than W_L and the plastic limit (W_P). The soils are in a plastic state, which means they can deform without cracking. All samples have consistency indices greater than one (1.46 to 2.72%). These indicate that the soil samples were below the plastic limit in their natural state during sampling. An increase in moisture content would directly affect the consistency of the soil, lowering its values and bringing the soil state close to zero. This would take the soil into the liquid state and thereby reduce slope stability. The plasticity index ranges from moderate to high, indicating that the soil types are made up of cohesive silty-clays.

Table 4.2.1: Consistency limits of six soil samples

Sample No	Liquid limit (W$_L$)	Plastic limit (W$_P$)	Plasticity index (I$_P$)	Shrinkage limit (S$_L$)
1	44.00	28.18	15.82	23.19
2	38.64	22.15	16.49	25.45
3	24.50	12.73	11.77	10.75
4	25.00	14.01	10.99	12.83
5	24.61	13.43	11.18	20.47

6	46.50	31.58	14.92	23.61

Samples 1, 2, 5, and 6 have very high shrinkage limits (20.47-25.45%) while samples 3 and 4 have moderate shrinkage limits (10.75-12.83%). According to Holtz and Gibbs (1956), soils such as 1, 2, 5, and 6 have low swelling potential and samples 3 and 4 have medium swelling potential. An increase in swelling capacity of the soil would reduce the slope FoS.

According to the plasticity chart (Fig. 4.2.2), soil samples 2, 3, 4, and 5 fall in the CL field, indicating inorganic clays with low to medium plasticity. Samples 1 and 6 are highly plastic with a silty to clayey composition.
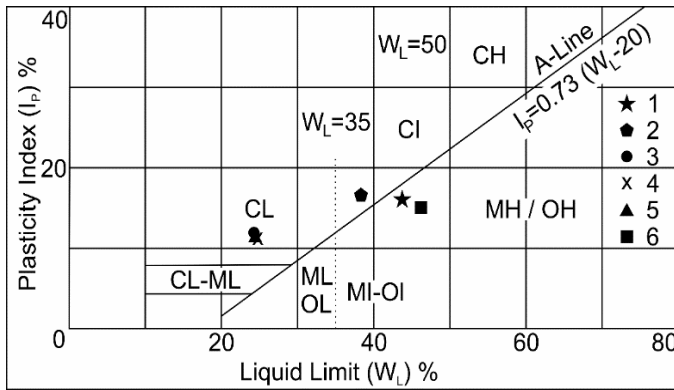
Fig. 4.2.2: Plasticity chart of the soil samples (M - Inorganic silt/very fine sand; C - Inorganic clay; O - Organic silt/clay; L - Low compressible and plastic silt/clay; I - Medium compressible and plastic silt/clay; H - High compressible and plastic silt/clay)

4.2.3 Direct Shear

The soil samples were tested for c, ϕ, and σ_{ci} (Table 4.2.2) and plotted (Fig. 4.2.3). Silty-clay typically has a 'c' value of 10-20 kPa and 'ϕ' value of 18°-32° under consolidated conditions (Geotechdata 2020). The samples exhibit unusually low 'c' values ranging from 5.86 to 16.56 kPa. This may be attributed to excessive rainfall (Matthew et al., 2013; He et al., 2022), which saturates soils and increase pore pressure. The 'ϕ' values range from 19.03° to 30.83°, indicating silty to sandy soils. Soil strengths range from extremely mild (<25 kPa) to strong (>400 kPa). According to Das and Sobhan (2018), soils with low to very low σ_{ci} values are typically weak and soft.

Table 4.2.2: Shear strength parameters of the soils obtained from direct shear test

Sample	Cohesion (C) (kPa)	Internal Friction Angle (ϕ)	σ_{ci} (kPa)
1	12.17	19.03	34.13

2	13.94	20.67	40.33
3	16.56	19.88	47.19
4	11.3	30.83	39.81
5	5.86	28.57	19.73
6	15.85	21.05	46.17
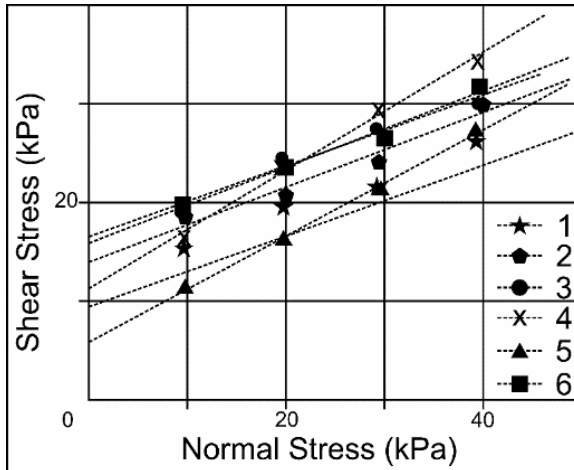
Fig. 4.2.3: Failure curves of samples

4.2.4   Back analysis

From back analysis of the slope, the probability of slope failure is estimated at 100%, whereas the FoS is 0.652 (Fig. 4.2.4). Therefore, the reliability index of the slope is -3.111, which is much below the safety limit of 3.
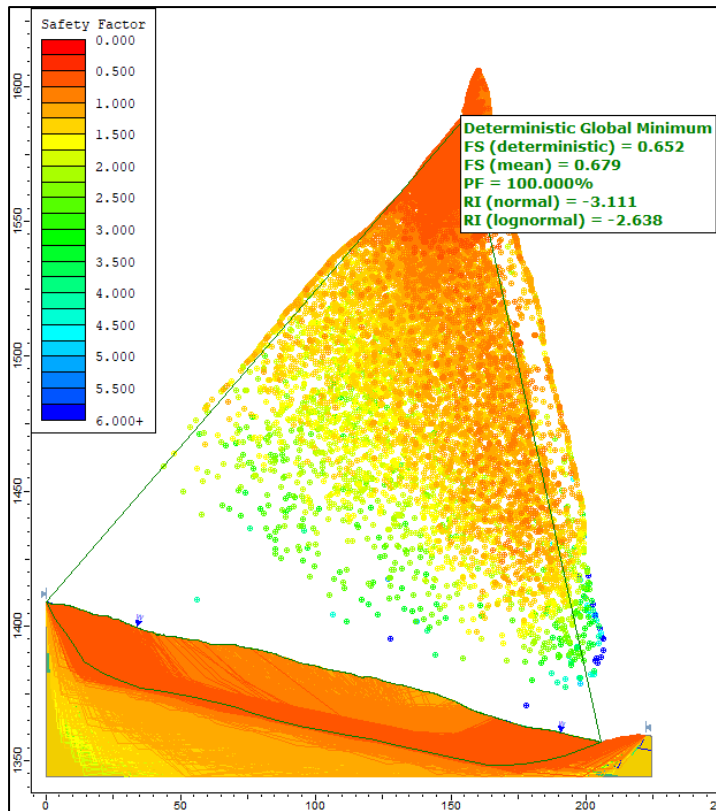
Fig. 4.2.4: Slope stability analysis with global minimum slip surface showing a safety factor of 0.652

4.2.5 *Precipitation analysis*

From 16 June to 15 July 2024, there were 29 rainy days. The total precipitation received was 377.0 mm, with a daily average of 24.32 mm (Table 4.2.3; Fig. 4.2.5). The days leading up to 11th July 2017 have seen intermittent days of above-average rainfall.

Table 4.2.3: Precipitation data of Peraciezie Colony

Date	Precipitation (mm)	Date	Precipitation (mm)	Date	Precipitation (mm)
16 Jun	22.66	26 Jun	12.01	06 Jul	06.41
17 Jun	06.66	27 Jun	26.46	07 Jul	05.96
18 Jun	04.39	28 Jun	15.58	08 Jul	05.84
19 Jun	05.83	29 Jun	02.51	09 Jul	47.26
20 Jun	05.47	30 Jun	30.94	10 Jul	23.49
21 Jun	06.00	01 Jul	16.35	11 Jul	21.33
22 Jun	13.47	02 Jul	20.67	12 Jul	11.46
23 Jun	10.08	03 Jul	04.41	13 Jul	05.96
24 Jun	08.19	04 Jul	10.91	14 Jul	07.06
25 Jun	02.33	05 Jul	04.69	15 Jul	12.68
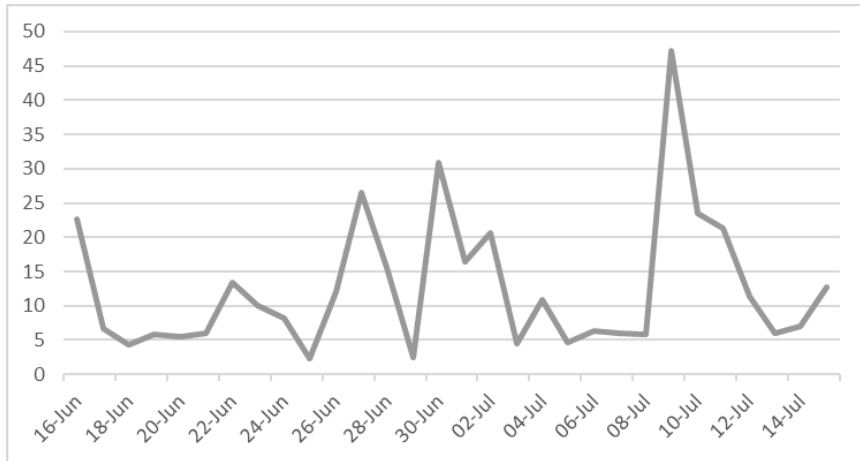
Fig. 4.2.5: Precipitation curve of Peraciezie Colony

4.3   Peraciezie Colony (2018)

4.3.1   Study area

The next year, on 1ˢᵗ August 2018, about 200 m southeast of PRC-A (25°41'14.40"N and 94°5'49.13"E), a larger slide, hereafter PRC-B, affected the colony (Fig. 4.3.1). At an elevation of about 1350 m, it blankets an area of ~54,000 m². The slide flowing in the southwest direction was of larger magnitude in terms of areal extent. Two houses of colony residents and three houses of the BRTF camp were affected (https://morungexpress.com/nagaland-natural-calamities-affect-over-150-families-kohima). A portion of a circular road within the camp was also damaged. The BRTF camp is perched at the crown of the slide. At the toe of the slide, the PRC-B slide destroyed a road connecting parts of Kohima. During the monsoon, this section of the road continues to be damaged by sliding debris and stream water flowing at the left edge of the slide.

53
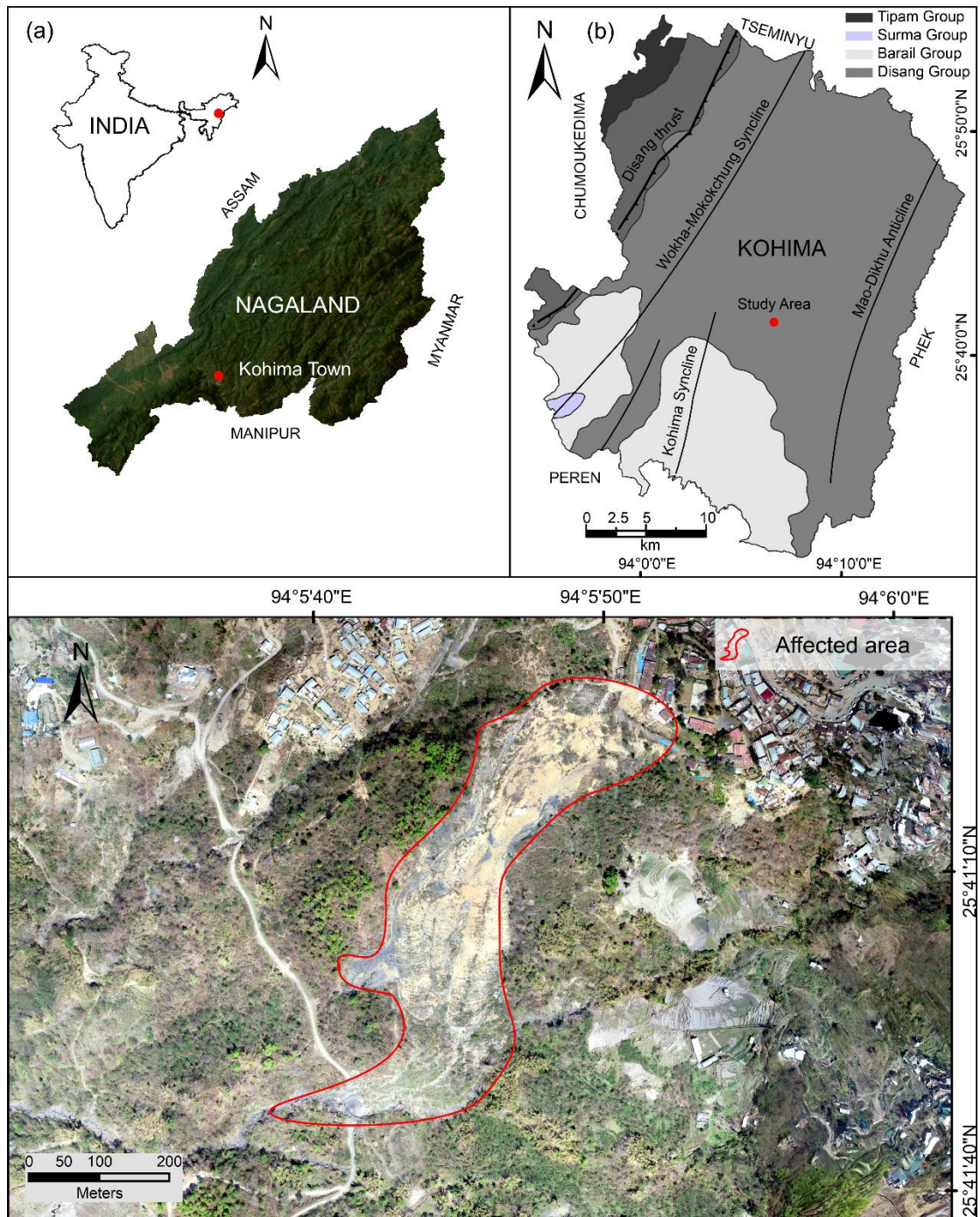
Fig. 4.3.1: Location map of Peraciezie Colony slide, 2018

The rocks of the study areas (PRC-A and PRC-B) consist predominantly of Disang shales with thin intercalations of siltstone. The rocks are highly crumpled, fractured, sheared, and weathered. Several lineaments pass through Kohima town, including some minor lineaments in the landslide-affected areas. These areas are saturated with water, leading to positive pore water, which decreases the shearing strength of the rocks. The lineaments contribute to the overall instability of the slopes. A first-order stream dissects PRC-A; at PRC-B it flows along the left of the slide zone,

touching the toe of the slide. According to Altin and Gökkaya (2018), such streams often cause slope failure. The major stream in the area is the Dzüchü Rü, which flows northwesterly to join the Dzüdza Rü.

4.3.2   Consistency limits

Soil samples were collected in March, the pre-monsoon month. The liquid limit (W_L) ranges from 21.14% to 40.15%. The plastic limit ranges from 12.65% to 24.51%. The plasticity chart shows most samples falling in the CL zone (W_L<35), which indicates inorganic clayey soils of low plasticity and liquid limits. These are also known as 'lean clays' due to their comparatively higher sandy and silty material content. Samples 2 and 6 near the CI field, indicate inorganic clays of moderate plasticity. With W_L between 35 and 50, samples 2 and 6 are intermediate compressible clays. Water contents in samples 1, 4, 5, 7, 8, and 9 are more than their respective plastic limits but less than the W_L, indicating that the soils are in the plastic state. Soils deform plastically at this stage without fracturing. Samples 2, 3, and 6 have consistency indices greater than one (1.02-1.38%), indicating that the soils were below the plastic limit in their natural state during sampling. The plasticity index of the samples indicate mild to very plastic conditions. All samples show very high shrinkage limits (18.74-33.87%); sample 3 has the lowest value. Sample 1, with the highest value, indicates that it will have a more remarkable change in volume relative to water content (Hobbs et al., 2018).

Table 4.3.1: Consistency limits of six soil samples

Sample No	Liquid limit (W_L)	Plastic limit (W_P)	Plasticity index (I_P)	Shrinkage limit (S_L)
1	21.14	12.65	08.49	33.87
2	40.15	24.51	15.64	27.63
3	32.56	16.81	15.75	18.74
4	29.35	13.64	15.71	32.54
5	24.61	12.94	11.67	21.69
6	39.64	23.15	16.49	27.51
7	24.25	14.28	09.97	30.45
8	28.63	20.51	08.12	24.78
9	26.20	18.09	08.11	30.15
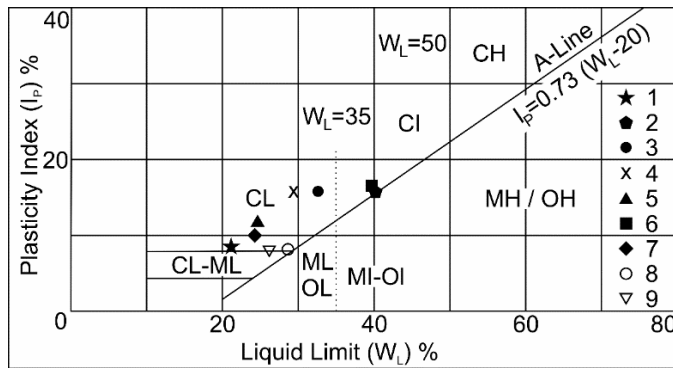
Fig. 4.3.2: Plasticity chart of the soil samples (M - Inorganic silt/very fine sand; C - Inorganic clay; O - Organic silt/clay; L - Low compressible and plastic silt/clay; I - Medium compressible and plastic silt/clay; H - High compressible and plastic silt/clay)

4.3.3 Direct Shear

The shear strength parameters c, ϕ, and σ_{ci} (Table 4.3.2) were determined from the failure envelope by plotting normal stress against shear stress (Fig. 4.3.3). The σ_{ci} values range from 26.04 to 67.03 kPa, which indicate soft and firm soils.

Table 4.3.2: Shear strength parameters of the soils obtained from direct shear test

Sample	Cohesion (C) (kPa)	Internal Friction Angle (ϕ)	σ_{ci} (kPa)
1	8.65	31.55	30.92
2	13.43	25.81	42.84
3	16.78	30.99	59.29
4	19.76	28.95	67.03
5	18.24	25.84	58.21
6	10.8	23.91	33.21
7	8.23	25.42	26.04
8	9.01	30.47	31.50
9	15.05	30.13	49.44
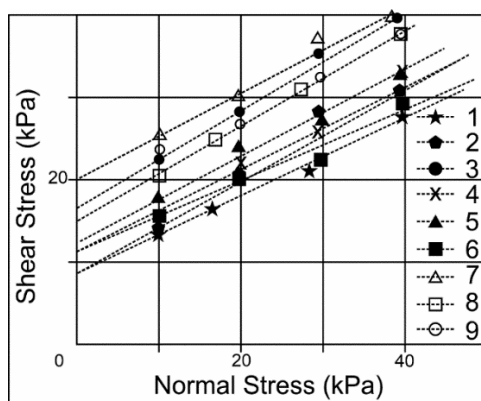
Fig. 4.3.3 Failure curves of the samples

4.3.4 Back analysis

56

The probability analysis (Fig. 4.3.4) indicates that the deterministic safety factor is 0.626, with a failure probability of 100%. This indicates that all analysed samples had a FoS <1. In this case a RI of -3.929 was obtained, which is insufficient for slope safety.
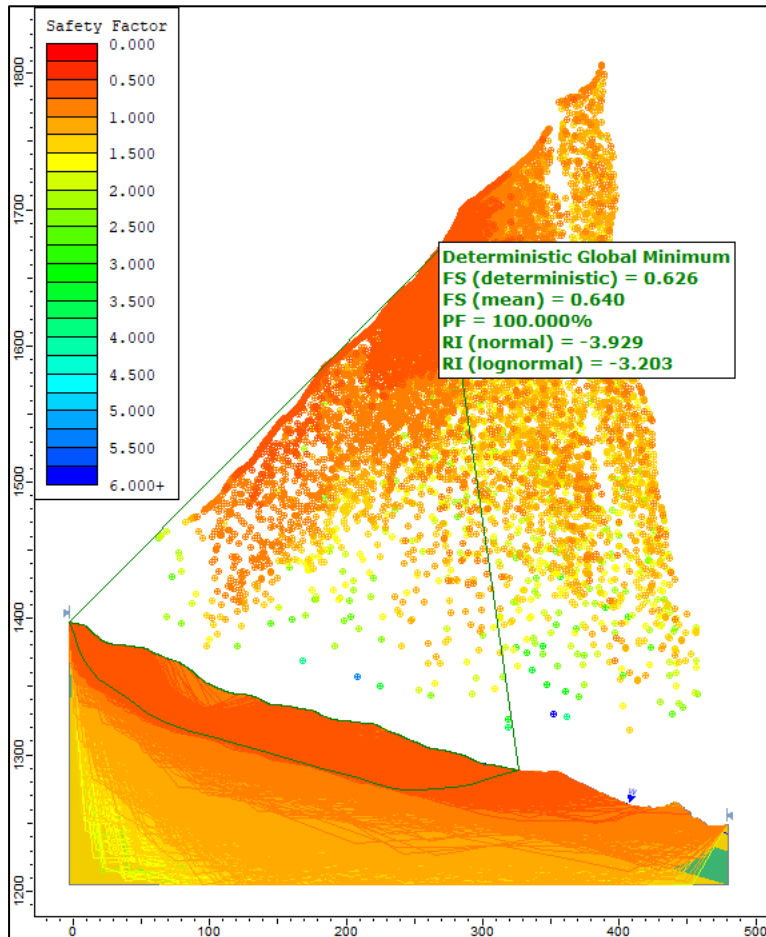
Fig. 4.3.4: Slope stability analysis with global minimum slip surface showing a safety factor of 0.626

4.3.5 Precipitation analysis

The days leading to the landslide event on 1st August 2018 experienced 16 rainy days from 16th to 31st July 2018. July 2018 received 434.22 mm of rainfall with a daily average of 14.01 mm (Table 4.3.3, Fig. 4.3.5). From the chart, it is notable that the days leading to 1st August 2018 had a higher amount of precipitation, which was more than three times the average rainfall of a day.

Table 4.3.3: Rainfall data of July-August 2018

Date	Precipitation (mm)	Date	Precipitation (mm)	Date	Precipitation (mm)
11 Jul	16.43	21 Jul	10.88	31 Jul	26.87

57

12 Jul	22.72	22 Jul	09.76	1 Aug	11.17
13 Jul	07.52	23 Jul	13.85	2 Aug	06.48
14 Jul	00.54	24 Jul	47.32	3 Aug	03.57
15 Jul	01.58	25 Jul	26.62	4 Aug	13.22
16 Jul	04.95	26 Jul	20.98	5 Aug	01.67
17 Jul	22.34	27 Jul	06.86	6 Aug	05.08
18 Jul	08.80	28 Jul	44.35	7 Aug	05.20
19 Jul	05.41	29 Jul	28.45	8 Aug	06.33
20 Jul	08.57	30 Jul	45.11	9 Aug	05.90
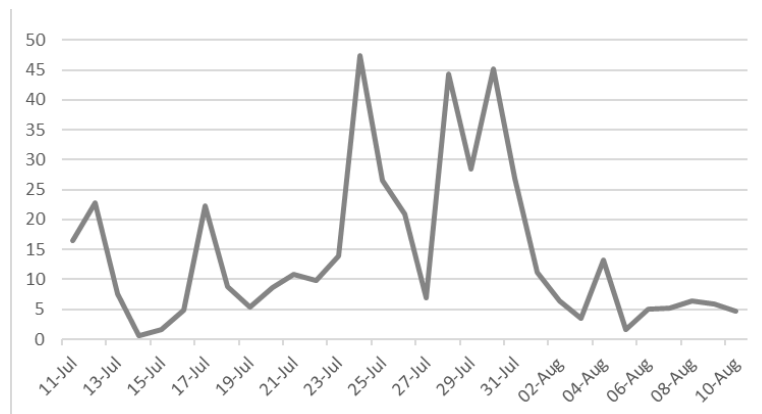
Fig. 4.3.5: Precipitation curve of the 2018 Peraciezie Colony slide

4.4 Nhachüko

4.4.1 *Study area*

This landslide occurred in the Nhachüko area, to the north of Kohima (Fig. 4.4.1). It is located at north latitude 25°41'30.72" and east longitude 94°6'44.58", approximately 1375 m above msl. Kohima receives an average rainfall of 2899 mm per year, with the highest received in July. The monsoon normally spreads from May to August/September.
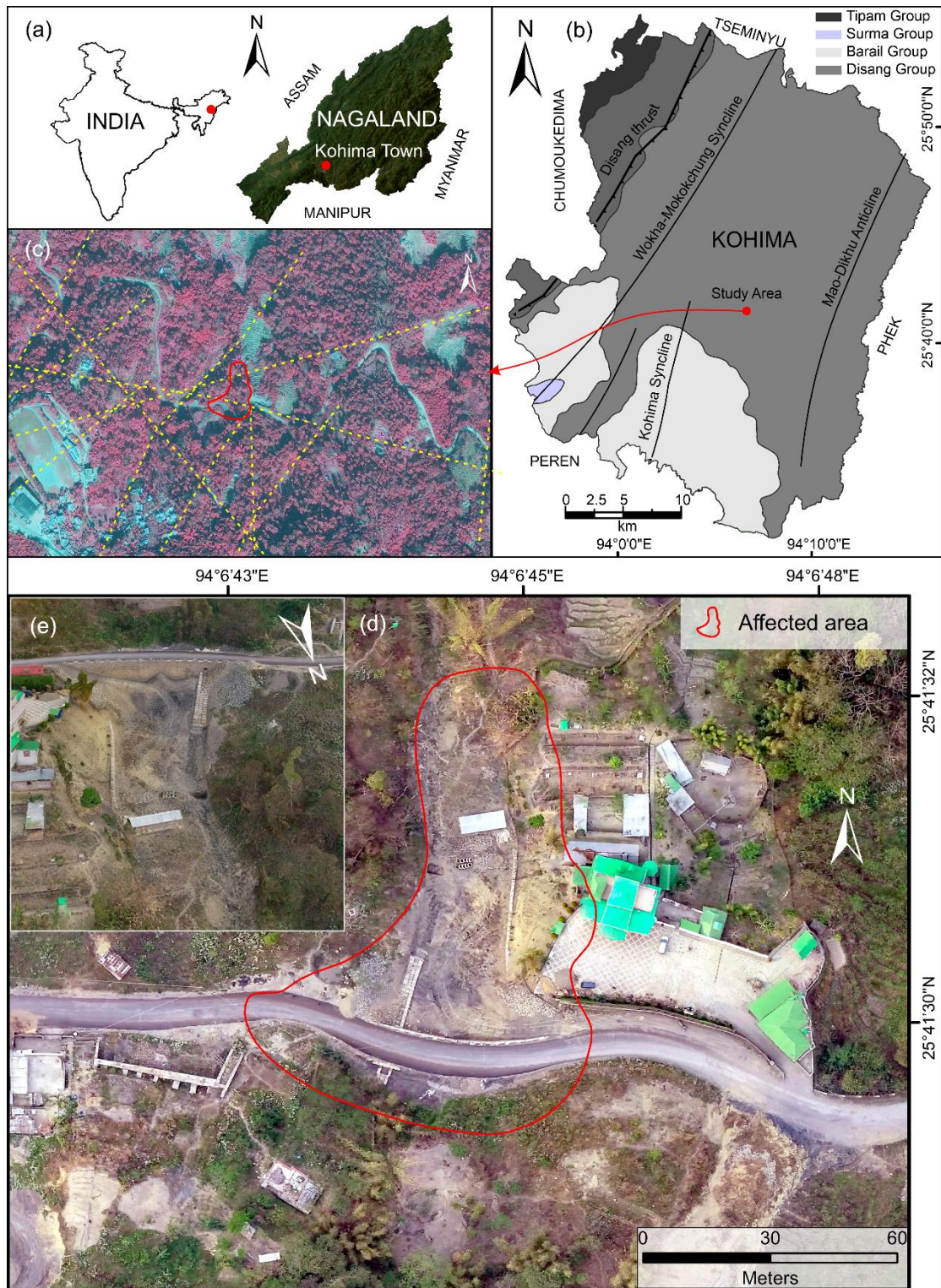
Fig. 4.4.1: Location map of Nhachüko area and affected area

The Civil Secretariat and other key offices of the state capital are located northwest of the landslide zone, while the Medical College is located east of the slide zone. Residential and agricultural properties surround the impacted area. The main scarp of the landslide was in the stream channel where water had accumulated prior to

failure. The slide zone is approximately 40 m broad, with most damage occurring in the head region where the main road passed. The slide measures around 100 m from crown to toe. The general slope is 35° and aspect is 15°. The fresh-cut slope dipped 55° towards 15°NNE. The major structural discontinuities are aligned 66° to 312° and 33° to 068°.

The owner of a plot of land above the road excavated the slope. However, against advice he dumped the excavated material into the narrow stream channel below the road bordering his property, which clogged the small-diameter hume-pipe culvert on the uphill side of the slope. This temporary dam blocked the passage of water downstream, which resulted in the retention of water along the upstream channel and surrounding areas. The situation was exacerbated by severe rains during the following days preceding the slide. Fresh seepages were noted in the area during this period, lending evidence of rising groundwater levels. The rocks and soils making up the steep, narrow channel and its banks were too weak for such a drastic change in hydrostatic pressure. The continuing increase in pore-water pressure resulted in the sudden collapse of the retaining wall that supported the road above, and the destruction of about 60 m of the road on 2nd June 2017. Portions of both banks of the channel were severely damaged. The boundary wall of a neighbouring building, three small houses, some ring wells, concrete footpaths, and a plantation in one of the neighbouring plots were completely damaged (Nagaland Post, 6th June 2017).

4.4.2 Consistency limits

The liquid limit (W_L) of the soil samples ranges between 32.00 and 39.00 (Table 4.4.1). The plasticity chart (Fig. 4.4.2) shows W_L vs I_P plots above the A-line for low compressible and plastic inorganic clay (CL) and medium compressible ad plastic clay (CI) regions. According to the chart the test samples can be classified as inorganic silts and clays of low to moderate plasticity.

Table 4.4.1: Consistency limits of six soil samples

Sample No	Liquid limit (W_L)	Plastic limit (W_P)	Plasticity index (I_P)	Shrinkage limit (S_L)
1	35.40	18.87	16.53	15.74
2	39.00	20.68	18.32	23.34
3	32.00	15.17	16.32	15.54
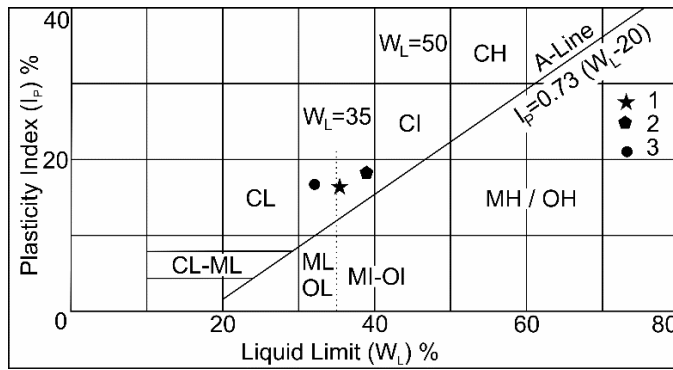
Fig. 4.4.2: Plasticity chart of the soil samples (M - Inorganic silt/very fine sand; C - Inorganic clay; O - Organic silt/clay; L - Low compressible and plastic silt/clay; I - Medium compressible and plastic silt/clay; H - High compressible and plastic silt/clay)

4.4.3 Direct Shear

Failure envelopes were used to obtain the shear strength parameters of c, ϕ, and σ_{ci} (Table 4.4.2; Fig. 4.4.3). UCS values range from 28.09 to 33.81 kPa. It is seen that UCS decreases significantly from moderately plastic soils (Sample 2) to low plastic soils (Samples 1 and 3).

Table 4.4.2: Shear strength parameters of the soils obtained from direct shear test

Sample	Cohesion (C) (kPa)	Internal Friction Angle (ϕ)	σ_{ci} (kPa)
1	9.02	24.59	28.09
2	11.01	23.86	33.81
3	9.33	23.46	28.43
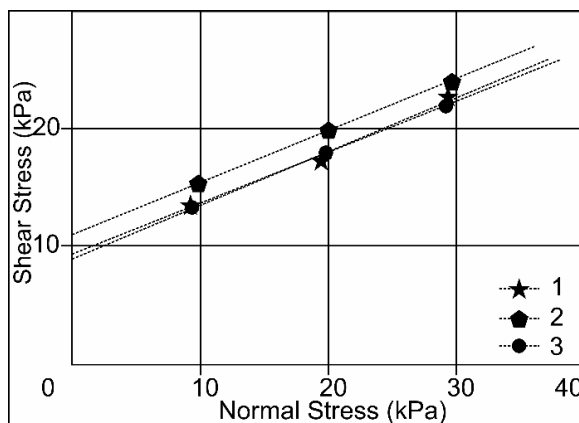
Fig. 4.4.3: Failure curves of samples

4.4.4 Back analysis

The probability analysis (Fig. 4.4.4) indicates that the deterministic safety factor is 0.542, with a failure probability of 100%. This indicates that all analysed samples

had a FoS <1. The minimum reliability index (RI) for slope safety is three (Kamien, 1997). However, in this area, an RI of -5.320 was obtained, which is insufficient for slope safety.

Fig. 4.4.4: Slope stability analysis with global minimum slip surface showing a safety factor of 0.542

4.4.5   Precipitation analysis

The area did not receive much rainfall during the later half of May prior to the landslide event on 2nd June 2017, except for 29 and 30 May 2017 (Table 4.4.3, Fig. 4.4.5), when the area suddenly received heavy rainfall of 32.68 and 51.6 mm respectively. Heavy rainwater percolation through the porous soils may have saturated the soils resulting in the formation of weak zones. Saturated soils reach a plastic state during this stage when plastic deformation sets in. Further saturation leads to the water content of the soil exceeding its W_L, causing it to behave like a viscous fluid. According to Lambe and Whitman (1979), there is a significant decrease in soil cohesiveness, friction angle, and bearing capacity during these transitions. In addition to the decrease

in strength, the weight of the soil increases when wet. This would have resulted in substantial pressure on the weak soils and rocks, primarily jointed and fractured, low-strength shales, as downslope stresses readily exceeded their resistances. Slope failure is imminent under such conditions.

Table 4.4.3: Precipitation data of Nhachüko slide for May-June 2017

Date	Precipitation (mm)	Date	Precipitation (mm)	Date	Precipitation (mm)
15 May	2.63	24 May	5.50	02 Jun	8.60
16 May	5.98	25 May	1.63	03 Jun	3.88
17 May	0.53	26 May	6.03	04 Jun	0.03
18 May	3.90	27 May	2.78	05 Jun	7.68
19 May	1.55	28 May	1.88	06 Jun	9.68
20 May	2.43	29 May	32.68	07 Jun	3.45
21 May	0.43	30 May	51.60	08 Jun	19.60
22 May	4.75	31 May	1.40	09 Jun	14.95
23 May	6.53	01 Jun	9.60	10 Jun	19.33
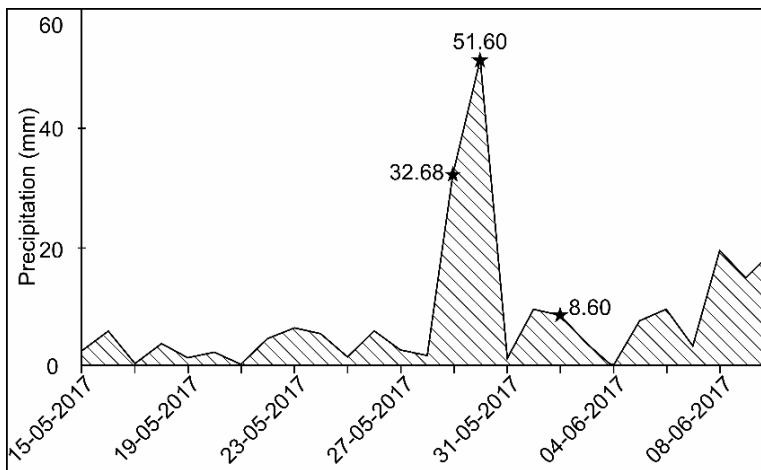
Fig. 4.4.5: Precipitation curve showing a spike in rainfall prior to the landslide event

4.5 Perizie Colony

4.5.1 Study area

The study area (Fig. 4.5.1) was affected by downslope movement of rock-soil masses on 22nd June 2018, and later again on 26th August 2018. Heavy rainfall in the area preceded the slide. The study area is located at 25°41'50.61"N latitude and 94° 5'40.50"E longitude, at an elevation of 1377 m above msl. Of about 100 houses or so in the colony, 46 were affected. Buildings of the Rüzhükhrie Government Higher Secondary School, Christ for the Nations Bible College, Directorate of Fishery, and Government Polytechnic were also affected by the slide. The affected families of the

colony were temporarily housed in the Khedi Baptist Fellowship complex, below the Government Polytechnic. Some of the families were later shifted to rented houses arranged by colony members.
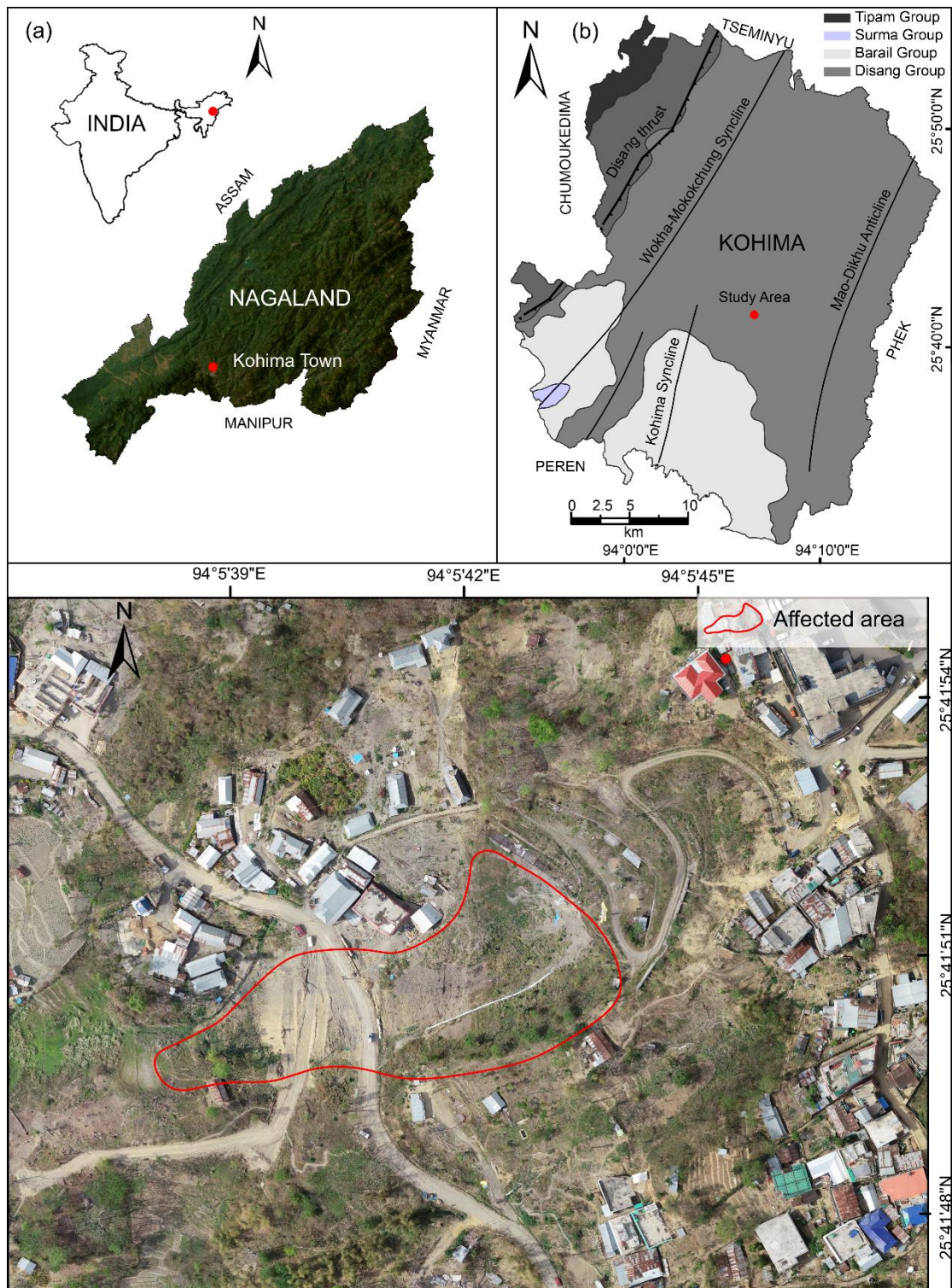
Fig. 4.5.1 Location map of the study area at Perizie colony

The landslide is about 146 m in length from the crown to the toe and a breadth of 53 m. It covered an area of about 5,700 square meters. The slide area may increase up to 12,059 square meters with a buffer of 14.7 m. The buffer being applied relates to tension cracks developed up to a distance of 14.7 m on the left flank of the slide along the road section. Tension cracks also developed above the crown. Along the crown, excess seepage of water into the subsurface was noted. This could further aggravate the situation.

The vegetative cover in the area is more or less moderate. A variety of indigenous shrubs and small trees cover the area and its surroundings. The landslide removed part of the vegetation along the slope. Removal of vegetative cover may increase the probability of further erosion (Choubey and Lallenmawia, 1987). A road passing through this slide zone was badly damaged. A pond was formed at the toe of the slide below this road. Sliding moved material about 8.5 m downslope, as is evident from the movement of concrete pillars supporting the iron gate of a house adjacent to the slide. Parts of the road also subsided about 2 m. Seven ring wells in the slide zone were covered up or sealed by debris.

The area is composed mainly of moderately to highly jointed shale, siltstone, and sandstone. Small natural drains and seepages of water are observed in and around the slide zone. Geotechnical investigations were carried out to evaluate surface instability and to understand the causes of the landslide.

4.5.2 *Consistency limits*

All four samples collected have consistency index values greater than 1, indicating that the soils are semisolid. According to test results, $I_C > 1$ suggests a semisolid state with a stiff nature. During sample collection, it was discovered that the soils were semisolid. All samples have a degree of shrinkage greater than 15 (Table 4.5.1), which indicates that the soils are deficient. When such soils dry, they shrink and desiccation fractures develop due to internal pressure in the shrunken soil mass. Subsidence occurs when such soils shrink. When wetted, the fissures close and the soils expand. The swelling process is primarily due to water molecules intercalating into the inter-plane area of smectitic clays (Schafer and Singer, 1976; Low and Margheim, 1979; Parker et al., 1980).

Table 4.5.1: Consistency limits of soil samples

Sample No	Liquid limit (W_L)	Plastic limit (W_P)	Plasticity index (I_P)	Shrinkage limit (S_L)
1	48.90	25.11	23.79	24.96
2	37.00	16.16	20.84	15.63
3	34.00	12.52	21.48	20.35
4	31.20	11.15	20.05	18.76

The plasticity chart shows soil samples 1 and 2 in the CI group (Fig. 4.5.2), indicating that they are inorganic clays of medium plasticity. Samples 3 and 4 belong to the CL category, which denotes inorganic clays with minimal plasticity. When compacted and soaked, such clays are impermeable and possess good shearing strength.
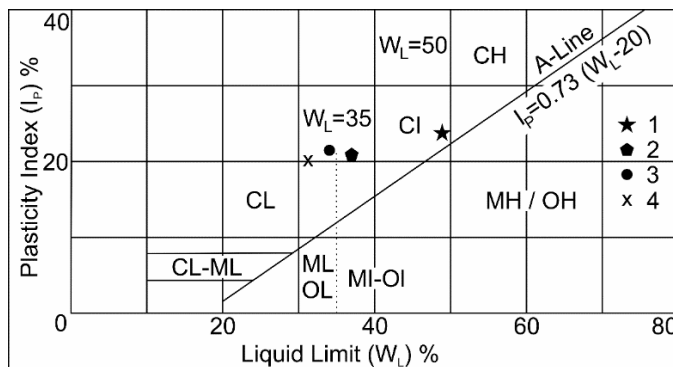
Fig. 4.5.2 Plasticity chart of the soil samples (M - Inorganic silt/very fine sand; C - Inorganic clay; O - Organic silt/clay; L - Low compressible and plastic silt/clay; I - Medium compressible and plastic silt/clay; H - High compressible and plastic silt/clay)

4.5.3 Direct Shear

Soil samples were analysed for c, ϕ, and σ_{ci} (Table 4.5.2; Fig. 4.5.3). The samples have very low 'c' values. According to Matthew et al. (2013) and He et al. 2022), heavy and continuous rainfall can saturate soils and raise the pore pressure to give such low values. The 'ϕ' values indicate loose packing of soils. The low to medium values of σ_{ci} suggest soft to firm type of soils, according to Das and Sobhan (2018).

Table 4.5.2 Shear strength parameters of the soils obtained from the direct shear test

Sample	Cohesion (C) (kPa)	Internal Friction Angle (ϕ)	σ_{ci} (kPa)
1	9.9	33.83	37.11
2	17.37	38.37	72.49
3	18.91	28.9	64.07
4	19.81	20.9	57.57
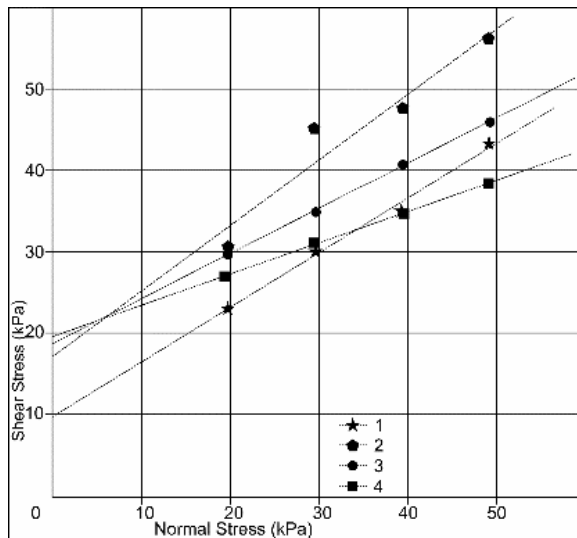
Fig. 4.5.3: Failure curves of the soil samples

4.5.4 Back analysis

The probability analysis (Fig. 4.5.4) indicates that the deterministic safety factor is 0.539, with a failure probability of 98.10%. This indicates that 981 out of 1000 samples analysed would have a FoS <1. An RI of -1.873 was obtained, which is insufficient for slope safety.
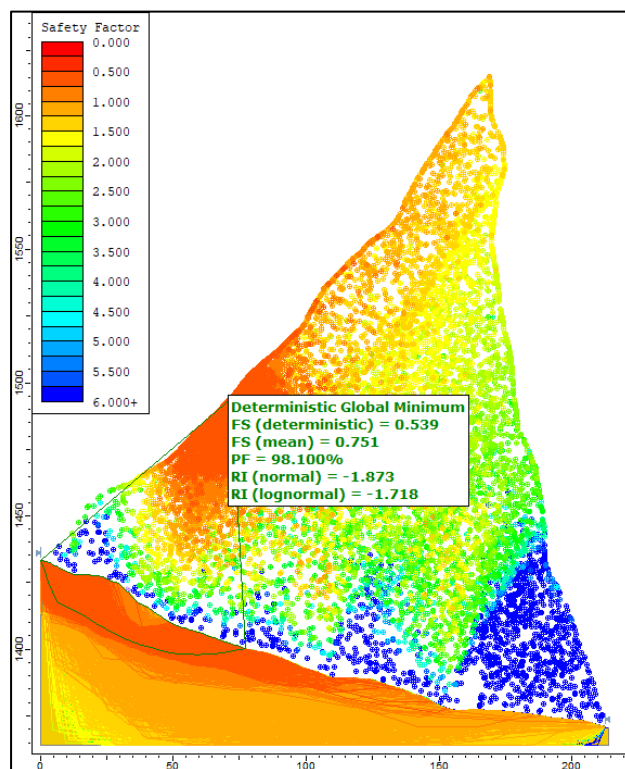
Fig. 4.5.4: Slope stability analysis with global minimum slip surface showing a safety factor of 0.539
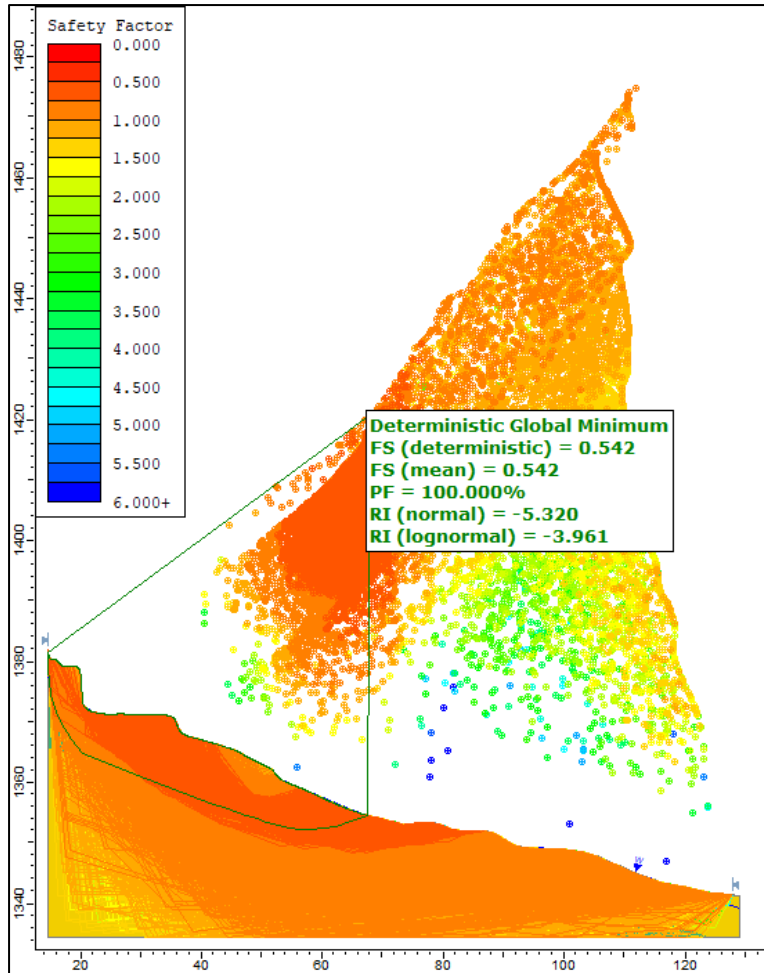
4.5.5 Precipitation analysis

The total precipitation in July 2018 was 434.22 mm with an average of 27.14 mm per day, while in August 2018 the total precipitation was 370.23 mm with a daily average of 23.14 mm. The days leading to 22nd June 2018 and 26th August 2018 (Table 4.5.4, Fig. 4.5.5) experienced light to moderate rainfall. However, both months have exhibited continuous rainy days. There were 33 rainy days between the two landslide events. The dates on which the landslides occurred did not show any unusual spike in the amount of precipitation. The area received above-average precipitation on 26th August 2018, which was when the landslide was initiated, leading to complete slope failure on 27th August 2018.

Table 4.5.3: Precipitation data of 2018

Date	Jun	Aug	Date	Jun	Aug	Date	Jun	Aug
1	01.99	11.17	12	22.72	13.54	23	13.85	17.15
2	03.05	06.49	13	07.53	22.76	24	47.32	18.76
3	06.27	03.57	14	00.54	04.16	25	26.62	12.93
4	02.14	13.22	15	01.58	01.48	26	20.98	30.89
5	02.53	01.67	16	04.95	04.06	27	06.86	12.42
6	04.29	05.08	17	22.34	29.06	28	44.35	40.73
7	06.95	05.19	18	08.80	30.50	29	28.45	08.73
8	08.45	06.33	19	05.41	02.64	30	45.11	00.86
9	15.37	05.89	20	08.57	06.39	31	26.87	21.42
10	03.32	04.67	21	10.88	04.45			
11	16.43	21.25	22	09.76	02.86			
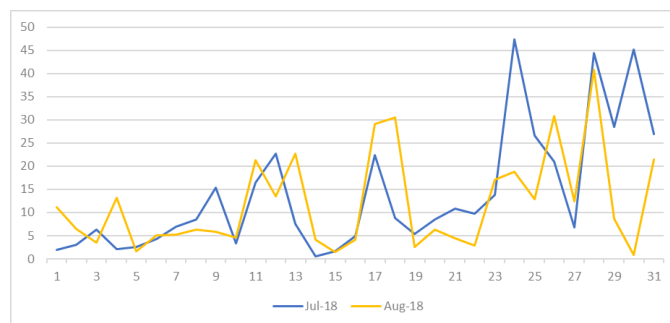
Fig. 4.5.5: Precipitation curve

4.6   Meriema area

4.6.1 Study area

The particular stretch of NH 2 near Meriema village, about 7.8 km from Kohima town, is continuously affected by slope failure. The first major event occurred on 30th October 2017 (https://easternmirrornagaland.com/landslide-cuts-off-kohima-wokha-

road/; https://nagalandpost.com/index.php/landslide-cuts-off-kma-wka-road/). About 32,520 square meters of the surface, at an elevation of 1410 m was affected. This area is located at latitude 25°43'0.25"N and longitude 94° 5'7.37"E (Fig. 4.6.1). The landslide area was preceded by heavy rainfall of 328.8 mm in September and 178.6 mm in October 2017.
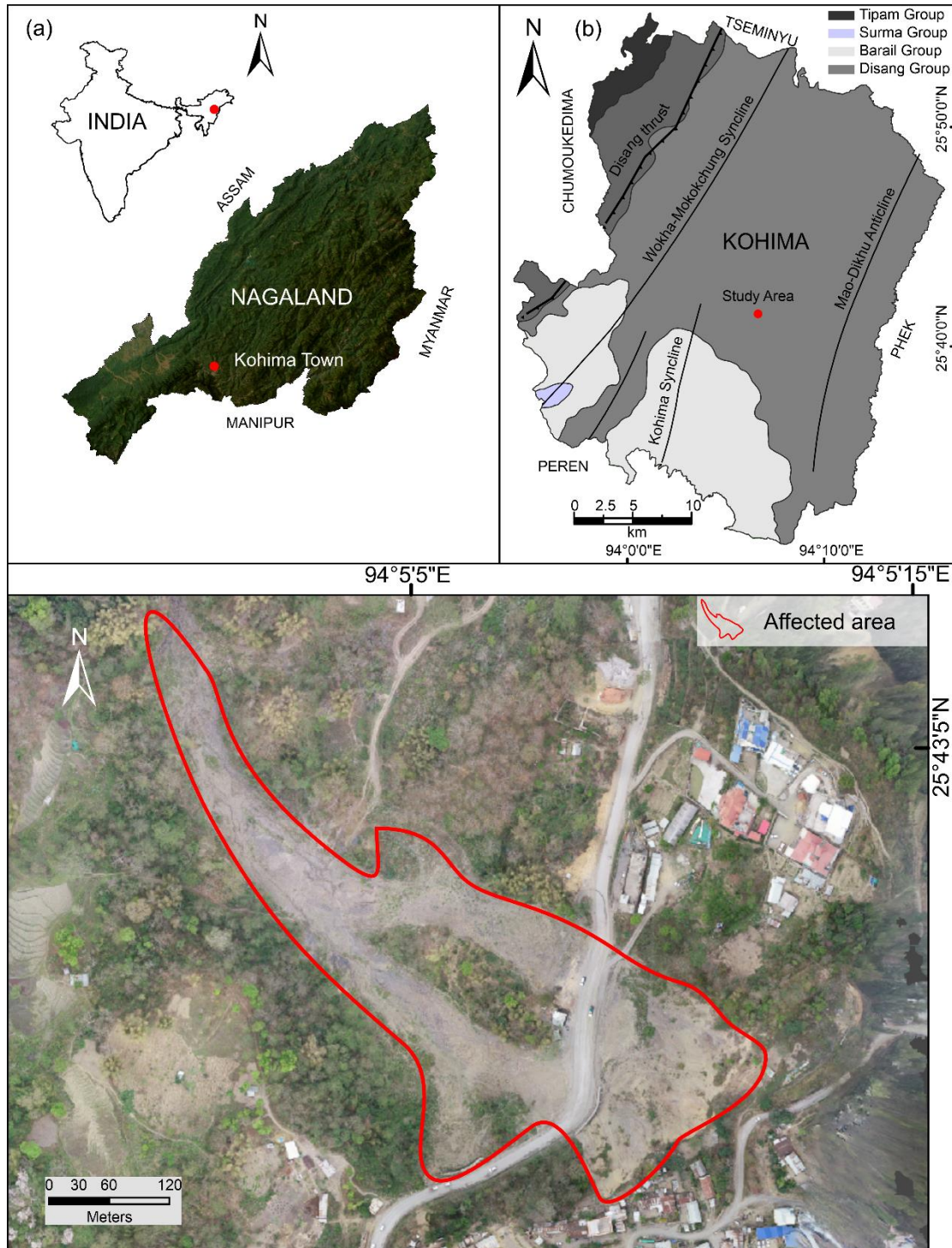
Fig. 4.6.1: Location map of Meriema area slide

The area has a general slope direction of 280°. Mass movement in the upper part of the area was initiated along the general direction of the slope. It diverted towards 320° further downslope. The total length of the slide is about 420 m. About 110 m of NH 2 was severely damaged, obstructing traffic for several days. The landslide affected an area of approximately 29,000 square meters. Residential houses surround the affected area. The slope is covered by variegated vegetation, with some agricultural lands in between. This highway connects most of the major districts of Nagaland with Kohima. At the crown is an agricultural tract, which shows signs of subsidence. Every year, this highway is damaged due to swelling and contraction of the earth material. Seepages are noted at several places, due to high groundwater levels.

4.6.2 Consistency limits

The liquid limit ranges from 25.00 to 62.00 (Table 4.6.1), which indicates low to very high swelling potential of the soils. The unusually high values of liquid limit points to the clayey nature of the soil, as exhibited by the plastic chart (Fig 4.6.2). The plasticity index ranges from 6.98 to 33.62, falling within the 0-35% range. Such soil types have a medium expansion potential (Peck et al., 1974), that is, they are prone to expansion on exposure to water, due to their clay mineral composition. The degree of shrinkage with values above 15 implies poor soil quality with the tendency to shrink when the soil dries. Samples 4 and 5 of this area exhibit medium soil quality. This is the moisture content when the soil stops shrinking. Except for samples 4 and 5, the remaining four samples exhibit S_L values above 15, indicating they have low swelling potential (Holtz and Gibbs, 1956). Sample 4 has very high swelling potential while sample 5 has medium swelling potential. The plasticity index also implies that samples 2, 3, 5, and 6 have high plasticity and cohesion (Prakash and Jain, 2002). While sample 1 is moderately plastic with a silt-clay composition, sample 4 is of low plasticity with a silty soil composition, which is partly cohesive.

Table 4.6.1: Consistency limits of six soil samples

Sample No	Liquid limit (W_L)	Plastic limit (W_P)	Plasticity index (I_P)	Shrinkage limit (S_L)
1	32.00	16.77	15.23	15.13
2	32.00	14.99	17.01	18.61
3	29.50	11.48	18.02	34.34
4	25.00	18.02	6.98	6.23
5	62.00	28.38	33.62	13.10
6	48.00	30.33	17.67	18.57
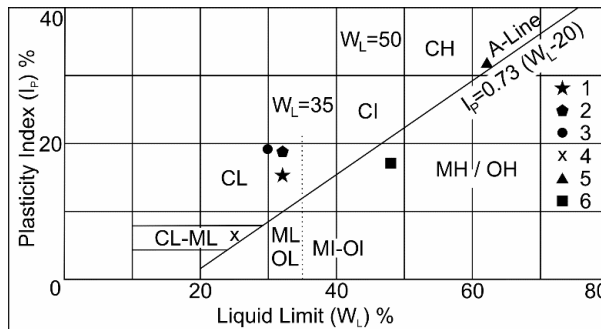
Fig. 4.6.2: Plasticity chart of the soil samples (M - Inorganic silt/very fine sand; C - Inorganic clay; O - Organic silt/clay; L - Low compressible and plastic silt/clay; I - Medium compressible and plastic silt/clay; H - High compressible and plastic silt/clay)

4.6.3   Direct Shear

The soil samples were tested for c, ϕ, and σ_{ci} (Table 4.6.2) and plotted (Fig. 4.6.3). The samples exhibit unusually low 'c' values that range from 8.23 to 19.76 kPa. Matthew et al. (2013) and He et al. (2022) attribute such values to excessive rainfall, which saturates the soils and increase the pore pressure. The 'ϕ' values range from 23.91° to 30.99°, indicating silty to sandy soils. According to Das and Sobhan (2018), low to medium values of σ_{ci}, as represented by the soils in this study, implies soft and firm soils.

Table 4.6.2: Shear strength parameters of the soils obtained from direct shear test

Sample	Cohesion (C) (kPa)	Internal Friction Angle (ϕ)	σ_{ci} (kPa)
1	08.65	31.55	30.92
2	13.43	25.81	42.84
3	16.78	30.99	59.29
4	19.76	28.95	67.03
5	18.24	25.84	58.21
6	10.80	23.91	33.21
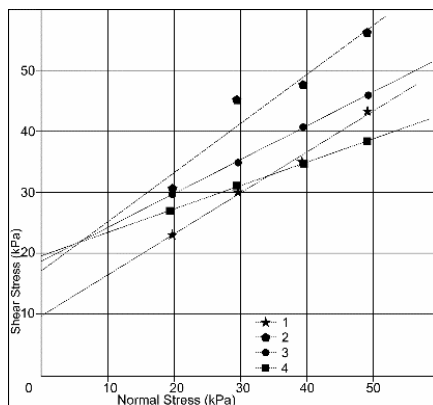
Fig. 4.6.3: Failure curves of samples

71

4.6.4 Back analysis

Probability analysis indicates that the deterministic safety factor is 0.415, with a failure probability of 100% (Fig. 4.6.4). This indicates that all analysed samples would have a FoS <1. In this area, an RI of -9.753 was obtained, which is insufficient for slope safety.
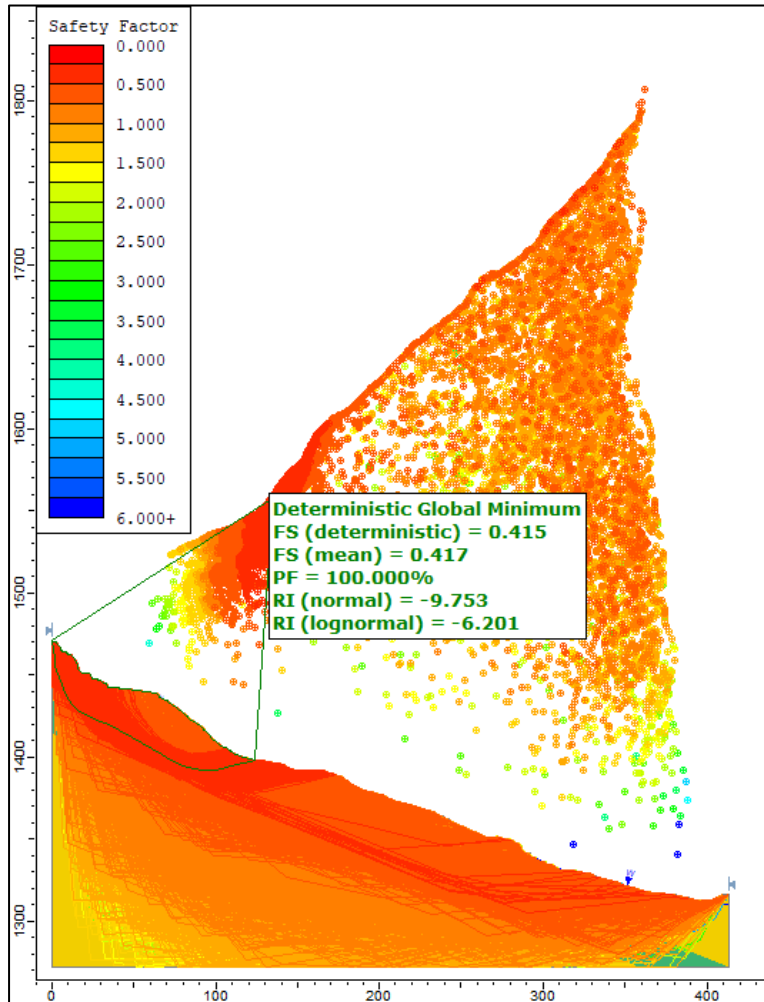
Fig. 4.6.4: Slope stability analysis with global minimum slip surface showing a safety factor of 0.415

4.6.5 Precipitation analysis

October, usually marking the beginning of the post-monsoon season, experiences comparatively lesser rainfall. October of 2017 exhibited a similar trend until 21st October 2017, and 29-30 October 2017 showed a dramatically high amount of rainfall. On 21st October, there was 69.96 mm of precipitation. At the same time, there was consecutive heavy rainfall on the 29 and 30 October 2017, with 54.35 mm and 44.8 mm, respectively. These were two to three times more than the daily average.

This sudden spike resulted in damage to the NH 2, affecting commuters in general. The month of October 2017 received 258.64 mm of rainfall, and September 2017 received 300.65 mm of rainfall.

Table 4.6.3: Precipitation data before and after the landslide event in October 2017

Date (October)	Precipitation (mm)	Date	Precipitation (mm)	Date	Precipitation (mm)
01	0.40	11	01.66	21	69.96
02	1.05	12	16.78	22	00.15
03	0.24	13	03.41	23	00.32
04	9.82	14	02.75	24	00.00
05	5.85	15	00.31	25	00.00
06	4.43	16	00.00	26	00.08
07	6.53	17	00.32	27	00.00
08	0.04	18	02.91	28	02.24
09	3.83	19	03.22	29	54.35
10	2.86	20	20.33	30	44.80
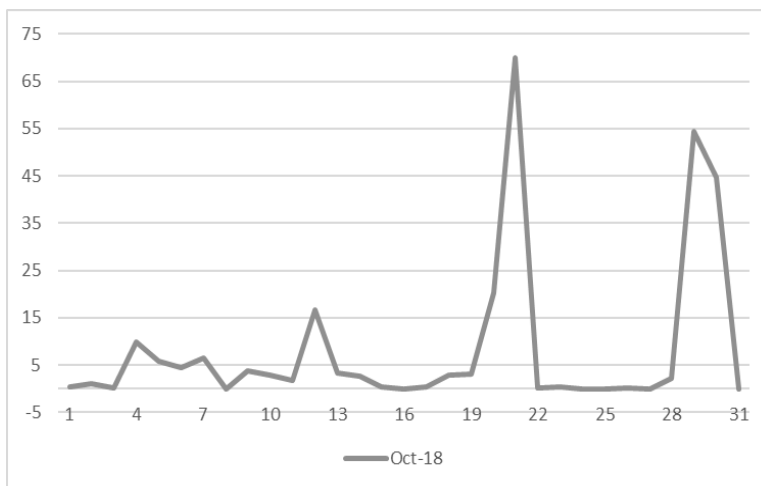
Fig. 4.6.5: Precipitation curve showing peak values at 32.68 and 51.60

CHAPTER 5

SMR, KINEMATIC AND STRUCTURAL ANALYSES

5.1   Pezielietsie Colony

5.1.1   Rock mass and slope mass rating

The point load test produced an average value of 4.8 MPa (Table 5.1.1). The value of 27 obtained for RMR falls in Class IV, which indicates weak rocks. The slope and dominant joint set J_1, with orientations of 60°-250° and 30°-281° respectively, were employed as factorial adjustments for the SMR. The score of 30.7 falls into Class IV, indicating unstable slope settings. Under such conditions planar or wedge failure may be expected.

Table 5.1.1: Slope mass rating

		Value or Condition	Rating
1	UCS	4.8 MPa	1
2	RQD	49%	8
3	Spacing of joints	75 mm	8
4	Condition of joints	Slickensided surface	10
5	Groundwater condition	Flowing	0
RMR = *1+2+3+4+5*			**27**
Class		IV	
6	$F_1 = (\alpha_j - \alpha_s)$	32°	0.15
7	$F_2 = \beta_j$	30°	0.70
8	$F_3 = \beta_j - \beta_s$ for plane failure where β_s = dip/angle of slope	-30°	-60
9	F_4 = Adjustment factor	Pre-splitting	10
SMR = *RMR+(F_1xF_2xF_3)+F_4*			***30.7***
Class		IV	
10	Description	Delicate rocks; unstable slope prone to wedge or planar failure	

5.1.2   Kinematic and structural analysis

The two other joint sets, J_2 and J_3, are orientated 40°-133° and 80°-108° respectively. The stereographic projection (Fig. 5.1.1) shows joint sets crossing to form a wedge to the southwest, which is consistent with the assumption made by SMR (Table 5.1.1). Field evidences also indicate wedge failure. The rose diagram of the joints of the study area depicts a significant NW-SE trend and a less prominent NNE-SSW trend (Fig. 5.1.2). The Anderson theory suggests that normal faulting has altered the rocks.

If faulting had occurred in both directions, either of the faults may have been reactivated.
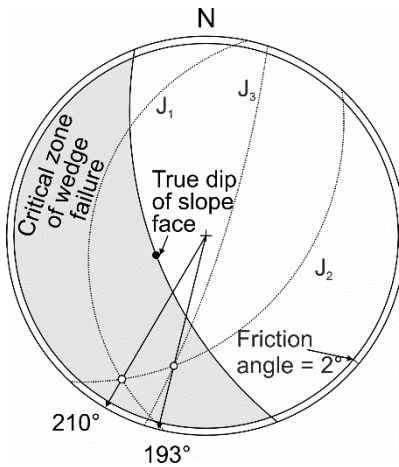
Fig. 5.1.1: Stereographic projection of slope and joints J_1, J_2 and J_3
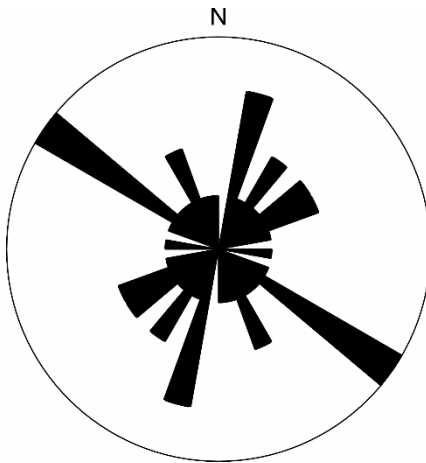
Fig. 5.1.2: Rose diagrams of rock joints of the study area

5.1.3 Paleostress analysis

Data from the first steam section was separated using function F5, resulting in a transpressive regime with tensors σ1 (34/188), σ2 (16/087), and σ3 (52/336) (Fig. 5.1.3a). With a stress ratio of 0.24 and a stress regime index (R') of 2.24, it has the greatest NNE-SSW shortening. Another tensor was determined using data collected from the upper horizon of the second stream section (Fig. 5.1.3b), south of F2. A purely strike-slip regime with tensors σ1 (21/241), σ2 (68/043), and σ3 (06/149) developed. It has a stress ratio of 0.44 and a R' of 1.56, with most stress in the NE-SW direction. The third tensor (Fig. 5.1.3c) was estimated from the lower horizon of the second stream section along plane F3, using σ1 (30/123), σ2 (09/027), and σ3 (58/282). It has a stress ratio of 0.67 and R' of 2.67 in pure compressive mode. The maximal horizontal stress

is oriented NNW-SSE. The NNE-SSW and NE-SW trends do not correspond to Nagaland regional compression pattern, which runs NW-SE. This may be attributed to the reactivation of faults in the study area.
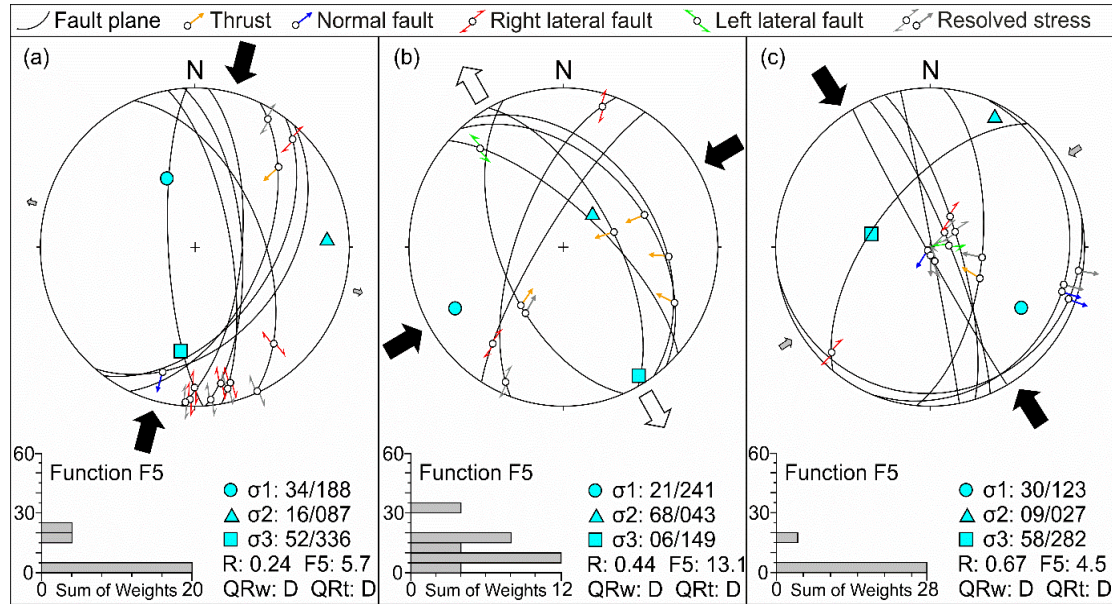
Fig. 5.1.3: Paleostress inversion of fault-slip data (Schmidt stereograph-lower hemisphere)

5.2   Peraciezie Colony (2017)

5.2.1   Rock mass rating and slope mass rating

An average value of 14.26 MPa was obtained from Point load tests (Table 5.2.1). The rock mass rating of the slope for rock condition falls in Class IV, which points to weak rocks. The slope and dominant joint set J_1, with orientations of 70° to 280° and 79° to 177° respectively, were employed as factorial adjustments for the SMR. The score of 36 falls in Class IV, indicating unstable slope settings; planar or wedge failure may be expected.

Table 5.2.1: Slope mass rating

		Value or Condition	Rating
1	UCS	14.26 MPa	2
2	RQD	23.09%	3
3	Spacing of joints	67.39mm	8
4	Condition of joints	Slickensided surface	10
5	Groundwater condition	Wet	7
RMR = 1+2+3+4+5			**30**
	Class	IV	
	Description	Poor rock	
6	$F_1 = (\alpha_j - \alpha_s)$	-103°	1

7	$F_2 = \beta_j$	79°	1
8	$F_3 = \beta_j - \beta_s$ for plane failure	9°	-6
9	F_4 = Adjustment factor	Pre-splitting	10
	$SMR = RMR+(F_1xF_2xF_3)+F_4$		**36**
	Class	IV	
10	Description	Bad; unstable; planar or big wedges	

5.2.2 Kinematic and structural analyses

The stereographic projection of the dominant joint and the slope attitude (Fig. 5.2.1) indicates wedge failure, which is also evident in the field. The rose diagram (Fig. 5.2.2) shows that the dominant trends of the joints are aligned along NE-SW, NNE-SSW, and WNW-ESE directions. The NE-SW trend corresponds with regional trend. The WNW-ESE trend points to synthetic shearing of the rocks.
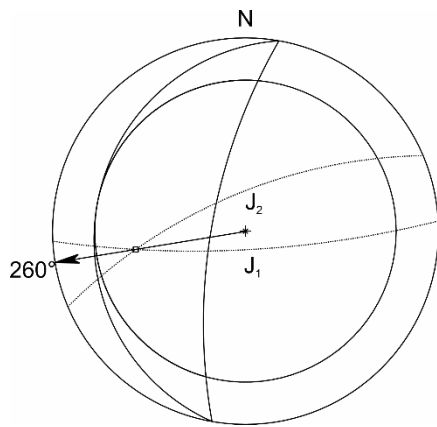
Fig. 5.2.1: Stereographic projection
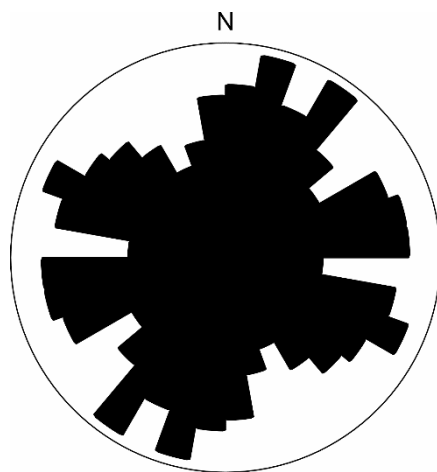
Fig. 5.2.2: Rosette

5.3 Peraciezie Colony (2018)

5.3.1 Rock mass rating and slope mass rating

The rock mass rating of the affected slope was evaluated after Bieniawski (1989) based on the five parameters of rock strength, rock quality designation, conditions of joints, and groundwater conditions in the field. The strength of the rock is determined at 2.4 MPa (Table 5.3.1) for the highly weathered and crumbled shales. This is equivalent to a rating of 7 on a rock mass rating system. The rock quality designation was calculated using the equation of Palmstorm (1982). A rock mass rating of 40 is obtained, which suggests that the rocks are of reasonable strength.

The slope and dominant joint set J_1, with orientations of 80° towards 245° and 77° towards 210° respectively, are used for the factorial adjustments to slope mass rating. The rating of 0 obtained, indicates Class V. It points to weak and very unstable slope conditions. Large planar or soil-like type of failure is expected on such slopes.

Table 5.3.1: Slope Mass Rating

		Value or Condition	**Rating**
1	Point Load Test	2.4 MPa	7
2	RQD	49%	8
3	Spacing of joints	73 mm	8
4	Condition of joints	Slickensided surface	10
5	Groundwater condition	Wet	7
RMR = 1+2+3+4+5			**40**
Class		IV	
Description		Poor rock	
6	$F_1 = (\alpha_j - \alpha_s)$	-35°	1
7	$F_2 = \beta_j$	77°	1
8	$F_3 = \beta_j - \beta_s$ for plane failure	-3°	-50
9	F_4 = Adjustment factor	Pre-splitting	10
SMR = RMR+(F_1xF_2xF_3)+F_4			**0**
Class		V	
10	Description	Weak and unstable slope prone to big planar and soil-like failure	

5.3.2   *Kinematic and structural analyses*

The cut slope and dominant joint sets (J_1 and J_2) are oriented 80° towards 245°, 77° towards 210°, and 82° towards 287° respectively. The joint sets J_1 and J_2 intersect to form a wedge towards S232°W (Fig. 5.3.1). This direction is related to the debris movement path at the landslide site. The joint set J_1 and the slope, with a strike difference of 35°, show some chance of planar failure. The rosette of the area shows a dominant NNE-SSW trend (Fig. 5.3.2). It also shows a WNW-ENE trend, which indicates synthetic shearing.
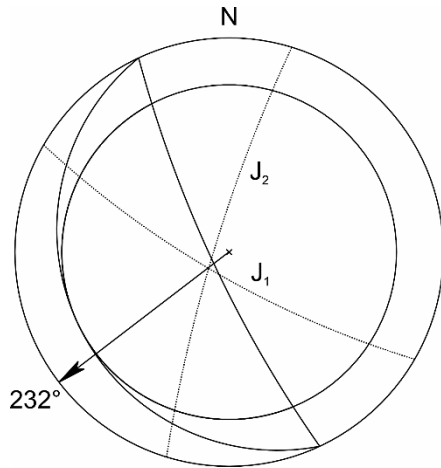
Fig. 5.3.1: Stereographic Projection
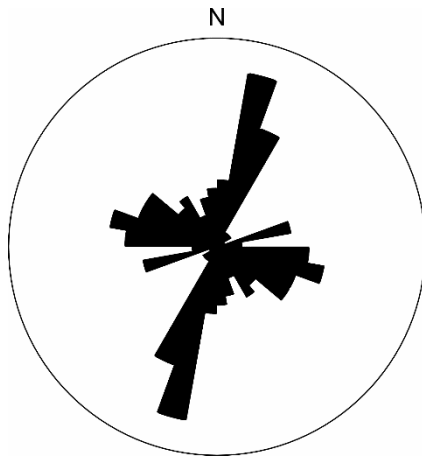
Fig. 5.3.2: Rosette

5.3.3 *Paleostress analysis*

A stress ratio of 0.28 and R' of 1.76 are obtained. The analyses yielded the following values: σ1 = 18/182, σ2 = 71/020, and σ3 = 05/274 (Fig. 5.3.3).
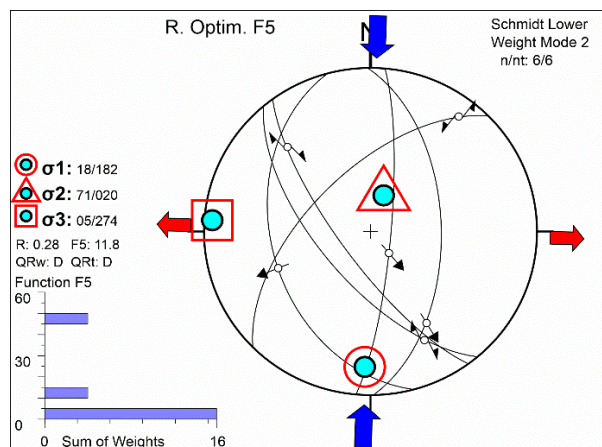
Fig. 5.3.3: Tensor generated by paleostress inversion as an effect of present-day thrusting in the region

79

5.4   Nhachüko

5.4.1   Rock mass rating and slope mass rating

The Disang shale samples of the study area exhibit low UCS values of 6.38 MPa (Table 5.4.1). These shale samples fall in stability Class IV. The Disang shales of a significant landslide near the present study area exhibit limited stability in Class IV. The RMR value of these rocks is 29. The SMR value for the slope is 39.

Table 5.4.1: Slope mass rating

		Value or Condition	**Rating**
1	UCS	6.38 MPa	2
2	RQD	34.15%	8
3	Spacing of joints	24.72 mm	5
4	Condition of joints	Slickensided surface, separation <1 mm	10
5	Groundwater condition	Dripping	4
RMR = 1+2+3+4+5			**29**
Class		IV	
Description		Poor rock	
6	$F_1 = (\alpha_j - \alpha_s)$	297°	0.15
7	$F_2 = \beta_j$	66°	1
8	$F_3 = \beta_j - \beta_s$ for plane failure	11°	0
9	F_4 = Adjustment factor	Pre-splitting	10
SMR = RMR+(F_1xF_2xF_3)+F_4			**39**
Class		IV	
10	Description	Unstable slope	

5.4.2   Kinematic and structural analysis

The joint data reveals two dominant joint sets (Fig. 5.4.1). Joint sets J_1 (66° due 312°) and J_2 (33° due 68°) form a wedge with a NNE (29°) trend. The combined data of the rocks in the rose diagram (Fig. 5.4.2) shows a NE-SW pattern, which is the regional trend in Nagaland.
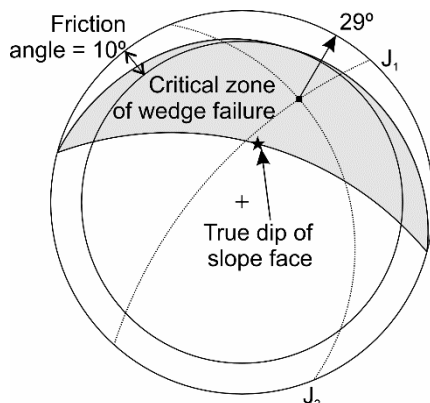
Fig. 5.4.1: Kinematic analyses depicting probable wedge failure towards 29° (wedge formed by the intersection of J_1 and J_2)
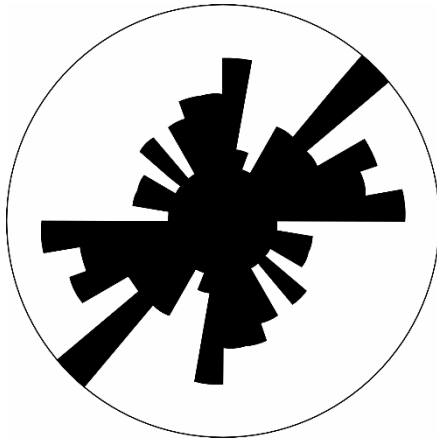
Fig. 5.4.2: Rose diagram of the joints of the study area

5.4.3   Paleostress analysis

Slickenside data was used to create a tensor (Fig. 5.4.3). The stress ratio of the stress ellipsoid (R) and the orientations of the three principal stress axes are four of six tensor components computed from the inversion of the slickenside data. A stress ratio of 0.49 was measured, resulting in a R' of 1.51. The analysis yielded the following values: $\sigma 1 = 04/135$, $\sigma 2 = 85/285$, and $\sigma 3 = 02/045$.
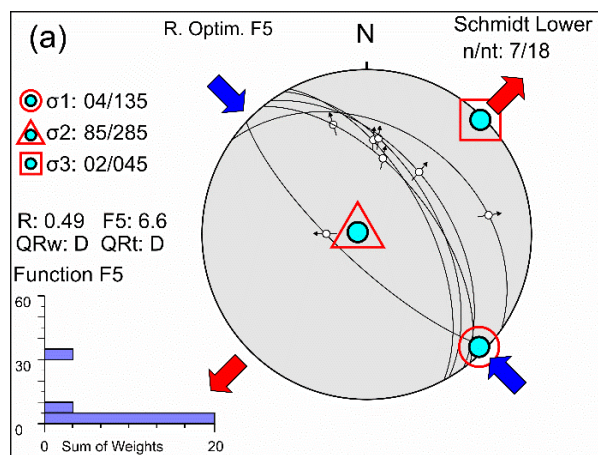
Fig. 5.4.3: Tensor generated by paleostress inversion as an effect of present-day thrusting in the region

5.5.   Perizie Colony

5.5.1   Rock mass rating and slope mass rating

An average value of 19.50 MPa was produced from point load tests (Table 5.5.1). The RMR value of 25 falls in Class IV, which indicates weak rocks. The slope and dominant joint set J_1, with orientations of 30° to 240° and 79° to 323° respectively, were used as factorial adjustments for the SMR. The SMR score of 35 falls into Class

IV, indicating unstable slope settings; planar or wedge collapse may be expected. Extensive corrective measures may be required.

Table 5.5.1: Slope mass rating

		Value or Condition	Rating
1	UCS	19.50 MPa	2
2	RQD	16.00%	3
3	Spacing of joints	221.16 mm	10
4	Condition of joints	Slickensided surfaces	10
5	Groundwater condition	Flowing	0
	***RMR* = 1+2+3+4+5**		**25**
	Class	IV	
	Description	Poor rock	
6	$F_1 = (\alpha_j - \alpha_s)$	83°	0.15
7	$F_2 = \beta_j$	79°	1
8	$F_3 = \beta_j - \beta_s$ for plane failure	49°	0
9	F_4 = Adjustment factor	Pre-splitting	10
	***SMR* = RMR+(F_1xF_2xF_3)+F_4**		**35**
	Class	IV	
10	Description	Poor, unstable, planar or large wedges, extensive corrective support required	

5.5.2   Kinematic and structural analyses

The cut slope and dominant joint sets (J_1 and J_2) are oriented 30° towards 240°, 79° towards 323°, and 51° towards 177° respectively. The joint sets J_1 and J_2 intersect to form a wedge towards S239°W (Fig. 5.5.1), which is the debris movement path in the slide zone. The rosette of the area shows NE-SW, NW-SE, and NNW-SSE trends (Fig. 5.5.2). These indicate normal faulting as well as thrusting and antithetic shearing in the region.
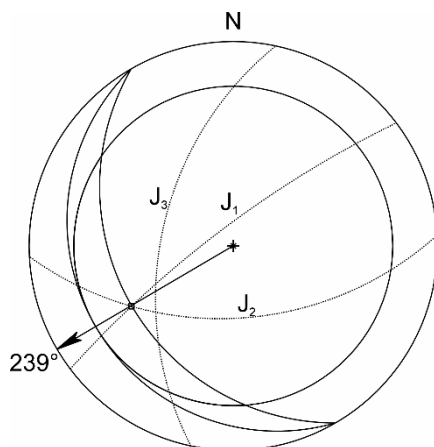
Fig. 5.5.1: Stereogram
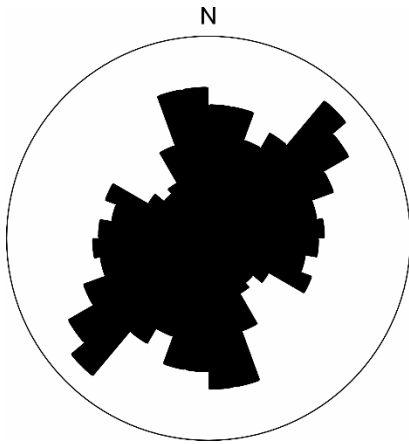
Fig. 5.5.2: Rose diagram

5.5.3   Paleostress analysis

A tensor was determined with σ_1 (13/278), σ_2 (08/186), and σ_3 (74/065) (Fig. 5.5.3). A stress ratio of 0.86 and R' of 2.86 was obtained. Data indicate a compressive regime.
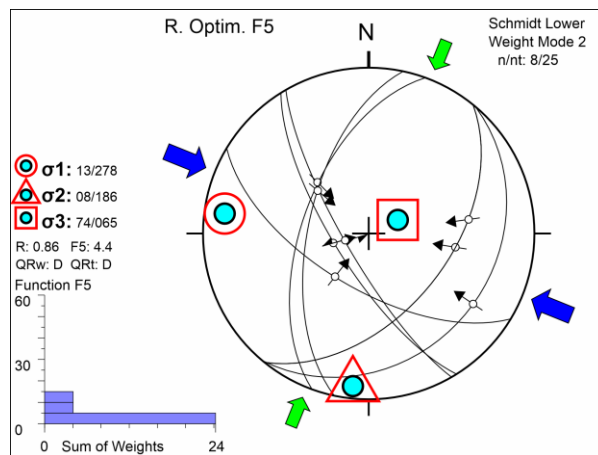
Fig. 5.5.3: Tensor generated by paleostress inversion as an effect of present-day thrusting in the region

5.6   Meriema area

5.6.1   Rock mass rating and Slope mass rating

Point load test results gave an average value of 20.66 MPa (Table 5.6.1). The RMR value of 35 obtained (Class IV) indicates weak rocks. The orientations of the slope and dominant joint set J_1 of 50° towards 320° and 51° towards 12° respectively, were employed as factorial adjustments for the SMR. The SMR score of 39 obtained falls into Class IV, indicating unstable slope conditions; planar or wedge failure may be expected.

Table 5.6.1: Slope Mass Rating

		Value or Condition	Rating
1	UCS	20.66 MPa	2
2	RQD	16.00%	3
3	Spacing of joints	221.16 mm	10
4	Condition of joints	Slickensided surfaces	10
5	Groundwater condition	Damp	10
RMR = 1+2+3+4+5			**35**
	Class	IV	
	Description	Poor rock	
6	$F_1 = (\alpha_j - \alpha_s)$	-308°	1
7	$F_2 = \beta_j$	51°	1
8	$F_3 = \beta_j - \beta_s$ for plane failure	1°	-6
9	F_4 = Adjustment factor	Pre-splitting	10
SMR = RMR+(F_1xF_2xF_3)+F_4			**39**
	Class	IV	
10	Description	Unstable slope condition; Planar or big wedges	

5.6.2   Kinematic and structural analyses

The cut slope and dominant joint sets (J_1 and J_2) are oriented 50° towards 320°, 51° towards 12°, and 80° towards 221° respectively. Joint sets J_1 and J_2 intersect to form a wedge towards N305°W (Fig. 5.6.2). This direction is related to the debris movement path in the slide zone. The rosette of the area shows NE-SW and NW-SE trends (Fig. 5.6.3). These suggest normal faulting as well as thrusting in the region.
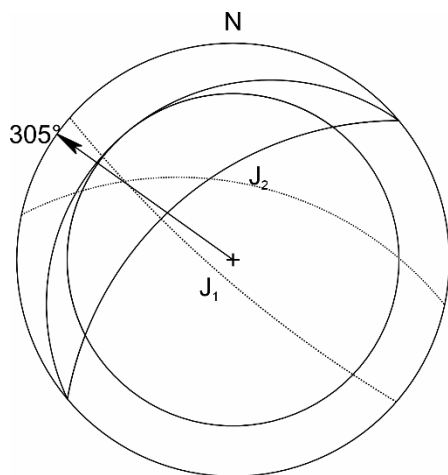
Fig. 5.6.1: Stereographic projection
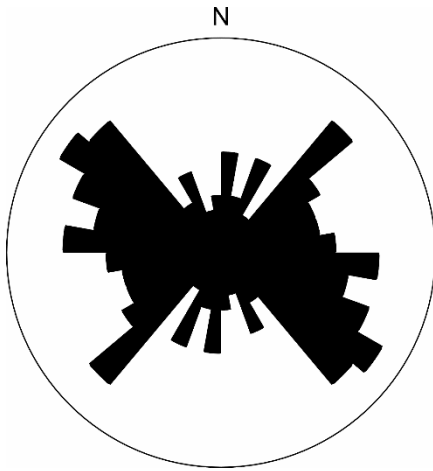
Fig. 5.6.2: Rosette

5.6.3 *Paleostress analysis*

Inversion of the slickenside data produced a tensor (Fig. 5.6.3) that was determined with σ_1 (63/334), σ_2 (09/083), and σ_3 (25/177). A stress ratio and R' of 0.82 were obtained, indicating an extensive regime.
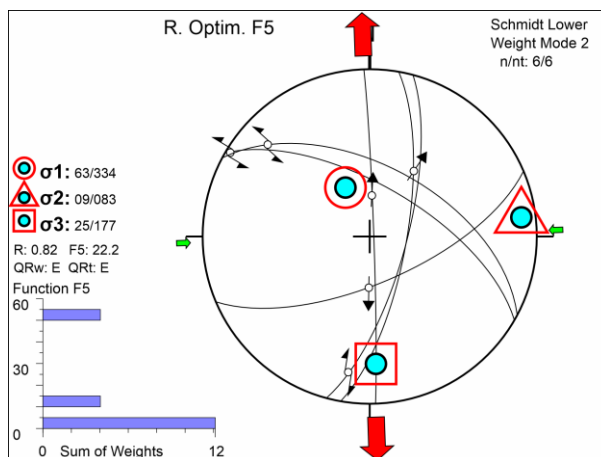
Fig. 5.6.3: Tensor generated by paleostress inversion as an effect of present-day thrusting in the region

CHAPTER 6

DISCUSSION, MITIGATION / REMEDIAL MEASURES AND CONCLUSION

6.1   Discussion

This study dwells on six landslide events during 2017 and 2018 in the northern part of Kohima Town of Nagaland. The six landslide zones experienced slope failure mainly due to the influence of water. The monsoon rains were responsible for the devastation of the slopes. Peraciezie Colony was affected by landslides adjacent to each other during both years (Fig. 6.1.1a, b). Pezielietsie (Fig. 6.1.1c), Nhachüko (Fig. 6.1.1d), Perizie (Fig. 6.1.1e), and Meriema (Fig. 6.1.1f) faced disasters during 2017.

The main focus of this chapter is the analysis of monsoon landslides and an anthropogenically induced landslide, emphasising on geological precursors, slope condition, and the role of human activity in the landslide events. The chapter highlights the need for awareness of the effects of human activity in worsening weak slopes and calls for the government to ensure a safer environment.

Fig. 6.1.1: Extent of damage at (a) Peraciezie, 2017, (b) Peraciezie, 2018, (c) Pezielietsie, (d) Nhachüko, (e) Perizie, and (f) Meriema

6.1.1   Geotechnical analyses

According to Snethen et al. (1977), liquid limit values of <30% have low swelling potential, while those with values >60% are considered very high. Samples with lower liquid limits tend to lose strength at lower moisture concentrations and are

thus prone to failure due to rainfall with the onset of monsoon. Of the 34 samples analysed from the six landslide zones, 35.29 percent of the samples exhibit low swelling potential, 47.06 percent show medium swelling potential, 14.71 percent have high swelling potential, and 2.94 percent show very high swelling potential. Most samples from the slide zones of Pezielietsie, Nhachüko, and Perizie colonies are in the medium category. One sample from the Meriema slide zone shows very high swelling potential, as the road bulges with the introduction of water (Fig. 6.1.2). These values are in line with the shrinkage limit values.

Fig. 6.1.2: Swelling of road sections along NH 2 at Meriema due to clayey soils

According to Casagrande (1948), soil samples with low, medium, and high plasticity exhibit varying compressibility levels. The abundance of fine sand in the various landslide masses may account for the low plasticity of the soils. According to the Bureau of Indian Standards (1970), the liquid limits of such soils indicate low to moderate compressibility. Dumbleton (1968) opines that such soils show moderate swelling potential. As subsurface water percolation rises, very fine soil particles in suspension move through the pervious crust and highly fissured subsurface rocks. This results in the retention of coarser particles, such as silt and fine sand, resulting in diminished soil flexibility, which some studies attribute to a reduced swelling potential (Al-Homoud et al., 1995), as observed in the analysis of the samples of the affected areas. According to Stanchi et al. (2016), soils with low liquid limit values, such as those seen in samples of the study area, can attain liquid limit more quickly, indicating the ability to rapidly transition from a semi-solid to liquid state when

moisture content increases. Any abrupt disturbance would cause the soil to flow, placing the slopes at risk of failure. According to Hobbs et al. (2019), soils with high shrinkage limits show more significant volume changes with changing water content. Frequent and cyclic drying and wetting during dry spells and heavy precipitation respectively, have a strong influence on soil shrink-and-swell behaviour, which can deform slopes and damage man-made structures (Guney et al., 2007; Nowamooz and Masrouri, 2008), as is common with the soils in the study area.

The consistency test and the plasticity chart help determine the type of soil present in each landslide area. The affected areas mostly have cohesive soils like silt and clay in varying combinations. Observations show that in areas of clayey soils, their expansive nature causes physical changes on slopes, which tend to be more destructive. Seasonal changes also create havoc to the slopes, as the shrink-swell nature of the soils ultimately render slopes unstable. This particular phenomenon is observed in the Meriema slide zone, where the affected area is damaged every monsoon (Fig. 6.1.2). Geotechnical analyses reveal weak soils that are prone to failure as water volume fluctuates.

As observed from the plasticity charts of all the affected areas (Figs. 4.1.2, 4.2.2, 4.3.2, 4.4.2, 4.5.2, and 4.6.2), silty, clayey, and sandy soils of low plasticity blanket the Disang shale that contain thin intercalations of mudstone and siltstone. The soils are fragile, with low cohesion, low UCS, and moderate internal friction angles, which are depicted from their shear strength charts (Figs. 4.1.3, 4.2.3, 4.3.3, 4.4.3, 4.5.3, and 4.6.3) and noted in the field.

According to Das and Sobhan (2018), UCS values reported from direct shear test, similar to that of the study area, indicate soft soils with low plasticity. These soils have limited flexibility because of high concentration of coarser particles. As a result, the water retention capacity is limited, and hence, the soils often fail, even at low water contents. According to Malizia and Shakoor (2018), the drop in UCS from moderate to low plasticity, in soils such as those of the study area, implies that the compressive strength of soil samples reduces as plasticity diminishes. Higher cohesion values in some areas are synonymous with higher values of liquid limit.

6.1.2   Slope mass rating

Except for the Peraciezie slide of 2018 (Table 5.3.1), the SMR values of the other slides fall in Class IV, indicating slope conditions with high risk of failure, particularly during or after continuous and/or heavy rainfall. The Class V status of the 2018 Peraciezie slide points to precarious slope conditions. This is evident from the extent of the slide (Fig. 6.1.3) as well as the continuous failure of the crown section after the main event (Fig. 6.1.4). The low values of point load test of the affected sites indicate that the rocks are very weak and highly prone to slope failure.

Fig. 6.1.3: Peraciezie slide, 2018

Bieniawski (1989) classifies rocks with RMR values of 25-40, as estimated in the study area (Tables 5.1.1, 5.2.1, 5.3.1, 5.4.1, 5.5.1, and 5.6.1), in Class IV. These are rocks with cohesiveness of 100-200 kPa and friction angles ranging from 15° to 25°. Clay infilling is widespread in these rock masses due to the ease with which surface runoff infiltrates the numerous joints and fractures. The low UCS values of these rocks indicate that they are still weathering due to seasonal changes in groundwater levels and artesian conditions.

The weathered shales are particularly sensitive to water. They are prone to rapid decrease in shearing strength in the presence of excess water, which reduces slope stability. Erguler and Ulusay (2009) found that increasing water content reduced UCS by up to 90 percent on clay-bearing rocks. Pellet et al. (2013) demonstrated that

water saturation lowers the cohesiveness and internal friction angle of clay-filled rocks, resulting in a 50 percent drop in strength. The fresh shales are fragile in some of the slides (Fig. 6.1.5).

Fig. 6.1.4: Fractured shale at crown (Box - unstable scarp) in Peraciezie, 2018. Changes at crown: a) 30th August 2018; b) 13th September 2018; c) 31st August 2019

Fig. 6.1.5: Shale outcrop with large open fractures at Pezielietsie slide zone (2018)

6.1.3 Kinematic and structural analyses

The lineaments of the study area, corroborated by joint data, indicate local-scale faults that may be splays of major faults in the region. These comprise normal, reverse, and strike-slip faults caused by tensile and shear loads centred in the NW-SE compression direction. The interaction of these forces has resulted in the formation of hybrid faults, which have significantly damaged the rocks. Part of these pulverised rocks have weathered to clays, making them more vulnerable to slope failure during the monsoon.

The rocks in and around fault zones are infested with slickensides (Fig. 6.1.6), which are caused by the grinding of rock layers and crystal deposition during slip (Ramsay and Huber, 1987). They can be used to determine the sense of shear on fault surfaces (Samant et al., 2017). Slickenside is a non-penetrative lineation that serves as a kinematic signal to assess the direction of sliding along a fault (Mukhopadhyay et al., 2019). Several writers have contributed to defining and classifying slickensides (Angelier, 1994; Doblas, 1998).

The two dominant joint sets, J_1 and J_2, form a wedge that trends SSW at Pezielietsie (Fig. 5.1.2), WSW at Peraciezie (2017) (Fig. 5.2.2), SW at Peraciezie (2018) (Fig. 5.3.2) and Perizie (Fig. 5.5.2), NNE at Nhachüko (Fig. 5.4.2), and NW at Meriema (Fig. 5.6.2). In the wedge mode of failure, the plunge of two intersecting discontinuities falls inside the critical zone. It is less than the dip angle of the slope face but larger than the friction angle of the slope material (Hoek and Bray, 1981). According to structural orientations, these conditions have been duly satisfied in this study, where the crossing joint sets are within the darkened section denoting the Critical Zone. Therefore, slope failure is inevitable when the frictional limit is exceeded.
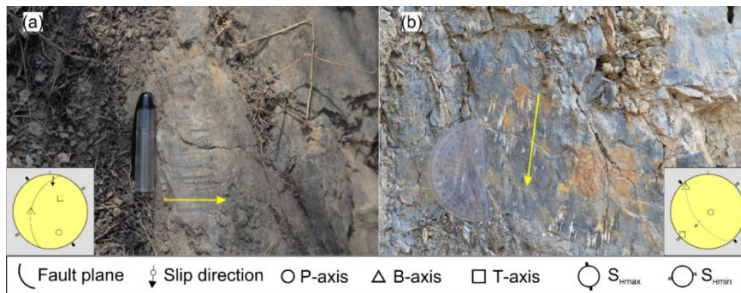
Fig. 6.1.6: Fault planes with slickensides (Inset-Schmidt stereonet displaying kinematic axes) and slide directions (yellow arrows) (a) Slickensided surface with reverse fault and sinistral movement; (b) Normal fault

The Disang rocks in all the landslide zones provide evidence of the interaction between the Indian Plate and the Burma microplate. The NE-SW pattern of rock joint data observed in most parts of the study area shows the influence of regional folding and thrusting in this area. Some NNW-SSE trends in the Perizie colony show antithetic shearing or sinistral strike-slip faulting, whereas the ENE-WSW trend at Peraciezie (2017) and Nhachüko show secondary synthetic shearing. The study area displays the effects of such interactions in the form of sheared (Fig. 6.1.7), fractured, and jointed rocks, and slickensided surfaces. The dominant WNW-ESE trend in Peraciezie (2018) and less conspicuous trends in Perizie and Meriema correspond to synthetic shearing of the rocks. The joints of the Pezielietsie colony and Meriema area exhibit NW-SE trends that align with the thrust direction of the region.
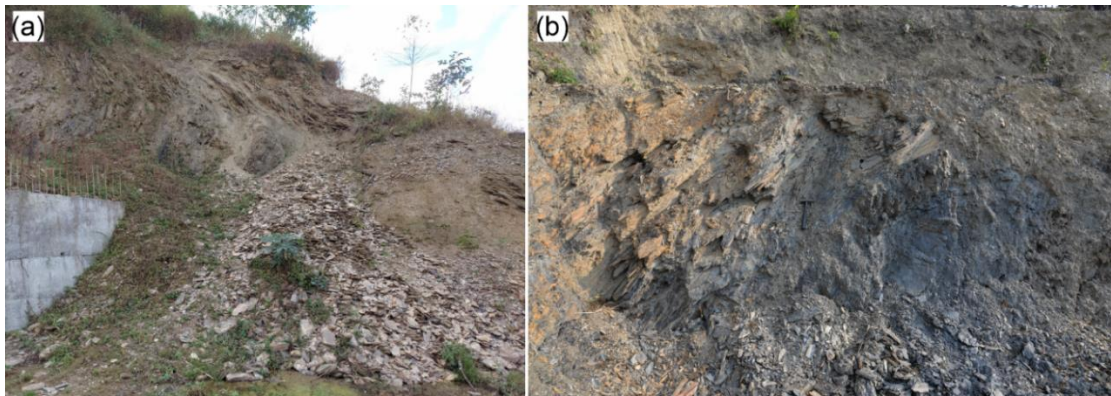
Fig. 6.1.7: (a) Folded and brittle rocks; (b) Sheared rocks

6.1.4 Back analyses

Back analysis of the affected slopes using the Cuckoo Search algorithm and the Janbu Simplified approach yield estimated FoS values ranging from 0.417 to 0.829, which indicate 85.90 to 100 percent probability of failure. A reliability index of 3 is considered the minimum value of slope reliability; hence reliability indices ranging from -9.753 to -1.096 indicate that the slopes are highly vulnerable to failure. The negative values of the reliability index of all the affected sites also imply that the mean factor of safety is below 1. In constructing a house or road in hilly terrain, a portion of the slope is cut to accommodate the development. In doing so, the stability of the slope becomes a crucial measure for which numerical modelling is integrated with geotechnical and geological studies so as not to be affected by future failure. To handle such situations, the reliability index and slope safety factor become very important tools in designing cut slopes. Though all the sites are vulnerable to failure,

the Meriema slide exhibits the highest vulnerability with a RI value of -9.753 (Fig. 4.6.4). The least vulnerable of the six sites is in the Pezielietsie colony with a RI value of -1.096 (Fig. 4.1.4). Back analysis shows that the friction angle of the soils has a greater impact on slope stability than cohesion (Fig. 4.1.5).

6.1.5   Paleostress analyses

σ1 is vertical in the Meriema slide (Fig. 5.6.3), pointing to an extensional stress axis. σ2 in Peraciezie (Fig. 5.3.3) and Nhachüko (Fig. 5.4.3) is synonymous with a strike-slip stress axis. σ3 in Perizie (Fig. 5.5.3) aligns with a compressional axis. In Pezielietsie, σ2 and σ3 are the vertical axes (Fig. 5.1.3). Besides the orientation of the three principal axes, σ1, σ2, and σ3, the stress ratio obtained from paleostress analysis also assists in determining the actual type of stresses acting in the study area. The stress ratio determines the direction of shear stress on each plane and defines the geometry of slip-on fault planes. In the Pezielietsie (Fig. 5.1.3a) and Peraciezie landslide zones (Fig. 5.1.3a), a transpressive regime with components of thrusting and strike-slip faulting is noted. A pure strike-slip regime was determined in Pezielietsie (Fig. 5.1.3b) and Nhachüko. A pure compressive regime affiliated to reverse faulting was defined at the Perizie and Pezielietsie colonies (Fig. 5.1.3c). Paleostress analysis of the Meriema slide zone indicates an extensive regime corresponding to normal faulting.

The stress ratio determines the direction of shear stress in each plane and defines the geometry of slip on fault planes. The greatest shortening (σ1) is oriented along the NW-SE direction, which is the compression and thrust direction of the region. The S_{Hmax} azimuth (maximum compression direction) of the slickenside is NW-SE (Fig. 5.4.3). This direction corresponds to normal faulting, which runs parallel to the regional compression direction. Slickenside data analysis is consistent with joint analysis. The slickened surfaces caused by stress are well retained along the joint planes.

The tensors obtained at Peraciezie have S_{Hmax} oriented NNE-SSW, NW-SE at Perizie, ENE-WSW at Meriema, NW-SW at Nhachüko, and NE-SW at Pezielietsie. The horizontal maximum shortening axis, S_{Hmax} (Fig. 5.1.3a) in Pezielietsie aligns with slope failure direction (Fig. 5.1.1) obtained from kinematic analysis. The S_{hmin} extensional directional of the paleostresses at Nhachüko aligns with that of the failure

direction of the slide obtained by the Markland's test (Fig. 5.4.1). The affinity of kinematic with paleostress analyses suggests that paleostresses in the study areas have been instrumental in the deformation of the rocks and overall instability of the slopes. The weakening of rock material due to paleostresses have facilitated the landslides of the study area, which other factors augment.

Paleostress analysis is especially useful because little is known of the relationship between instability and discontinuity. By isolating fracture systems and deriving paleostress tensors such as transtensional and compressive stress tensors, the study identifies locations at high risk of slope collapse due to structural orientations and weaknesses. This approach provides useful insights into the elements that contribute to slope instability and aids in projecting future failures, allowing for better risk assessment and disaster mitigation tactics in areas prone to structure-controlled landslides (Igwe and Okonkwo, 2016). All types of stress regimes have been observed in and around the township. The combination of all these faults within a small area can imply the dynamic nature of tectonism that this area has experienced.

6.1.6 *Precipitation Analyses*

The six landslide areas experienced slope failure due to the influence of water. The monsoon heralded the devastation of slopes in 2017 and 2018. Two portions of Peraciezie colony adjacent to each other, were affected by landslides during these years. Pezielietsie, Perizie, Meriema, and Nhachüko faced disastrous events in 2017. As regards the impact of precipitation on landslides, the Meriema slide was significant, compared to the five others in that it occurred after the monsoon.

Even during the dry season the landslide zones of the study area have an abundance of subsurface water, which has led to extensive weathering of the fractured rocks. Thus, the slopes are extremely weak. The study areas experienced considerable rains days before failure of the slopes. Rainwater percolation through the pervious soils would have produced severe pore-water pressure at saturation. The saturated soils reached the plastic stage, where plastic deformation occurred. Further saturation increased the water content of the soils above the liquid limit, creating viscous fluids. Lambe and Whitman (1979) found that soil cohesiveness, friction angle, and bearing capacity decrease significantly through the change from plastic deformation to a viscous fluid state. In addition to a decrease in strength, the weight of saturated soils

increase. This significantly strains weak soils, loose debris, and underlying rocks (Chung, 2019), mostly low-strength shales, and downslope forces quickly exceed their resistance in the landslide areas. Under such conditions, slope collapse is almost certain.

Excess rains lead to percolation of water into the pore spaces of soils, which serve as matric suction and hold the soil particles together. Matric suction, in turn, contributes to soil stability. With increasing groundwater percolation and levels, the matric suction is reduced, thereby reducing the factor of slope safety. It has been observed that rapid reduction in matric suction leads to shallow failure at the toe of landslides, which implies that a gentle slope could also experience failure (Mao et al., 2020; Balakrishnan and Ganapathy, 2022). With increase in pore pressure, slope stability and matric suction decrease gradually (Li et al., 2020). Therefore, landslide areas are expected to experience increased pore pressure and reduced matric suction, which ultimately reduce slope stability during heavy and continuous downpours.

Water interacts with clayey soils to alter their internal structure, which reduces the overall strength of the soil (Wang et al., 2020). Each landslide has some clayey soil that could have been affected by interaction with rainwater. The Meriema slide exhibited swelling deformation at the time of slope failure, which can be attributed to the interaction of rainwater as well as high groundwater levels with the clayey soils. The other five areas also have high clay content, which may be the cause of slope failure.

Five of the study areas, except for Meriema, experienced heavy rainfall with elevated groundwater levels prior to failure. The Meriema slide was a post-monsoon event, which was also marked by high groundwater levels. Similar situations have been observed in the other landslide areas, where high precipitation and elevated groundwater levels triggered medium- to large-scale landslides. Water from rainfall reduces the shear strength of soils, thereby affecting their overall stability, which in turn reduces the factor of safety. The extensively fractured top soils and subterranean rocks soon absorbed most water.

6.2   Mitigation / Remedial measures

6.2.1   *Efficient drainage system*

Water is a major contributor to landslides, so draining surface and shallow subsurface water at vulnerable sites can enhance the stability of landslide-prone slopes. Surface water should not be permitted to accumulate or flow on landslide-prone slopes. Surface water should be diverted away from landslide-prone areas by channelling into lined ditches or sewage pipes to the base of slopes. Trenches loaded with gravel, perforated pipes, and pumped water wells can be used to drain shallow groundwater. Sewers should be kept in good condition to avoid leaks, and lawns and vegetation should be watered sparingly. Clayey soils and shales are low in hydraulic conductivity, so may be difficult to drain. Drains were constructed from the head of the slide to channelise water in the Pezielietsie and Peraciezie colonies after the 2017 slide (Fig. 6.2.1). At the right edge of the Perizie colony slide, a temporary drain was excavated to train water out of the landslide zone.

Fig. 6.2.1: Drainage construction for surface runoff at Peraciezie colony, 2017

Awareness of the benefits of good drainage systems is important in all affected areas, which should include Kohima town as well. Landslides at the Pezielietsie,

Peraciezie, and Perizie colonies could have been averted if good drainage systems were in place earlier. The construction of such basic infrastructures can help reduce the impact of worsening slope conditions.

6.2.2 *Retaining walls and gabions*

On the basis of estimation of slope mass rating following Romana (1985), some remedial and/or mitigation measures may be suggested from detailed fieldwork and engineering. From SMR values that range from 25-40 in the six landslide zones, re-excavation of the walls may be a good idea. Shallow surface and deep drains along the slopes is necessary for all the landslide areas. Retaining walls have been constructed at the toe of the 2017 Peraciezie slide (Fig. 6.2.2a), the crown of the Nhachüko slide (Fig. 6.2.2b), and along the highway section of the Meriema slide (Fig. 6.2.2c) to arrest further movement of slope material. Gabions filter water, reduce erosion, and help stabilize slopes by lowering groundwater levels, supporting load variations, and improving safety factors. Hence, they reduce landslide formation (Trojnar, 2020;Fan et al., 2021). An example of this can be seen along the Meriema slide zone to control further sliding of slope debris (Fig. 6.2.3).

Fig. 6.2.2: Construction of retaining walls (a) at the toe of 2017 Peraciezie slide, (b) Nhachüko slide zone, (c) along the National Highway at Meriema

Fig. 6.2.3: Gabion wall at Meriema slide zone

6.2.3   Bamboo piling to arrest further sliding of affected slopes

Bamboo is a viable and environmentally beneficial material for stabilising landslide-prone slopes. This bioengineering strategy for slope stabilisation can be used in mountainous areas where bamboo is abundant, to support civil constructions (Maddalwar et al., 2024). The benefits of bamboo have been demonstrated in slope stabilisation and erosion prevention. Bamboo can be utilised as reinforcement material, either in its natural state or processed to form bamboo tube piles. Such structures stabilise the soil by allowing air and water seepage without interfering with soil interaction and material transfer. This traditional method of arresting slope movement by bamboo piling has been used in most of the affected areas (Fig 6.2.4a, b).

Fig. 6.2.4: Bamboo piling at (a) 2017 Peraciezie slide; (b) Perizie slide

6.2.4   Agroforestry

Trees and grass can reduce the amount of water that enters the soil and prevent erosion due to surface water flows. Though vegetation cannot prevent a landslide, removing vegetation from a landslide-prone slope may cause one. Agroforestry with trees, grass cover, and crops may be a valuable management method and a viable option for sustainable agricultural systems on sloping terrain, since it lowers soil erosion. The various layers of agroforestry can be used to stabilise and recover landslide-affected areas, contribute to land management, and limit the adverse effects of landslides (Moreira et al., 2012; Mufidawati et al., 2021). Though plants and trees can enhance soil strength, raise slope safety, and decrease landslide risk caused by rainfall, not all are suitable for landslide mitigation (Naredla and Sangeetha, 2022).

6.2.5 Restriction of constructions on unstable slopes

Constructions on unstable slopes should be discouraged, particularly at the crown and toe (Parkash, 2019). Proper slope engineering practices have to be considered when undertaking any construction work. Terracing with reinforced bamboo walls is an effective way to control construction on unstable slopes as it tends to reduce the probability of slope failure, thereby increasing the factor of safety and reliability index of the slope. Slope stability analysis using LEM and FEM methods can be used to analyse slope conditions by incorporating several physical measures and examining their impact on the slope (Kamal et al., 2023). Knowledge gained from deducing the shear strength characteristics of slope material, slope height and gradient, etc. can help restrict construction on unstable slopes (Zeng et al., 2024). But ultimately, government policies have to be firmly in place.

6.2.6 Public Awareness

Researchers, public, and the government should work together to improve slope stability and reduce the future impact of affected slopes. The effects of human activity on weak slopes must be discussed in public. A terrain such as Kohima, which is criss-crossed by numerous fault splays, and located between several large faults of the region, is liable to be affected by ongoing tectonism. Human actions can aggravate the situation on unstable slopes. The local community and government together need to enhance disaster risk reduction through commitment, regular audit, and increased stakeholder involvement to improve the landslide disaster mitigation system (Fathani et al., 2016). Studies by several researchers in the region can be used to protect buildings, lives, and the environment from landslides through better planning (Samodra et al., 2018).

6.2.7 Monitoring slope movements

Slopes affected by landslides continue to be in a state of movement that pose danger to residential areas, as well as commuters on roads. Hence, it is important to monitor slope movements to assess the danger, and mitigate potential loss to lives and properties. Continuous drone mapping can enable the detection of change in slope movements (An et al., 2018; Xin et al., 2024). Various techniques using Lidar, radar, total station, GPS, and micro-seismic monitoring can assist in monitoring changes along slopes (Singh et al., 2024). A cost-effective method based on wireless image transmission using GPRS technology, offers accurate detection while saving time

(Peng et al., 2020). Using multi-point tilting sensors and pipe strain gauges, in addition to water levels and rain gauges, have proven to be successful in detecting slope movements and offering early warnings (Sheikh et al., 2020).

6.3   Conclusion

Multiple landslides affected Kohima town in 2017 and 2018 following heavy and continuous rains. Of the affected areas, six covering the northern part of the township were taken up for this study. One of the purposes of this study was to determine the role of human activity in inducing landslides in Kohima town. These landslide zones are part of a tectonically dynamic terrain, where active faulting is responsible for weakening of the lithology. Geotechnical analysis indicates that the soils are weak. Numerous tension fractures in the soils and rocks of the study area have rendered them weak and highly pervious. In such areas of fissured soils and rocks with high infiltration rates, the slopes tend to become unstable during continuous and heavy rainfall. At Pezielietsie, if further sliding occurs, the peripheral subsidence zones are also in danger of sliding down. Geotechnical studies indicates that these weak soils are prone to further failure with changes in water volume. Even during the dry season, the affected area has a significant groundwater level, which is evident from the seepages at Perizie, Nhachüko, and Meriema. Springs and wells are common in Pezielietsie, Peraciezie, and Meriema. High water tables have contributed to the continuing deterioration of the rocks and soils.

The exposed shales show varying degrees of weathering. RMR data reveal weak Disang rock masses, while SMR data indicate unstable slope conditions. Kinematic studies reveal that the rock slopes fail as wedges. These findings confirm that the slopes are usually very weak. Back analysis highlights unsafe slope conditions. The subsurface shales of the slopes in all the study areas are fresh but very brittle and commonly fractured; geomechanical analysis indicates weak rocks that are highly prone to failure. The rocks of the slide zone are highly jointed, fractured, and sheared to varying extents.

The hillside seepages and high water tables in some open wells observed in the study areas may be due to faults. Deposits of black clays noted at lower elevations of stream channels, such as at the slide zone in the Pezielietsie colony are possible

indicators of active faulting. Numerous studies have shown that the region is tectonically active, so it is natural that the rocks of the study area will be further pulverised. The numerous faults that have been reactivated in recent times, and their splays in the study area, point to continuous deformation of the rocks.

The study area received very heavy rainfall prior to failure of the slopes, which is attributed to the highly fissured surface soils and subsurface rocks. The artificial drain at Pezielietsie was choked with debris, which caused water to overflow onto the surface during heavy rainfall. This caused the build-up of pore-water pressure in the fissured surface and subsurface material, triggering the landslide on 31st July 2018. Human action can further aggravate the condition of slopes, as observed in the Nhachüko area. The dumping of hillside excavated material into the waterway resulted in the formation of an artificial dam. This area experienced significant precipitation for two days before slope failure. With the channel blocked, the natural flow of the stream was disrupted, causing water to accumulate behind the debris and the excess to flow on the surface. This increase in weight along with the development of severe pore-water pressure resulted in a drastic decrease in the cohesion and friction angle values of the already weak subsurface, resulting in breach of the dam, which suddenly triggered the landslide. Thus, aggravating and triggering factors played vital roles in this event. The disaster could have been avoided if the slope-cut debris had been dumped in a safer area, seeing that this slope was very weak.

Besides precipitation and detrimental human activity, the paleostresses of the region aided the landside events in the study area. The bedded rocks are distorted by multi-directional compressional and extensional stresses, which caused the formation of folds, joints, fractures, and faults. Where rainwater seeps into the subsurface, the slopes are further weakened. Tectonic signals confirm that thrusting and faulting are common in the region. Such geologic processes have weakened the rocks of the study area.

BIBLIOGRAPHY

Acker, J. G., & Leptoukh, G. (2007). Online Analysis Enhances Use of NASA Earth Science Data. *Eos, Transactions American Geophysical Union, 88(2),* 14. https://doi.org/10.1029/2007EO020003

Agliardi, F., Crosta, G., & Zanchi, A. (2001). Structural constraints on deep-seated slope deformation kinematics. *Engineering Geology*, *59*(1–2), 83–102. https://doi.org/10.1016/S0013-7952(00)00066-1

Aier, I. (2005). Landslides along the Kohima-Dimapur road: their causes and possible remedial measures. In *Unpublished Ph. D. Thesis, Department of Geology, Nagaland University, Kohima*.

Aier, I., Supongtemjen, M. K., Khalo, M., & Thong, G. T. (2009a). Geotechnical assessment of the Mehrülietsa slide (179 km) along NH 39, Kohima, Nagaland. *Earth System Sciences. Concept Publishing Company, New Delhi*, 81–88.

Aier, I., Supongtemjen, & Thong, G.T. (2009b). Slope mass rating and kinematic analyses along part of NH 61, Nagaland, NE India.

Aier, I., Luirei, K., Bhakuni, S. S., Thong, G. T., & Kothyari, G. C. (2011). Geomorphic evolution of Medziphema intermontane basin and Quaternary deformation in the schuppen belt, Nagaland, NE India. *Zeitschrift Fur Geomorphologie*, *55*(2), 247–265. https://doi.org/10.1127/0372-8854/2011/0055-0048

Aier, I., Singh, M. P., Thong, G. T., & Ibotombi, S. (2012). Instability analyses of Merhülietsa slide, Kohima, Nagaland. *Natural Hazards*, *60*(3), 1347–1363. https://doi.org/10.1007/s11069-011-9913-6

Akın, M. (2017). Reliability of Shear Strength Parameters for a Safe Slope Design in Highly Jointed Rock Mass. In *Advancing Culture of Living with Landslides*. https://doi.org/10.1007/978-3-319-53487-9_52

Al-Homoud, A. S., Basma, A. A., Malkawi, A. I. H., & Al Bashabsheh, M. A. (1995). Cyclic swelling behavior of clays. *Journal of Geotechnical Engineering*, *121*(7). https://doi.org/10.1061/(ASCE)0733-9410(1995)121:7(562)

Alejano, L. R. (2021). Considerations on failure mechanisms of rock slopes involving

toppling. *IOP Conference Series: Earth and Environmental Science*, *833*(1), 012004. https://doi.org/10.1088/1755-1315/833/1/012004

Aleotti, P., & Chowdhury, R. (1999). Landslide hazard assessment: summary review and new perspectives. *Bulletin of Engineering Geology and the Environment*, *58*(1), 21–44. https://doi.org/10.1007/s100640050066

Alok, A., Burman, A., Samui, P., R. Kaloop, M., & Eldessouki, M. (2024). A Generalized Limit Equilibrium-Based Platform Incorporating Simplified Bishop, Janbu and Morgenstern–Price Methods for Soil Slope Stability Problems. *Advances in Civil Engineering*, *2024*, 1–16. https://doi.org/10.1155/2024/3053923

Altın, T. B., & Gökkaya, E. (2018). Assessment of landslide-triggering factors and occurrence using morphometric parameters in Geyraz basin, tokat, Northern Turkey. *Environmental Earth Sciences*, *77*(4). https://doi.org/10.1007/s12665-018-7315-8

Ambrosi, C., & Crosta, G. B. (2006). Large sackung along major tectonic features in the Central Italian Alps. *Engineering Geology*, *83*(1–3), 183–200. https://doi.org/10.1016/j.enggeo.2005.06.031

Aminpour, M., Discipline, I. E., Alaie, R., Kardani, N., Discipline, I. E., Moridpour, S., Discipline, I. E., Nazem, M., & Discipline, I. E. (2021). Slope stability predictions on spatially variable random fields using machine learning surrogate models. *Engineering Geology*, *November 2021*.

An, H., Seo, T., Choi, D., & Lee, C. G. (2018). Slope Detection Method Based on Web Camera Image for UAV application. *2018 22nd International Computer Science and Engineering Conference (ICSEC)*, 1–3. https://doi.org/10.1109/ICSEC.2018.8712733

Angelier, J. (1994). Fault Slip Analysis and Paleostress Reconstruction. In P. L. Hancock (Ed.), *Continental Deformation* (pp. 53–100). Pergamon Press, Oxford.

Anon, O. H. (1979). Classification of rocks and soils for engineering geological mapping. Part 1: rock and soil materials. *Bull Int Assoc Eng Geol*, *19*, 355–371.

Aoki, T., Kaneko, Y., & Kearse, J. (2023). Dynamic simulations of coseismic slickenlines on non-planar and rough faults. *Geophysical Journal International*,

233(2), 1124–1143. https://doi.org/10.1093/gji/ggac501

Assis, L. C., Calijuri, M. L., Salvador, M. M., Castro, J. de S., & Carvalho, C. F. (2019). Identification of Susceptible Rainfall-Induced Landslide Areas Based on Field Experiments and Multi-criteria Analysis in GIS Environment: A Proposal for Non-inventoried Areas. *Geotechnical and Geological Engineering*, *37*(5), 4473–4489. https://doi.org/10.1007/s10706-019-00922-0

ASTM D421−85. (2007). Standard Practice for Dry Preparation of Soil Samples for Particle-Size Analysis and Determination of Soil Constants (Withdrawn 2016). *ASTM International, West Conshohocken, PA*. https://doi.org/10.1520/D0421-85R07.2

Atterberg, A. (1911). Physical soil examination about the plasticity of the clays. *International Communications for Soil Science*, *1*.

Bai, D., Lu, G., Zhu, Z., Zhu, X., Tao, C., & Fang, J. (2022). Using Electrical Resistivity Tomography to Monitor the Evolution of Landslides' Safety Factors under Rainfall: A Feasibility Study Based on Numerical Simulation. *Remote Sensing*, *14*(15). https://doi.org/10.3390/rs14153592

Balakrishnan, M., & Ganapathy, P. G. (2022). Failure Mechanism Of An Unsaturated Slope In The Nilgiris District, Tamil Nadu, India. *Indian Geotechnical Conference IGC 2022*, 1–7.

Bhattacharjee, C.C., Rahman, S., Sarmah, R.N., & Thong, G.T. (1998). Landslides and road instability along NH 39, between Kohima and Chumukedima, Nagaland. *Proc. Intl. Conf. Dis. Man.*, Guwahati, pp. 556-568.

Bieniawski, Z. T. (1973). Engineering classification of jointed rock masses. *Transactions of the South African Institution of Civil Engineers*, *15*(12), 335–343. https://linkinghub.elsevier.com/retrieve/pii/0148906274909243

Bieniawski, Z. T. (1989). Engineering rock mass classifications: a complete manual for engineers and geologists in mining, civil, and petroleum engineering. In *Engineering rock mass classifications: a complete manual for engineers and geologists in mining, civil, and petroleum engineering*. John Wiley and Sons.

Bogoslovsky, V. A., & Ogilvy, A. A. (2012). Geophysical methods for the investigation

of landslides. *Geophysics, 42*(3), 562–571. https://doi.org/10.1190/1.1440727

Borradaile, G. (2015). Faults. In *Understanding Geology Through Maps* (pp. 111–139). Elsevier. https://doi.org/10.1016/B978-0-12-800866-9.00009-0

Borrelli, L., Ciurleo, M., & Gullà, G. (2018). Shallow landslide susceptibility assessment in granitic rocks using GIS-based statistical methods: the contribution of the weathering grade map. *Landslides*, *15*(6), 1127–1142. https://doi.org/10.1007/s10346-018-0947-7

Bradley, K., Mallick, R., Andikagumi, H., Hubbard, J., Meilianda, E., Switzer, A., Du, N., Brocard, G., Alfian, D., Benazir, B., Feng, G., Yun, S. H., Majewski, J., Wei, S., & Hill, E. M. (2019). Earthquake-triggered 2018 Palu Valley landslides enabled by wet rice cultivation. *Nat Geosci*, *12*(11), 935–939. https://doi.org/10.1038/s41561-019-0444-1

Brandes, C., & Tanner, D. C. (2019). Fault mechanics and earthquakes. In *Understanding Faults: Detecting, Dating, and Modeling*. https://doi.org/10.1016/B978-0-12-815985-9.00002-3

Brunsden, D., & Prior, D. B. (1987). *Slope instability*. Wiley.

Bucci, F., Santangelo, M., Cardinali, M., Fiorucci, F., & Guzzetti, F. (2016). Landslide distribution and size in response to Quaternary fault activity: the Peloritani Range, NE Sicily, Italy. *Earth Surface Processes and Landforms*, *41*(5), 711–720. https://doi.org/10.1002/esp.3898

Bui, D. T., Long, N. Q., Bui, X., & Nghia, N. V. (2018). Advances and Applications in Geospatial Technology and Earth Resources. *Advances and Applications in Geospatial Technology and Earth Resources*, *November 2017*. https://doi.org/10.1007/978-3-319-68240-2

Bureau of Indian Standards. (1970). *IS: 1498: Classification and Identification of Soils for General Engineering Purposes*.

Bureau of Indian Standards. (1972). *IS: 2720-6: Method of test for soils: Determination of shrinkage factors (First Revision) (Reaffirmed 2001)*. Bureau of Indian Standards.

Bureau of Indian Standards. (1985). Methods of test for soils: Determination of liquid

limit and plastic limit. In *Indian Standards*.

Bureau of Indian Standards. (1986). *IS: 2720-13: Method of test for soils: Direct shear test (Second Revision) (Reaffirmed 2002)*. Bureau of Indian Standards.

Burns, S. (2013). Processes, Transport, Deposition, and Landforms: Slides. In *Treatise on Geomorphology* (pp. 152–157). Elsevier. https://doi.org/10.1016/B978-0-12-374739-6.00159-7

Cai, J., Jibin, L., Ting, X., & Yongyue, S. (2020). Study on Fast Test and Calculation Method of Integrity Coefficient of Surrounding Rock during Tunnel Construction. *IOP Conference Series: Earth and Environmental Science*, *474*(4). https://doi.org/10.1088/1755-1315/474/4/042014

Campbell, D. A. (1951). Types of erosion prevalent in New Zealand. *Assoc. Intl. d'Hydrologie Scientifique, Assemblee Generale de Bruxelles. Tome II*.

Casagrande, A. (1932). Research on the Atterberg Limits of Soils. *Public Roads*, *13*(8).

Casagrande, A. (1948). Classification and Identification of Soils. *Transactions of the American Society of Civil Engineers*, *113*(1), 901–930. https://doi.org/10.1061/TACEAT.0006109

Central Road Research Institute (2000a). Preliminary report on correction of landslide at km-174 and km-180 on NH 39 in Nagaland, pp. 1-6.

Central Road Research Institute (2000b). Correction of landslides on NH 39 in Nagaland. *Suppl. Rep*.

Cerri, R. I., Reis, F. A. G. V., Gramani, M. F., Giordano, L. C., & Zaine, J. E. (2017). Landslides Zonation Hazard: Relation between geological structures and landslides occurrence in hilly tropical regions of Brazil. *Anais Da Academia Brasileira de Ciencias*, *89*(4), 2609–2623. https://doi.org/10.1590/0001-3765201720170224

Chang, C. N., Ezung, M., Apon, M., Supongtemjen, Walling, T., & Thong, G. T. (2021). Assessment of Landslides Along NH 29 in the Kevüza Area, Kohima, Nagaland. *Indian Geotechnical Journal*, *51*(4), 841–860. https://doi.org/10.1007/s40098-021-00566-z

Chang, K.-J., Chan, Y.-C., Chen, R.-F., & Hsieh, Y.-C. (2018). Geomorphological evolution of landslides near an active normal fault in northern Taiwan, as revealed by lidar and unmanned aircraft system data. *Natural Hazards and Earth System Sciences*, *18*(3), 709–727. https://doi.org/10.5194/nhess-18-709-2018

Chen, A., Darbon, J., & Morel, J.-M. (2014). Landscape evolution models: A review of their fundamental equations. *Geomorphology*, *219*, 68–86. https://doi.org/10.1016/j.geomorph.2014.04.037

Chen, G., Zhang, K., Wang, S., Xia, Y., & Chao, L. (2023). iHydroSlide3D v1.0: an advanced hydrological-geotechnical model for hydrological simulation and three-dimensional landslide prediction. *Geoscientific Model Development*, *16*(10). https://doi.org/10.5194/gmd-16-2915-2023

Chen, L., Guo, Z., Yin, K., Shrestha, D. P., & Jin, S. (2019). The influence of land use and land cover change on landslide susceptibility: a case study in Zhushan Town, Xuan'en County (Hubei, China). *Natural Hazards and Earth System Sciences*, *19*(10), 2207–2228. https://doi.org/10.5194/nhess-19-2207-2019

Chiang, S. H., & Chang, K. T. (2011). The potential impact of climate change on typhoon-triggered landslides in Taiwan, 2010-2099. *Geomorphology*, *133*(3–4). https://doi.org/10.1016/j.geomorph.2010.12.028

Choubey, V.D. Lallenmawia, H. (1987). Landslides and other mass movements in Aizawl, NE India, Mizoram state. *5th Intl. Conf.*, 113–120.

Chung, S. H. (2019). Study of the rainfall infiltration effect and soil strength variation on unsaturated laterite terraces. *World Congress on Civil, Structural, and Environmental Engineering*, 1–8. https://doi.org/10.11159/icgre19.184

Ciccarese, G., Mulas, M., Alberoni, P. P., Truffelli, G., & Corsini, A. (2020). Debris flows rainfall thresholds in the Apennines of Emilia-Romagna (Italy) derived by the analysis of recent severe rainstorms events and regional meteorological data. *Geomorphology*, *358*, 107097. https://doi.org/10.1016/j.geomorph.2020.107097

Cignetti, M., Godone, D., & Giordan, D. (2019). Shallow landslide susceptibility, Rupinaro catchment, Liguria (northwestern Italy). *Journal of Maps*, *15*(2), 333–345. https://doi.org/10.1080/17445647.2019.1593252

Coch, N. K. (1995). *Geohazards: Natural and Human*. Prentice Hall Inc.

Conte, E., Pugliese, L., & Troncone, A. (2022). A Simple Method for Predicting Rainfall-Induced Shallow Landslides. *Journal of Geotechnical and Geoenvironmental Engineering*, *148*(10). https://doi.org/10.1061/(ASCE)GT.1943-5606.0002877

Crozier, M. J. (1973). Techniques for the morphometric analysis of landslips. *Zeitschrift Für Geomorphologie*, *17*(1). https://doi.org/10.1127/zfg/17/1973/78

Crozier, M. J. (1984). Field Assessment of Slope Instability. In D. Brunsden & D. Prior (Eds.), *Slope Instability*. John Wiley & Sons.

Crozier, M. J. (1986). *Landslides : causes, consequences & environment*. 252.

Crozier, M. J. (2010). Deciphering the effect of climate change on landslide activity: A review. *Geomorphology*, *124*(3–4), 260–267. https://doi.org/10.1016/j.geomorph.2010.04.009

Cruden, D. M. (1978). A method of distinguishing between single and double plane sliding of tetrahedral wedges. *International Journal of Rock Mechanics and Mining Sciences & Geomechanics Abstracts*, *15*(4), 217. https://doi.org/10.1016/0148-9062(78)91228-7

Cruden, D. M. (1991). A simple definition of a landslide. *Bulletin of the International Association of Engineering Geology*, *43*(1), 27–29. https://doi.org/10.1007/BF02590167

Cruden, D. M., & Varnes, D. J. (1996). Landslide types and processes. *Special Report - National Research Council, Transportation Research Board*, 36–75.

Dabral, P. P., Dada, M., & Odi, H. (2019). Probability analysis of rainfall at Kohima (Nagaland) for crop planning. *Journal of Soil and Water Conservation*, *18*(4), 364. https://doi.org/10.5958/2455-7145.2019.00051.1

Dai, F., & Lee, C. (2002). Landslide characteristics and slope instability modeling using GIS, Lantau Island, Hong Kong. *Geomorphology*, *42*(3–4), 213–228. https://doi.org/10.1016/S0169-555X(01)00087-3

Das, I., Sahoo, S., van Westen, C., Stein, A., & Hack, R. (2010). Landslide

susceptibility assessment using logistic regression and its comparison with a rock mass classification system, along a road section in the northern Himalayas (India). *Geomorphology*, *114*(4), 627–637. https://doi.org/10.1016/j.geomorph.2009.09.023

Das, B. M., & Sobhan, K. (2018). Principles of Geotechnical Engineering 9th Edition. In *Cengage Learning*.

Deere, D. U., Hendron, A. J., Patton, F. D., & Cording, E. J. (1966). Design of surface and near-surface construction in rock. *8th U.S. Symposium on Rock Mechanics, USRMS 1966*.

Delvaux, D. (1993). The TENSOR program for paleostress reconstruction: examples from the east African and the Baikal rift zones. *EUG VII Strasbourg, France, 4-8 April 1993, Abstracts Supplement N°1 to TERRA Nova, Vol. 5*, 216.

Delvaux, D., & Sperner, B. (2003). New aspects of tectonic stress inversion with reference to the TENSOR program. *Geological Society, London, Special Publications*, *212*(1), 75–100. https://doi.org/10.1144/GSL.SP.2003.212.01.06

Delvaux, D., Moeys, R., Stapel, G., Petit, C., Levi, K., Miroshnichenko, A., Ruzhich, V., & San'kov, V. (1997). Paleostress reconstructions and geodynamics of the Baikal region, Central Asia, Part 2. Cenozoic rifting. *Tectonophysics*, *282*(1–4), 1–38. https://doi.org/10.1016/S0040-1951(97)00210-2

Devdas, V., & Gandhi, P. (1985). *Systematic geological mapping in Maromi- Akuluto-Suruhuto areas, Zunheboto district, Nagaland*.

Diabat, A. A. (2009). Structural and stress analysis based on fault-slip data in the Amman area, Jordan. *Journal of African Earth Sciences*, *54*(5), 155–162. https://doi.org/10.1016/j.jafrearsci.2009.03.011

Directorate of Geology & Mining, N. (1978). *Miscellaneous Publication No. 1*.

Djeffal, H., & Belkacemi, S. (2023). Slope Reliability Analysis in Locating and Observing the Direction of Failure Propagation. *Engineering, Technology and Applied Science Research*, *13*(1). https://doi.org/10.48084/etasr.5509

Doblas, M. (1998). Slickenside kinematic indicators. *Tectonophysics*, *295*, 187–197. https://doi.org/10.1016/S0040-1951(98)00120-6

Doglioni, A., & Simeone, V. (2014). Geomorphometric analysis based on discrete wavelet transform. *Environmental Earth Sciences*, *71*(7), 3095–3108. https://doi.org/10.1007/s12665-013-2686-3

Dorren, L. K. A. (2003). A review of rockfall mechanics and modelling approaches. *Progress in Physical Geography: Earth and Environment*, *27*(1), 69–87. https://doi.org/10.1191/0309133303pp359ra

Dumbleton, M. (1968). *The classification and description of soil for engineering purposes. A suggested British System RRL report classification, LR 182, UK*.

Duncan, J. M., Wright, S. G., & Brandon, T. L. (2014). Soil Strength and Slope Stability, 2nd Edition. In *John Wiley & Sons*.

Erguler, Z. A., & Ulusay, R. (2009). Water-induced variations in mechanical properties of clay-bearing rocks. *International Journal of Rock Mechanics and Mining Sciences*, *46*(2). https://doi.org/10.1016/j.ijrmms.2008.07.002

Fan, Z., Zhenxue, Z., Chao, S., Jianjian, D., Heng, Z., & Yujun, M. (2021). Particle flow analysis of basalt fiber gabion slope under conditions of rapid drawdown of water level. *IOP Conference Series: Earth and Environmental Science*, *643*(1), 012030. https://doi.org/10.1088/1755-1315/643/1/012030

Fathani, T. F., Karnawati, D., & Wilopo, W. (2016). An integrated methodology to develop a standard for landslide early warning systems. *Natural Hazards and Earth System Sciences*, *16*(9). https://doi.org/10.5194/nhess-16-2123-2016

Fookes, P. G., & Wilson, D. D. (1966). The geometry of discontinuities and slope failures in siwalik clay. *Geotechnique*, *16*(4). https://doi.org/10.1680/geot.1966.16.4.305

Froude, M. J., & Petley, D. N. (2018). Global fatal landslide occurrence from 2004 to 2016. *Natural Hazards and Earth System Sciences*, *18*(8), 2161–2181. https://doi.org/10.5194/nhess-18-2161-2018

Galeandro, A., Doglioni, A., Guerricchio, A., & Simeone, V. (2013). Hydraulic stream network conditioning by a tectonically induced, giant, deep-seated landslide along the front of the Apennine chain (south Italy). *Natural Hazards and Earth System Sciences*, *13*(5), 1269–1283. https://doi.org/10.5194/nhess-13-1269-2013

Garcia-Delgado, H., Petley, D. N., Bermúdez, M. A., & Sepúlveda, S. A. (2022). Fatal landslides in Colombia (from historical times to 2020) and their socio-economic impacts. *Landslides*, *19*(7), 1689–1716. https://doi.org/10.1007/s10346-022-01870-2

Gentier, S., Riss, J., Archambault, G., Flamand, R., & Hopkins, D. (2000). Influence of fracture geometry on shear behavior. *International Journal of Rock Mechanics and Mining Sciences*, *37*(1–2), 161–174. https://doi.org/10.1016/S1365-1609(99)00096-9

Geological Survey of India (2011). Geology and Mineral resources of Manipur, Mizoram, Nagaland, and Tripura. *Miscellaneous Publication*, No 30, Part IV, vol. 1 (Part-2).

Geotechdata. (2020). *Geotechnical parameters*. http://www.geotechdata.info/parameter/

Geotechnical Info. (2012). *Soil unit weight*. http://www.geotechnicalinfo.com/soil_unit_weight.html

Ghose, N., Agrawal, O., & Chatterjee, N. (2010). Geological and mineralogical study of eclogite and glaucophane schists in the Naga Hills Ophiolite, Northeast India. *Island Arc*, *19*, 336–356.

Gokceoglu, C., Sonmez, H., & Ercanoglu, M. (2000). Discontinuity controlled probabilistic slope failure risk maps of the Altindag (settlement) region in Turkey. *Engineering Geology*, *55*(4), 277–296. https://doi.org/10.1016/S0013-7952(99)00083-6

Goodman, R. E., & Bray, J. W. (1976). Toppling of Rock Slopes. *Specialty Conference on Rock Engineering for Foundations and Slopes (Boulder: American Society of Civil Engineering)*, 739–760.

Goodman, R. E., & Kieffer, D. S. (2000). Behavior of Rock in Slopes. *Journal of Geotechnical and Geoenvironmental Engineering*, *126*(8), 675–684. https://doi.org/10.1061/(ASCE)1090-0241(2000)126:8(675)

Guiraud, M., Laborde, O., & Philip, H. (1989). Characterization of various types of deformation and their corresponding deviatoric stress tensors using microfault

analysis. *Tectonophysics*, *170*(3–4), 289–316. https://doi.org/10.1016/0040-1951(89)90277-1

Guney, Y., Sari, D., Cetin, M., & Tuncan, M. (2007). Impact of cyclic wetting-drying on swelling behavior of lime-stabilized soil. *Handbook of Environmental Chemistry, Volume 5: Water Pollution*, *42*(2). https://doi.org/10.1016/j.buildenv.2005.10.035

Guo, J., & Wang, J. (2018). Mechanism Analysis of the Failure for a Safe Jointed Rock High Slope: Tectonic Structures and Damage. *Geotechnical and Geological Engineering*, *36*(1), 455–467. https://doi.org/10.1007/s10706-017-0339-0

Guo, Y., Zhang, F., Liu, Z., & Meng, Q. (2023). Effects of water content change path on laboratory and field compaction of lime stabilized expansive soil. *Frontiers in Earth Science*, *11*. https://doi.org/10.3389/feart.2023.1282044

Hancock, P. L., & Barka, A. A. (1987). Kinematic indicators on active normal faults in Western Turkey. *Journal of Structural Geology*, *9*(5–6), 573–584. https://doi.org/10.1016/0191-8141(87)90142-8

Handwerger, A. L., Fielding, E. J., Huang, M. H., Bennett, G. L., Liang, C., & Schulz, W. H. (2019). Widespread Initiation, Reactivation, and Acceleration of Landslides in the Northern California Coast Ranges due to Extreme Rainfall. *Journal of Geophysical Research: Earth Surface*, *124*(7). https://doi.org/10.1029/2019JF005035

Hasan, M., Shang, Y., Meng, H., Shao, P., & Yi, X. (2021). Application of electrical resistivity tomography (ERT) for rock mass quality evaluation. *Scientific Reports*, *11*(1). https://doi.org/10.1038/s41598-021-03217-8

Hazreek, Z. A. M., Rosli, S., Fauziah, A., Wijeyesekera, D. C., Ashraf, M. I. M., Faizal, T. B. M., Kamarudin, A. F., Rais, Y., Md Dan, M. F., Azhar, A. T. S., & Hafiz, Z. M. (2018). Determination of Soil Moisture Content using Laboratory Experimental and Field Electrical Resistivity Values. *Journal of Physics: Conference Series*, *995*(1). https://doi.org/10.1088/1742-6596/995/1/012074

He, K., Li, J., Li, B., Zhao, Z., Zhao, C., Gao, Y., & Liu, Z. (2022). The Pingdi landslide in Shuicheng, Guizhou, China: instability process and initiation mechanism.

Bulletin of Engineering Geology and the Environment, *81*(4).
https://doi.org/10.1007/S10064-022-02596-0

Henriques, C., Zêzere, J. L., & Marques, F. (2015). The role of the lithological setting
on the landslide pattern and distribution. *Engineering Geology*, *189*.
https://doi.org/10.1016/j.enggeo.2015.01.025

Hobbs, P. R. N., Jones, L. D., Kirkham, M. P., Gunn, D. A., & Entwisle, D. C. (2018).
Shrinkage limit test results and interpretation for clay soils. *Quarterly Journal of
Engineering Geology and Hydrogeology*, *52*(2).
https://doi.org/10.1144/qjegh2018-100

Hocking, G. (1976). A method for distinguishing between single and double plane
sliding of tetrahedral wedges. *International Journal of Rock Mechanics and
Mining Sciences And*, *13*(7). https://doi.org/10.1016/0148-9062(76)91697-1

Hoek, E., & Bray, J. W. (1981a). *Rock slope engineering* (3rd ed.). The Institute of
Mining and Metallurgy.

Hoek, E., & Brown, E. T. T. (1997). Practical estimates of rock mass strength.
International Journal of Rock Mechanics and Mining Sciences, *34*(8), 1165–1186.
https://doi.org/10.1016/S1365-1609(97)80069-X

Hoek, E., & Marinos, P. (2000). Predicting tunnel squeezing problems in weak
heterogeneous rock masses. *Tunnels and Tunnelling International Part*,
1(December).

Holtz, W., & Gibbs, H. (1956). Engineering Properties of Expansive Clays.
Transactions ASCE, *121*(1), 641–663.

Hounguè, N. R., Ogbu, K. N., Almoradie, A. D. S., & Evers, M. (2021). Evaluation of
the performance of remotely sensed rainfall datasets for flood simulation in the
transboundary Mono River catchment, Togo and Benin. *Journal of Hydrology:
Regional Studies*, *36*, 100875. https://doi.org/10.1016/j.ejrh.2021.100875

Huang, B., Cai, S., Li, J., Wu, K., & Yang, W. (2023). Undrained strength of clay
determined from simple shear test. *Frontiers in Earth Science*, *10*.
https://doi.org/10.3389/feart.2022.1098846

Huffman, G. J., Stocker, E. F., Bolvin, D. T., Nelkin, E. J., & Tan, J. (2019). GPM

IMERG final precipitation L3 1 day 0.1 degree x 0.1 degree V06. *Edited by Andrey Savtchenko, Greenbelt, MD, Goddard Earth Sciences Data and Information Services Center (GES DISC). Accessed: [24-03-2020].* https://doi.org/10.5067/GPM/IMERGDF/DAY/06

Hungr, O., Evans, S. G., Bovis, M. J., & Hutchinson, J. N. (2001). A review of the classification of landslides of the flow type. *Environmental and Engineering Geoscience*, *7*(3), 221–238. https://doi.org/10.2113/gseegeosci.7.3.221

Hungr, O., Leroueil, S., & Picarelli, L. (2014). The Varnes classification of landslide types, an update. *Landslides*, *11*(2), 167–194. https://doi.org/10.1007/s10346-013-0436-y

Hussain, M., Stark, T., & Akhtar, K. (2010). Back-analysis procedure for landslides. *International Conference on Geotechnical Engineering*.

Igwe, O., & Okonkwo, I. A. (2016). Application of paleostress analysis for the identification of potential instability precursors within the Benue Trough Nigeria. *Geoenvironmental Disasters*, *3*(1), 17. https://doi.org/10.1186/s40677-016-0051-z

Iverson, R. M. R. M. (2000). Landslide triggering by rain infiltration. *Water Resources Research*, *36*(7), 1897–1910. https://doi.org/10.1029/2000WR900090

Jaboyedoff, M., Crosta, G. B., & Stead, D. (2011). Slope tectonics: a short introduction. *Geological Society, London, Special Publications*, *351*(1), 1–10. https://doi.org/10.1144/SP351.1

Jaboyedoff, M., Michoud, C., Derron, M. H., Voumard, J., Leibundgut, G., Sudmeier-Rieux, K., Michoud, C., Nadim, F., & Leroi, E. (2016). Human-Induced Landslides: Toward the analysis of anthropogenic changes of the slope environment. In *Landslides and Engineered Slopes. Experience, Theory and Practice* (Vol. 1, pp. 217–232). CRC Press. https://doi.org/10.1201/b21520-20

Jaboyedoff, M., Penna, I., Pedrazzini, A., Baroň, I., & Crosta, G. B. (2013). An introductory review on gravitational-deformation induced structures, fabrics and modeling. *Tectonophysics*, *605*, 1–12. https://doi.org/10.1016/j.tecto.2013.06.027

Jaffari, S. H. K. H. (2014). Comparison in Limit Equilibrium Methods of Slices in Slope

Stability Analysis. *Journal of Applied Science and Agriculture*, *9*(4), 1440–1451.

Jamir, N., Aier, I., Supongtemjen, & Thong, G. (2011). An appraisal of the debris slide in Artang Ward, Mokokchung Town, Nagaland, NE India. *Proceedings of the National Seminar on Geodynamics, Sedimentation and Biotic Response in the Context of India-Asia Collision, Mizoram University. Memoirs of the Geological Society of India*, 259–268.

Jamir, M., Chang, C. N., Jamir, I., Thong, G. T., & Walling, T. (2022). Landslide susceptibility mapping of Noklak Town, Nagaland, North-east India using bivariate statistical method. *Geological Journal*, *57*(12), 5250–5264. https://doi.org/10.1002/GJ.4595

Jamir, N. (2013). Landslide investigation and susceptibility mapping of Mokokchung town, Nagaland. Unpublished Ph.D. thesis, Nagaland University, Kohima.

Johnston, E. C., Davenport, F. V., Wang, L., Caers, J. K., Muthukrishnan, S., Burke, M., & Diffenbaugh, N. S. (2021). Quantifying the Effect of Precipitation on Landslide Hazard in Urbanized and Non-Urbanized Areas. *Geophysical Research Letters*, *48*(16). https://doi.org/10.1029/2021GL094038

Kamal, A. S. M. M., Hossain, F., Ahmed, B., Rahman, M. Z., & Sammonds, P. (2023). Assessing the effectiveness of landslide slope stability by analysing structural mitigation measures and community risk perception. *Natural Hazards*, *117*(3). https://doi.org/10.1007/s11069-023-05947-6

Kamien, D. J. (1997). *Engineering and Design: Introduction to Probability and Reliability Methods for Use in Geotechnical Engineering* (p. 14). Corps Of Engineers.

Kandpal, G. C., & Pant, G. (1995). Geological evaluation of instability along Balia Nala, Dist. UP. *Symp. Rec. Adv. Geol. Studies, NE Himalayas*, 2123.

Kearse, J., & Kaneko, Y. (2020). On-Fault Geological Fingerprint of Earthquake Rupture Direction. *Journal of Geophysical Research: Solid Earth*, *125*(9). https://doi.org/10.1029/2020JB019863

Kearse, J., Kaneko, Y., Little, T., & Van Dissen, R. (2019). Curved slickenlines preserve direction of rupture propagation. *Geology*, *47*(9), 838–842.

https://doi.org/10.1130/G46563.1

Kedovikho, Y., & Krishnaiah, Y. V. (2020). Assessing landslide vulnerability in Kohima city, Nagaland: A geospatial approach. *National Geographical Journal of India*, *66*(3), 274–287. https://doi.org/10.48008/ngji.1747

Keller, E. A., & Blodgett, R. H. (2007). *Riesgos naturales : procesos de la Tierra como riesgos, desastres y catástrofes*. Pearson Educación. https://books.google.co.in/books?id=c63SMAAACAAJ

Kemas, K., Thong, G.T., & Walling, T. (2004). Chokidzü debris slide - A case study. *Nagaland University Research Journal*, vol. 2, pp. 89-94.

Khalo, M. (2016). Slope stability investigations between Kohima and Mao with special reference to NH-39. *Unpublished Ph.D. thesis, Nagaland University, Kohima*.

Kidd, C., Takayabu, Y. N., Skofronick-Jackson, G. M., Huffman, G. J., Braun, S. A., Kubota, T., & Turk, F. J. (2020). The Global Precipitation Measurement (GPM) Mission. In *Advances in Global Change Research* (Vol. 67). https://doi.org/10.1007/978-3-030-24568-9_1

Kirschbaum, D., & Stanley, T. (2018). Satellite-Based Assessment of Rainfall-Triggered Landslide Hazard for Situational Awareness. *Earth's Future*, *6*(3), 505–523. https://doi.org/10.1002/2017EF000715

Kirschbaum, D. B., Huffman, G. J., Adler, R. F., Braun, S., Garrett, K., Jones, E., McNally, A., Skofronick-Jackson, G., Stocker, E., Wu, H., & Zaitchik, B. F. (2017). NASA's Remotely Sensed Precipitation: A Reservoir for Applications Users. *Bulletin of the American Meteorological Society*, *98*(6), 1169–1184. https://doi.org/10.1175/BAMS-D-15-00296.1

Kliche, C. A. (1999). *Rock Slope Stability*. Society for Mining, Metallurgy, and Exploration, Inc.

Koutnik, T., Wei, L., & Singh, J. (2008). *A Case Study of Safety Factor Comparison of Different Slope Stability Methods for Levee Design in New Orleans*. https://doi.org/10.1061/40971(310)62

Kusre, B. C., & Singh, K. S. (2012). Study of spatial and temporal distribution of

rainfall in Nagaland (India). *International Journal of Geomatics and Geosciences*, *2*(3), 712–722.

Kwan, A. K. H. (2004). Dip and strike angles method for yield line analysis of reinforced concrete slabs. *Magazine of Concrete Research*, *56*(8), 487–498. https://doi.org/10.1680/macr.2004.56.8.487

Lambe, T. W., & Whitman, R. V. (1979). *Soil Mechanics, Si Version*. John Wiley & Sons.

Lee, J. J., Song, M. S., Yun, H. S., & Yum, S. G. (2022). Dynamic landslide susceptibility analysis that combines rainfall period, accumulated rainfall, and geospatial information. *Scientific Reports*, *12*(1). https://doi.org/10.1038/s41598-022-21795-z

Lehmann, P., Gambazzi, F., Suski, B., Baron, L., Askarinejad, A., Springman, S. M., Holliger, K., & Or, D. (2013). Evolution of soil wetting patterns preceding a hydrologically induced landslide inferred from electrical resistivity survey and point measurements of volumetric water content and pore water pressure. *Water Resources Research*, *49*(12), 7992–8004. https://doi.org/10.1002/2013WR014560

Li, X., Liu, H., Pan, J., Li, D., & Wang, J. (2020). Rainfall thresholds of shallow landslides in Wuyuan County of Jiangxi Province, China. *Open Geosciences*, *12*(1), 821–831. https://doi.org/10.1515/geo-2020-0120

Lotha, K.A. (1994). A note on the geotechnical investigation on landslide at Cheipfutsiepfe, Lower AG colony, Kohima Town, Nagaland. *Unpubl. Rep. Geoenvir. Cell, DGM, Nagaland*.

Low, P. F., & Margheim, J. F. (1979). The Swelling of Clay: I. Basic Concepts and Empirical Equations. *Soil Science Society of America Journal*, *43*(3), 473–481. https://doi.org/10.2136/sssaj1979.03615995004300030010x

Luirei, K., Mehta, M., Iqpal, A., Nazir, S., & Kothyari, G. C. (2023). Factors influencing the slope instability of the Mussoorie-Bhitarli area, Garhwal Himalaya. *Geosciences Journal*, *27*(3), 337–350. https://doi.org/10.1007/s12303-022-0036-8

Luo, J., Pei, X., Jiang, R., Li, T., Sun, H., Jin, B., & Li, Q. (2023). The Characteristics

and Seepage Stability Analysis of Toppling-Sliding Failure under Rainfall. *Sustainability (Switzerland)*, *15*(10). https://doi.org/10.3390/su15107736

Macklin, C., Kaneko, Y., & Kearse, J. (2021). Coseismic slickenlines record the emergence of multiple rupture fronts during a surface-breaking earthquake. *Tectonophysics*, *808*, 228834. https://doi.org/10.1016/j.tecto.2021.228834

Maddalwar, S., Kumar, T., Tijare, G., Agashe, A., Kotangale, P., Sawarkar, A., & Singh, L. (2024). A global perspective on a bioengineering approach to landslide mitigation using bamboo diversity. *Advances in Bamboo Science*, *8*, 100093. https://doi.org/10.1016/j.bamboo.2024.100093

Malizia, J. P., & Shakoor, A. (2018). Effect of water content and density on strength and deformation behavior of clay soils. *Engineering Geology*, *244*. https://doi.org/10.1016/j.enggeo.2018.07.028

Mallet, F. R. (1876). On the coal fields of the Naga Hills, bordering the Lakhimpur and Sibsagar Districts. In *Geological Survey of India, Memoir* (Vol. 12, Issue 2, pp. 269–363). Geological Survey of India.

Mandal, J., Narwal, S., & Gupte, S. S. (2017). Back Analysis of Failed Slopes - A Case Study. *International Journal of Engineering Research & Technology*, *6*(5), 1070–1078.

Mandal, N., & Chakraborty, C. (1989). Fault motion and curved slickenlines: A theoretical analysis. *Journal of Structural Geology*, *11*(4), 497–501. https://doi.org/10.1016/0191-8141(89)90026-6

Mao, J.-Z., Guo, J., Fu, Y., Zhang, W.-P., & Ding, Y.-N. (2020). Effects of Rapid Water-Level Fluctuations on the Stability of an Unsaturated Reservoir Bank Slope. *Advances in Civil Engineering*, *2020*, 1–10. https://doi.org/10.1155/2020/2360947

Markland, J. T. (1972). A useful technique for estimating the stability of rock slopes when the rigid wedge sliding type of failure is expected. *Imperial College Rock Mech. Res. Rep. No. 19*.

Massonnet, D., & Feigl, K. L. (1998). Radar interferometry and its application to changes in the earth's surface. *Reviews of Geophysics*, *36*(4).

https://doi.org/10.1029/97RG03139

Mathew, J., Babu, D. G., Kundu, S., Kumar, K. V., & Pant, C. C. (2013). Integrating intensity–duration-based rainfall threshold and antecedent rainfall-based probability estimate towards generating early warning for rainfall-induced landslides in parts of the Garhwal Himalaya, India. *Landslides*, *11*(4), 575–588. https://doi.org/10.1007/s10346-013-0408-2

Mathur, L. P., & Evans, P. (1964). Oil in India. In *22nd Session International Geological Congress*. Int. Geol. Congress, 22nd Session.

Mavrouli, O., Corominas, J., & Jaboyedoff, M. (2015). Size Distribution for Potentially Unstable Rock Masses and In Situ Rock Blocks Using LIDAR-Generated Digital Elevation Models. *Rock Mechanics and Rock Engineering*, *48*(4), 1589–1604. https://doi.org/10.1007/s00603-014-0647-0

Mebrahtu, T. K., Heinze, T., Wohnlich, S., & Alber, M. (2022). Slope stability analysis of deep-seated landslides using limit equilibrium and finite element methods in Debre Sina area, Ethiopia. *Bulletin of Engineering Geology and the Environment*, *81*(10). https://doi.org/10.1007/S10064-022-02906-6

Mehrotra, G. S., Dharmaraju, R., & Prakash, S. (1994). Morphometric appraisal of slope instability of Chilla landslide, Garhwal Himalaya. *Journal - Geological Society of India*, *44*(2), 203–211.

Melo, R., Oliveira, S. C., & Zêzere, J. L. (2022). Mass-Movement Processes: Shallow Landslides. In *Treatise on Geomorphology* (pp. 106–113). Elsevier. https://doi.org/10.1016/B978-0-12-818234-5.00024-9

Montoya-Araque, E. A., & Montoya-Noguera, S. (2023). Sensitivity Analysis of a Physically Based Model to Assess Rainfall-Triggered Shallow Landslides. *Geotechnical and Geological Engineering*, *41*, 2797–2814. https://doi.org/10.1007/s10706-023-02427-3

Moreira, A., Moraes, L. A. C., & Fageria, N. K. (2012). Nutritional limitations in multi-strata agroforestry system with native amazonian plants. *Journal of Plant Nutrition*, *35*(12), 1791–1805. https://doi.org/10.1080/01904167.2012.706676

Msilimba, G. G. (2002). *Landslides: Geohazard assessment of the Vunguvungu/Banga*

Catchment Area in Rumphi District. M.Sc. Environmental Science. University of Malawi, Zomba.

Mufidawati, H., Damayanti, A., & Supriatna. (2021). Vegetative conservation for landslide mitigation in bungaya sub-district, gowa regency, south sulawesi province. *IOP Conference Series: Earth and Environmental Science*, *683*(1), 012064. https://doi.org/10.1088/1755-1315/683/1/012064

Mukhopadhyay, M., Biswas, U., Mandal, N., & Misra, S. (2019). On the Development of Shear Surface Roughness. *Journal of Geophysical Research: Solid Earth*, *124*(2), 1273–1293. https://doi.org/10.1029/2018JB016677

Murthy, V. N. S. . (2003). Geotechnical Engineering- Principles and Practices of Soil Mechanics and Foundation Engineering. In *Taylor & Francis* (Vol. 6, Issue October).

Nagy-Göde, F. K., & Török, Á. (2022). The probabilistic analysis of steep lakeside slopes; geotechnical-geological-hydrogeological constraints and numerical analysis, an example from Hungary. *The Evolution of Geotech - 25 Years of Innovation*. https://doi.org/10.1201/9781003188339-59

Nassirzadeh, R., Dini, A., & Balagar, V. (2024). Back analysis of cohesion and friction angle of failed slopes using probabilistic approach: two case studies. *International Journal of Geo-Engineering*, *15*(1). https://doi.org/10.1186/s40703-024-00205-5

Nasution, S. N., Rachman, S., & Pramudito, H. (2021). Slope stability analysis using bishop method and kinematic analysis. *IOP Conference Series: Materials Science and Engineering*, *1098*(6), 062041. https://doi.org/10.1088/1757-899X/1098/6/062041

Naredla, P., & Sangeetha, S. (2022). A Study on the Influence of Vegetation Growth on Slope Stability. *IOP Conference Series: Earth and Environmental Science*, *1032*(1), 012003. https://doi.org/10.1088/1755-1315/1032/1/012003

Nguyên, T. T. T., Doanh, T., Le Bot, A., & Dalmas, D. (2019). On the role of pore pressure in dynamic instabilities of saturated model granular materials. *Granular Matter*, *21*(3). https://doi.org/10.1007/s10035-019-0915-5

Nowamooz, H., & Masrouri, F. (2008). Hydromechanical behaviour of an expansive

bentonite/silt mixture in cyclic suction-controlled drying and wetting tests. *Engineering Geology*, *101*(3–4). https://doi.org/10.1016/j.enggeo.2008.04.011

Oktarianty, H. (2019). Influence of DifferenceDip Direction on The Relationship of Friction Angle and Factor of Safety in Wedge Failure for Rock Slope. *IOP Conference Series: Earth and Environmental Science*, *353*(1), 012028. https://doi.org/10.1088/1755-1315/353/1/012028

Oluyemi-Ayibiowu, B. D., & Akinleye, T. O. (2019). Factors Influencing the Soil-Water Characteristics of Unsaturated Tropical Silty Sand. *Journal of Geoscience and Environment Protection*, *07*(05). https://doi.org/10.4236/gep.2019.75019

Oorthuis, R., Hürlimann, M., Vaunat, J., Moya, J., & Lloret, A. (2023). Monitoring the role of soil hydrologic conditions and rainfall for the triggering of torrential flows in the Rebaixader catchment (Central Pyrenees, Spain): Role of soil hydrologic conditions and rainfall for torrential flows in the Rebaixader catchment. *Landslides*, *20*(2), 249–269. https://link.springer.com/article/10.1007/s10346-022-01975-8

Palmström, A. (1982). The volumetric joint count - A useful simple measure of the degree of rock jointing. *Fourth Congress, IAEG*, 221–228.

Pan, X., Wu, H., Chen, S., Nanding, N., Huang, Z., Chen, W., Li, C., & Li, X. (2023). Evaluation and Applicability Analysis of GPM Satellite Precipitation over Mainland China. *Remote Sensing*, *15*(11), 2866. https://doi.org/10.3390/rs15112866

Pandey, P., Chauhan, P., Bhatt, C. M., Thakur, P. K., Kannaujia, S., Dhote, P. R., Roy, A., Kumar, S., Chopra, S., Bhardwaj, A., & Aggrawal, S. P. (2021). Cause and Process Mechanism of Rockslide Triggered Flood Event in Rishiganga and Dhauliganga River Valleys, Chamoli, Uttarakhand, India Using Satellite Remote Sensing and in situ Observations. *Journal of the Indian Society of Remote Sensing*, *49*(5), 1011–1024. https://doi.org/10.1007/s12524-021-01360-3

Parkash, S. (2019). *Landslide Preparedness Guidelines for Safety of Buildings on Slopes*. National Institute of Disaster Management (NIDM), Ministry of Home Affairs, New Delhi-110001.

Parker, J. C., Zelazny, L. W., & Amos, D. F. (1980). Swelling Components of Compacted Ca-Montmorillonite. *Clays and Clay Minerals*, *28*(2), 135–141. https://doi.org/10.1346/CCMN.1980.0280210

Peck, R., Hanson, W., & Thornburn, T. (1974). *Foundation Engineering*. Wiley.

Pellet, F. L., Keshavarz, M., & Boulon, M. (2013). Influence of humidity conditions on shear strength of clay rock discontinuities. *Engineering Geology*, *157*. https://doi.org/10.1016/j.enggeo.2013.02.002

Peng, J., Jin, F., Yang, Y., Dong, K., Song, J., & Mo, W. (2020). Design of Image Transmission for Slope Monitoring Based on GPRS. *2020 IEEE 11th International Conference on Software Engineering and Service Science (ICSESS)*, 236–239. https://doi.org/10.1109/ICSESS49938.2020.9237734

Penna, I. M., Abellán, A., Humair, F., Jaboyedoff, M., Daicz, S., & Fauqué, L. (2017). The role of tectonic deformation on rock avalanche occurrence in the Pampeanas Ranges, Argentina. *Geomorphology*, *289*, 18–26. https://doi.org/10.1016/j.geomorph.2016.07.006

Peruccacci, S., Brunetti, M. T., Luciani, S., Vennari, C., & Guzzetti, F. (2012). Lithological and seasonal control on rainfall thresholds for the possible initiation of landslides in central Italy. *Geomorphology*, *139–140*. https://doi.org/10.1016/j.geomorph.2011.10.005

Petit, J. P. P. (1987). Criteria for the sense of movement on fault surfaces in brittle rocks. *Journal of Structural Geology*, *9*(5–6), 597–608. https://doi.org/10.1016/0191-8141(87)90145-3

Picarelli, L., Santo, A., Di Crescenzo, G., Vassallo, R., Urciuoli, G., Silvestri, F., & Olivares, L. (2022). A complex slope deformation case—history. *Landslides*, *19*(7), 1649–1665. https://doi.org/10.1007/s10346-022-01866-y

Pirzada, M. A., Bahaaddini, M., Andersen, M. S., & Roshan, H. (2023). Coupled Hydro-Mechanical Behaviour of Rock Joints During Normal and Shear Loading. *Rock Mechanics and Rock Engineering*, *56*(2). https://doi.org/10.1007/s00603-022-03106-0

Piteau, D. R., & Peckover, F. L. (1989). *Engineering of rock slopes. In: Goodman, R.E.*

(Ed.), Introduction to Rock Mechanics (2nd ed.). John Wiley & Sons.

Prakash, S., & Jain, P. K. (2002). *Engineering soil testing*. Nem Chand. http://catalog.hathitrust.org/api/volumes/oclc/9359193.html

Punmia, B.C. (1994). *Soil Mechanics and Foundations* (13th ed.). Laxmi Publications (P) Ltd.

Rahimi, A., Rahardjo, H., & Leong, E.-C. (2011). Effect of Antecedent Rainfall Patterns on Rainfall-Induced Slope Failure. *Journal of Geotechnical and Geoenvironmental Engineering*, *137*(5), 483–491. https://doi.org/10.1061/(ASCE)GT.1943-5606.0000451

Rahman, A. U., Zhang, G., A. AlQahtani, S., Janjuhah, H. T., Hussain, I., Rehman, H. U., & Shah, L. A. (2023). Geotechnical Assessment of Rock Slope Stability Using Kinematic and Limit Equilibrium Analysis for Safety Evaluation. *Water*, *15*(10), 1924. https://doi.org/10.3390/w15101924

Ramsay, J. G. (1967). *Folding and fracturing of rocks*. Blackburn Press.

Ramsay, J. G., & Huber, M. I. (1987). The techniques of modern structural geology: Folds and fractures. In *Folds and fractures*. Academic Press.

Ran, Q. hua, Qian, Q., Li, W., Fu, X. dong, Yu, X., & Xu, Y. ping. (2015). Impact of earthquake-induced-landslides on hydrologic response of a steep mountainous catchment: a case study of the Wenchuan earthquake zone. *Journal of Zhejiang University: Science A*, *16*(2), 131–142. https://doi.org/10.1631/JZUS.A1400039

Ritchie, A. M. (1963). *Evaluation of rockfall and its control. Highway Research Record*.

Rocscience Inc. (2005). *RocData Version 5.0 - Rock, Soil, and Discontinuity Strength Analysis. www.rocscience.com, Toronto, Ontario, Canada*. www.rocscience.com

Roda-Boluda, D. C., D'Arcy, M., McDonald, J., & Whittaker, A. C. (2018). Lithological controls on hillslope sediment supply: insights from landslide activity and grain size distributions. *Earth Surface Processes and Landforms*, *43*(5). https://doi.org/10.1002/esp.4281

Romana, M. (1985). New adjustment ratings for application of Bieniawski

classification to slopes. *Proceedings of the International Symposium on Role of Rock Mechanics, Zacatecas, Mexico*, 49–53.

Roy, R. K., & Kacker, R. N. (1986). Cenozoic deformation pattern and mechanism in the belt of Schuppen and their role in hydrocarbon accumulation; further exploratory concepts for Assam-Arakan Basin. In N. C. Ghose & S. Varadarajan (Eds.), *Ophiolites and Indian Plate margin* (pp. 197–221). Sumna Publishers & Distributors, Patna.

Samant, H., Pundalik, A., D'souza, J., Sheth, H., Lobo, K. C., D'souza, K., & Patel, V. (2017). Geology of the Elephanta Island fault zone, western Indian rifted margin, and its significance for understanding the Panvel flexure. *Journal of Earth System Science*, *126*(1), 9. https://doi.org/10.1007/s12040-016-0793-8

Samodra, G., Chen, G., Sartohadi, J., & Kasama, K. (2018). Generating landslide inventory by participatory mapping: an example in Purwosari Area, Yogyakarta, Java. *Geomorphology*, *306*. https://doi.org/10.1016/j.geomorph.2015.07.035

Sarma, H. (1985). *Systematic geological mapping around Pukha-Lungwa-Chenwentyu-Champang areas of Mon district*.

Sati, S. P., Asim, M., Sundriyal, Y. P., Rana, N., Bahuguna, V., & Sharma, S. (2023). Unstable slopes and threatened livelihoods of the historical Joshimath town, Uttarakhand Himalaya, India. *Current Science*, *124*(12), 1384–1392. https://doi.org/10.18520/cs/v124/i12/1384-1392

Schafer, W. M., & Singer, M. J. (1976). A New Method of Measuring Shrink-Swell Potential Using Soil Pastes. *Soil Science Society of America Journal*, *40*(5), 805–806. https://doi.org/10.2136/sssaj1976.03615995004000050050x

Sen, S., Mitra, S., Debbarma, C., & De, S. K. (2015). Impact of faults on landslide in the Atharamura Hill (along the NH 44), Tripura. *Environmental Earth Sciences*, *73*(9). https://doi.org/10.1007/s12665-014-3778-4

Shabbir, W., Omer, T., & Pilz, J. (2023). The impact of environmental change on landslides, fatal landslides, and their triggers in Pakistan (2003–2019). *Environmental Science and Pollution Research*, *30*(12). https://doi.org/10.1007/s11356-022-24291-z

Sharda, Y. P., & Bhambay, G. C. (1980). *Kohima town, Nagaland: A decade of environmental geoscientific studies. GSI Sp. Publ. Series, No. 9.*

Sheikh, M. R., Nakata, Y., Shitano, M., & Kaneko, M. (2020). *Unstable Slope Monitoring and Early Warning by Multi-point Tilting Sensor and Pipe Strain Gauge* (pp. 1225–1232). https://doi.org/10.1007/978-981-15-2184-3_161

Sidle, R. C., & Bogaard, T. A. (2016). Dynamic earth system and ecological controls of rainfall-initiated landslides. *Earth-Science Reviews*, *159*, 275–291. https://doi.org/10.1016/j.earscirev.2016.05.013

Sidle, R. C., & Ochiai, H. (2006). Natural Factors Influencing Landslides. In *Landslides: Processes, Prediction, and Land Use* (pp. 41–119). https://doi.org/https://doi.org/10.1002/9781118665954.ch3

Simón, J. L. (2019). Forty years of paleostress analysis: has it attained maturity? *Journal of Structural Geology*, *125*, 124–133. https://doi.org/10.1016/j.jsg.2018.02.011

Singh, P. K., Ratan, D., Singh, K. K., & Singh, T. N. (2016). *Landslide in fractured and stratified rocks - A case from Aizawl, Mizoram, India. Rare*, 375–380. https://doi.org/10.2991/rare-16.2016.59

Singh, R. A., Negi, R., Singh, P. K., & Singh, T. N. (2021). Landslide Studies Between Devprayag and Pali along National Highway-7, Tehri District, Garhwal Lesser Himalaya. *Journal of Scientific Research*, *65*(01), 32–38. https://doi.org/10.37398/JSR.2021.650105

Singh, M.P., Soibam, I., Thong, G.T., & Aier, I. (2008). Impact of human settlement and land use on slope stability: Phikomei (Mao) Slide, an example from NH 39, Imphal-Mao road section, Manipur. Bulletin of the Indian Geologists' Association, vol. 41, pp. 25-39.

Singh, T. N., Kainthola, A., Venkatesh, A., & Venkatesh A. (2012). Correlation Between Point Load Index and Uniaxial Compressive Strength for Different Rock Types. *Rock Mechanics and Rock Engineering*, *45*(2), 259–264. https://doi.org/10.1007/s00603-011-0192-z

Singh, V. K., Masood, M. M., & Verma, T. (2024). Slope Monitoring Techniques in

Opencast Mines: A Review of Recent Advances. *Journal of Mines, Metals and Fuels*, 83–92. https://doi.org/10.18311/jmmf/2024/36294

Sinha, N. K., Chatterjee, B. P., & Satsangi, P. P. (1982). *Status of paleontological researches in North Eastern region*. Geol. Surv. India Record, No. 112.

Skilodimou, H., Bathrellos, G., Koskeridou, E., Soukis, K., & Rozos, D. (2018). Physical and Anthropogenic Factors Related to Landslide Activity in the Northern Peloponnese, Greece. *Land*, *7*(3), 85. https://doi.org/10.3390/land7030085

Smith, K. (2013). *Environmental Hazards Assessing Risk and Reducing Disaster* (6th ed.). Routledge.

Snethen, D. R., Johnson, L. D., & Patrick, D. M. (1977). *An evaluation of expedient methodology for identification of potentially expansive soils. Soil and Pavements Laboratory, US Army Engineering, Waterway Experiment Station, Vicksburg, Mississippi. Report No. FHWA (Federal Highway Administration)-RE-77-94, N*.

Soibam, I. (1998). *Structural and tectonic analysis of Manipur with special reference to evolution of the Imphal valley*. Manipur University, Imphal.

Sondhi, V. P. (1941). *A note on landslips on the Dimapur-Manipur road, Assam*.

Sothu, H.N., Aier, I., & Thong, G.T., (2009). Evaluation of two unstable sites along NH 150, SE of Kohima Town, Nagaland. Indian Landslides, vol. 2, pp. 27-30.

Sothu, H.N., Aier, I., & Thong, G.T. (2011). Analysis of Chakhabama subsidence and its surroundings along NH 150, Nagaland, NE India. Disaster and Development, vol. 5, pp. 131-137.

Springman, S., Kienzler, P., Casini, F., & Askarinejad, A. (2009). Landslide triggering experiment in a steep forested slope in Switzerland. *Proceedings of the 17th International Conference on Soil Mechanics and Geotechnical Engineering: The Academia and Practice of Geotechnical Engineering*, *2*. https://doi.org/10.3233/978-1-60750-031-5-1698

Stanchi, S., D'Amico, M., Zanini, E., & Freppaz, M. (2016). Liquid and plastic limits of mountain soils as a function of the soil and horizon type. *Catena*, *135*. https://doi.org/10.1016/j.catena.2015.07.021

Stoffel, M., & Huggel, C. (2012). Effects of climate change on mass movements in mountain environments. In *Progress in Physical Geography* (Vol. 36, Issue 3). https://doi.org/10.1177/0309133312441010

Su, M., Cheng, K., Liu, Y., Xue, Y., Wang, P., Zhang, K., & Li, C. (2021). Combining geophysical methods, drilling, and monitoring techniques to investigate carbonaceous shale landslides along a railway line: a case study on Jiheng Railway, China. *Bulletin of Engineering Geology and the Environment*, *80*(10), 7493–7506. https://doi.org/10.1007/s10064-021-02365-5

Subashchandrabose, E., & Jeyapriya, S. P. (2023). Determination of Drained Residual Shear Strength Parameters of C Soil Using Ring Shear Apparatus. *International Journal for Research in Applied Science and Engineering Technology*, *11*(6). https://doi.org/10.22214/ijraset.2023.53901

Summerfield, M. A. (2014). *Global Geomorphology*. Routledge. https://doi.org/10.4324/9781315841182

Sun, T., Deng, Z., Xu, Z., & Wang, X. (2020). Volume Estimation of Landslide Affected Soil Moisture Using TRIGRS: A Case Study of Longxi River Small Watershed in Wenchuan Earthquake Zone, China. *Water*, *13*(1), 71. https://doi.org/10.3390/w13010071

Supongtemjen. (2012). *Geological investigation of land instability between Kohima and Zhadima*. Nagaland University.

Supongtemjen, & Thong, G.T. (2014). Risk analyses along part of NH 2, north of Kohima town, Nagaland. Indian Landslides, vol.7, pp. 35-44.

Supongtemjen, Walling, T., Tep, S., & Thong, G.T. (2015). Stability analyses of two fresh cut slopes along NH 2, Meriema, Nagaland. Proceedings of the National Seminar on Landslides: Management and Mitigation Strategies. Journal of Engineering Geology, vol. XL, pp. 158-170.

Tabbal, D., Saleh, M., & Bashir, H. (2019). Geotechnical and Numerical analysis of Bcharreh Landslide stability. *MATEC Web of Conferences*, *281*, 02005. https://doi.org/10.1051/matecconf/201928102005

Tang, Z. C., & Wong, L. N. Y. (2016). New criterion for evaluating the peak shear

strength of rock joints under different contact states. *Rock Mechanics and Rock Engineering*, *49*(4). https://doi.org/10.1007/s00603-015-0811-1

Terzaghi, K. (1950). Mechanism of Landslides. In *Application of Geology to Engineering Practice* (pp. 83–123). Geological Society of America. https://doi.org/10.1130/Berkey.1950.83

Thong, G. T., Aier, I., & Walling, T. (2004). *Preliminary geological report of Mao slide. BRO Report*.

Tranos, M. D., Neofotistos, P. G., Kokkalas, S. A., & Tourigny, G. L. (2022). Insights into the Paleostress Analysis of Heterogeneous Fault-Slip Data by Comparing Different Methodologies: The Case of the Voltri Massif in the Ligurian Alps (NW Italy). *Applied Sciences*, *12*(19), 10098. https://doi.org/10.3390/app121910098

Trisnawati, D., Najib, Hidayatillah, A. S., & Najib. (2022). The Relationship of Lithology with Landslide Occurrences in Banyumanik and Tembalang Districts, Semarang City. *IOP Conference Series: Earth and Environmental Science*, *1047*(1). https://doi.org/10.1088/1755-1315/1047/1/012026

Trojnar, K. (2020). *Numerical Analysis of the Landslide Geohazards - Case Study with Gabions and Piles Solutions* (pp. 474–479). https://doi.org/10.1007/978-3-030-27011-7_60

Tsai, C.-H., Huang, C.-L., Hsu, S.-K., Doo, W.-B., Lin, S.-S., Wang, S.-Y., Lin, J.-Y., & Liang, C.-W. (2018). Active normal faults and submarine landslides in the Keelung Shelf off NE Taiwan. *Terrestrial, Atmospheric and Oceanic Sciences*, *29*(1), 31–38. https://doi.org/10.3319/TAO.2017.07.02.01

Turner, A. K. (2018). Social and environmental impacts of landslides. *Innovative Infrastructure Solutions*, *3*(1), 70. https://doi.org/10.1007/s41062-018-0175-y

Umili, G., Bonetto, S. M. R., Mosca, P., Vagnon, F., & Ferrero, A. M. (2020). In Situ Block Size Distribution Aimed at the Choice of the Design Block for Rockfall Barriers Design: A Case Study along Gardesana Road. *Geosciences*, *10*(6), 223. https://doi.org/10.3390/geosciences10060223

Varnes, D. (1978). Slope Movement Types and Processes. In R. J. Schuster & R. J. Krizek (Eds.), *Transportation Research Board Special Report* (Issue 176, pp. 11–

33). National Academy of Sciences.

Velayudham, J., Kannaujiya, S., Sarkar, T., Champati Ray, P. K., Taloor, A. K., Singh Bisht, M. P., Chawla, S., & Pal, S. K. (2021). Comprehensive study on evaluation of Kaliasaur Landslide attributes in Garhwal Himalaya by the execution of geospatial, geotechnical and geophysical methods. *Quaternary Science Advances*, *3*, 100025. https://doi.org/10.1016/j.qsa.2021.100025

Vidrih, R., Ribičič, M., & Suhadolc, P. (2001). Seismogeological effects on rocks during the 12 April 1998 upper Soča Territory earthquake (NW Slovenia). *Tectonophysics*, *330*(3–4), 153–175. https://doi.org/10.1016/S0040-1951(00)00219-5

Vishal, V., Pradhan, S. P., & Singh, T. N. (2010). Instability assessment of mine slope-A Finite Element Approach. *International Journal of Earth Sciences and Engineering*, *3*, 11–23.

Wallace, R. E. (1951). Geometry of Shearing Stress and Relation to Faulting. *The Journal of Geology*, *59*(2), 118–130. https://doi.org/10.1086/625831

Walling, T. (2005). *Geological investigation of land instability in Kohima town Nagaland* [Nagaland University]. http://hdl.handle.net/10603/118894

Walling, T., Supongtemjen, Chang, C.N., & Thong, G.T. (2016). Geotechnical analyses of debris slide near Secretariat junction, Kohima, Nagaland. In: Srivastava, S.K. (Ed), Recent Trends in Earth Science Research with Special Reference to NE India, Today and Tomorrow Publishers, New Delhi, pp. 277-289.

Wang, F., Wang, S., Yao, W., Li, X., Meng, F., & Xia, K. (2023). Effect of roughness on the shear behavior of rock joints subjected to impact loading. *Journal of Rock Mechanics and Geotechnical Engineering*, *15*(2), 339–349. https://doi.org/10.1016/j.jrmge.2022.04.011

Wang, N., Liu, W., Sun, F., Yao, Z., Wang, H., & Liu, W. (2020). Evaluating satellite-based and reanalysis precipitation datasets with gauge-observed data and hydrological modeling in the Xihe River Basin, China. *Atmospheric Research*, *234*. https://doi.org/10.1016/j.atmosres.2019.104746

Wang, Z.Y., Lee, J. H. W., & Melching, C. S. (2015). Debris Flows and Landslides. In

River Dynamics and Integrated River Management (pp. 193–264). Springer Berlin Heidelberg. https://doi.org/10.1007/978-3-642-25652-3_5

Wieczorek, G. F., Nishenkod, S. P., & Varnes, D. J. (1995). Analysis of rockfalls in the Yosemite Valley, California. In J. J. K. Daemen & R. A. Schultz (Eds.), *Rock mechanics: proceedings of the 35th US symposium* (pp. 85–89).

Wieczorek, G. F., Snyder, J. B., Waitt, R. B., Morrissey, M. M., Uhrhammer, R. A., Harp, E. L., Norris, R. D., Bursik, M. I., & Finewood, L. G. (2000). Unusual July 10, 1996, rock fall at Happy Isles, Yosemite National Park, California. *Geological Society of America Bulletin*, *112*(1), 75–85. https://doi.org/10.1130/0016-7606(2000)112<75:UJRFAH>2.0.CO;2

Willenberg, H., Loew, S., Eberhardt, E., Evans, K. F., Spillmann, T., Heincke, B., Maurer, H., & Green, A. G. (2008). Internal structure and deformation of an unstable crystalline rock mass above Randa (Switzerland): Part I — Internal structure from integrated geological and geophysical investigations. *Engineering Geology*, *101*(1–2), 1–14. https://doi.org/10.1016/j.enggeo.2008.01.015

Wu, X., Ren, J., & Vanapalli, S. K. (2020). The Influence Of Temperature And Water Content On The Behavior Of Soils. *International Journal of GEOMATE*, *18*(70). https://doi.org/10.21660/2020.70.9439

Xin, Y., Feng, H., Yiqiang, Y., Wei, Z., Dingyi, Z., & Zhi, H. (2024). Application of UAV 3D Point Cloud Data in Highway Slope Disaster Investigation. *IOP Conference Series: Earth and Environmental Science*, *1334*(1), 012031. https://doi.org/10.1088/1755-1315/1334/1/012031

Yadav, M., Pal, S. K., Singh, P. K., & Gupta, N. (2023). Landslide Susceptibility Zonation Mapping Using Frequency Ratio, Information Value Model, and Logistic Regression Model: A Case Study of Kohima District in Nagaland, India. In *Landslides: Detection, Predict. and Monit.: Technol. Dev.* (pp. 333–363). Springer International Publishing. https://doi.org/10.1007/978-3-031-23859-8_17

Yamaguchi, Y., Makinoshima, F., & Oishi, Y. (2023). Simulating the entire rainfall-induced landslide process using the material point method for unsaturated soil with implicit and explicit formulations. *Landslides*. https://doi.org/10.1007/S10346-023-02052-4

Yang, J., Cai, J., Yao, C., Li, P., Jiang, Q., & Zhou, C. (2019). Comparative Study of Tunnel Blast-Induced Vibration on Tunnel Surfaces and Inside Surrounding Rock. *Rock Mechanics and Rock Engineering*, *52*(11), 4747–4761. https://doi.org/10.1007/S00603-019-01875-9

Ykhlef, B., Belouar, A., & Boulfoul, A. (2023). Experimental Studies on Some Clays Leading to Instability. *Civil Engineering Journal (Iran)*, *9*(2). https://doi.org/10.28991/CEJ-2023-09-02-012

Yu, L., Zhang, D., Fang, Q., Cao, L., Zhang, Y., & Xu, T. (2020). Face stability of shallow tunnelling in sandy soil considering unsupported length. *Tunnelling and Underground Space Technology*, *102*, 103445. https://doi.org/10.1016/j.tust.2020.103445

Yu, X., Gong, B., & Tang, C. (2021). Study of the slope deformation characteristics and landslide mechanisms under alternating excavation and rainfall disturbance. *Bulletin of Engineering Geology and the Environment*, *80*(9), 7171–7191. https://doi.org/10.1007/S10064-021-02371-7

Zaruba, Q., & Mencl, V. (1969). Landslides and their control. Developments in geotechnical engineering. vol 2. In *Czechoslovakia Academy of Sciences*.

Zellmer, J. T. (1987). The unexpected rockfall hazard. *Bulletin of the Association of Engineering Geologists*, *24*(2), 281–283.

Zeng, Y., Zhang, Y., Hu, W., Chen, M., Hu, Q., Liu, X., & Zhu, X. (2024). A case study on soil slope landslide failure and parameter analysis of influencing factors for safety factor based on strength reduction method and orthogonal experimental design. *PLOS ONE*, *19*(5), e0300586. https://doi.org/10.1371/journal.pone.0300586

Zhang, J., Tang, W. H., & Zhang, L. M. (2010). Efficient Probabilistic Back-Analysis of Slope Stability Model Parameters. *Journal of Geotechnical and Geoenvironmental Engineering*, *136*(1), 99–109. https://doi.org/10.1061/(asce)gt.1943-5606.0000205

Zhang, T., Yin, Y., Li, B., Liu, X., Wang, M., Gao, Y., Wan, J., & Gnyawali, K. R. (2023). Characteristics and dynamic analysis of the February 2021 long-runout

disaster chain triggered by massive rock and ice avalanche at Chamoli, Indian Himalaya. *Journal of Rock Mechanics and Geotechnical Engineering*, *15*(2), 296–308. https://doi.org/10.1016/j.jrmge.2022.04.003

Zhang, X., Wang, L., Krabbenhoft, K., & Tinti, S. (2020). A case study and implication: particle finite element modelling of the 2010 Saint-Jude sensitive clay landslide. *Landslides*, *17*(5), 1117–1127. https://doi.org/10.1007/s10346-019-01330-4

Zhang, Z., Yang, C., & Yang, M. (2023). Stability analysis and prevention suggestions for a landslide in Sichuan Province**. In *Advances in Traffic Transportation and Civil Architecture* (pp. 811–818). CRC Press. https://doi.org/10.1201/9781003402220-91

Zheng, Y., Wang, R., Chen, C., & Meng, F. (2021). Analysis of Flexural Toppling Failure in Rock Slopes Using Discrete Element Method. *Frontiers in Earth Science*, *9*. https://doi.org/10.3389/feart.2021.773088

Zhong, N., Jiang, H., Li, H., Su, D., Xu, H., Liang, L., & Fan, J. (2022). The potential of using soft-sediment deformation structures for quantitatively reconstructing paleo-seismic shaking intensity: progress and prospect. *Environmental Earth Sciences*, *81*(16). https://doi.org/10.1007/S12665-022-10504-8

Zieher, T., Gallotti, G., Rianna, G., Reder, A., & Pfeiffer, J. (2023). Exploring the effects of climate change on the water balance of a continuously moving deep-seated landslide. *Natural Hazards*, *115*(1), 357–387. https://doi.org/10.1007/s11069-022-05558-7

Zischinsky, U. (1966). On the deformation of high slopes. *1st ISRM Congress 1966*.